

Politecnico di Torino

Master of Science in Energy and Nuclear Engineering

**Thermochemical Energy Storage
for Concentrated Solar Power**



Fabio Scaiola

Supervisor:
Ricardo Chacartegui
Vittorio Verda

Abstract

This thesis is focused on the study of a new way of storing thermal energy coupled with already mature CSP technologies in order to enhance their competitiveness in the energy market. Currently the main solutions for existing CSP plants, as thermal energy storage, are based on sensible heat storage technology made using molten salt at high temperature. The alternative way studied in this work is instead based on the exploitation of chemical bonds. The heat is not simply stored but is used to drive an endothermic reversible chemical reaction where the products act as the actual energy storage. The inverse exothermic reaction is then the energy releasing step. This process, called chemical looping, permit to store thermal energy for theoretically infinite time without any losses during the storage period. The system performance and behaviour of the process are strongly affected by the chosen chemical reaction. The focus of this work is on the chemical looping based on calcium hydroxide. The chemical looping process is then composed by two different reactions: the dehydration of the hydroxide, that is the endothermic reaction, and the hydration of the oxide, that is the exothermic one. Their characteristics show that they are suitable for medium-low temperature processes (150 – 600 °C). This range of temperature is high enough to permit the exploitation of a Rankine-Hirn cycle with superheated steam for power production. The effect of reaction temperature and pressure are evaluated in order to enhance the TES performance and its integration with the power production system. Many system modifications are hypothesized in order to improve the system efficiency and the pinch point analysis has been used to see how the management of the available heat sources should be done. The direct integration of a steam turbine in the discharge process of the TES system has been studied in order to enhance the overall performance of the system. It has also been studied the exploitation of ORC, with toluene or cyclopentane as working fluids, for the power generation.

Index

1. Energy Storage	5
1.1. Overview	5
1.2. TES Characterization	8
1.2.1. Sensible heat storage TES	9
1.2.2. Latent heat storage TES	11
1.2.3. Thermochemical heat storage TES.....	12
2. Calcium Hydroxide Chemical Looping	17
2.1. Ca(OH)₂ / CaO Main Information	17
2.2. Ca(OH)₂ Dehydration / CaO Hydration Reactions Kinetics	20
3. Calcium Hydroxide TES System	24
3.1. Reactor Choice	24
3.2. Reference layout	27
3.3. Base Layout	33
3.3.1. Description	33
3.3.2. Parametric analysis 1	37
3.3.3. Parametric analysis 2.....	42
3.3.4. Pinch analysis.....	45
4. Plant Configuration	53
4.1. Plant Size	53
4.2. Direct and Indirect Dehydration Reactor Integration	57
4.3. Pinch analysis.....	60
5. TES System Modification	66
5.1. System Pressure Modification	66
5.2. Dehydration Steam Partial Pressure Reduction	67
5.2.1. Pinch Analysis.....	78
5.3. Series of Dehydration Reactors	85
5.3.1. Pinch Analysis.....	92
5.4. Hydration Pressure Modification	97
5.4.1. Pinch analysis.....	102
6. Power Block Integration	107
6.1. Rankine-Hirn Steam Cycle	108
6.1.1. Rankine-Hirne PB integration with base case TES layout after pinch analysis.....	115

6.1.2.	Rankine-Hirne PB integration with N ₂ modified TES layout after pinch analysis	116
6.1.3.	Rankine-Hirn PB integration with modified 3 dehydration reactor TES after pinch analysis	117
6.2.	Higher TES heat output temperature level by higher hydration temperature	118
6.3.	Direct Steam Turbine integration.....	123
6.3.1.	Pinch analysis.....	131
6.4.	Organic Rankine Cycle.....	137
6.4.1.	Toluene.....	139
6.4.2.	Toluene ORC PB integration with low hydration temperature TES.....	146
6.4.3.	Cyclopentane.....	147
6.4.4.	Cyclopentane ORC PB integration with low hydration temperature TES	150
7.	Conclusions	151
7.1.	TES system modification results and analysis	156
7.2.	Power block integration results and analysis.....	159
8.	Bibliography	162

1. Energy Storage

1.1. Overview

Our society and our world are dependent of energivorous technologies for the fulfilment of many activities and this addiction is constantly increasing and spreading due to the variation of the consumers habit and the rapid increase of the population. This evolution requires, and will means, an always higher amount of energy to work. The complexity of our energy network and its need to be more and more efficient and flexible has already shown the importance to be able to store energy and to convert it in an efficient way. With the penetration on the market of the main renewable energy sources we know today, the importance of energy storage ability has risen more and more due to the intermittency of their functioning. Renewable sources have many differences on the way they can be adequately exploited and so, the best choice of storage technology can be very different between the various sources and between the intended applications. We can divide the energy we mainly use in two main groups: thermal and electrical, figure 1. As can be seen in figure 1, there is a wide ser of available energy storage technologies for the different energy modes [1].

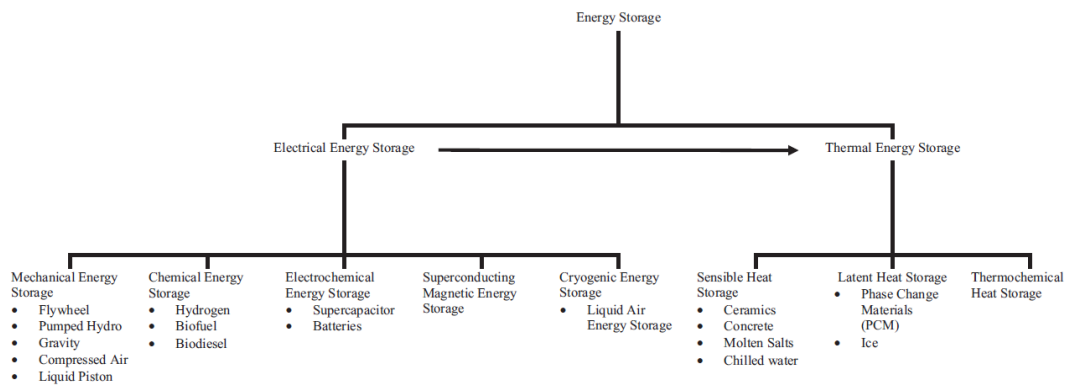


Figure 1: energy storage technology overview [1]

Electricity is one of the most used form of energy of our society, its production and distribution on large scale represents a very complex problem. The balance of the grid that, with the increased decentralization of production and the penetration of renewable sources, went harder making indispensable the energy storage as an instrument to be fulfilled. Different ways of storing electrical energy has already been studied; in any case electricity has to be transformed in order to be stored.

In the case of thermal energy, the ways in which it can be stored are mainly related to technologies that don't need previously a conversion in other form of energies but anyway they change its quality and shows some efficiency over the conversion. Thermal energy can be also converted into electrical energy with a power cycle and then stored with one of the available methods for electricity.

Any energy storage technology shows specific characteristics that make it suitable for specific storage applications. The most important features related to energy storage, that can be taken into account to make a comparison or an evaluation, are [1]:

- Energy density, defined as the amount of energy that can be stored for unit of mass or volume of the storage medium;
- Power density, that represents the amount of rated power that the storage medium can release for each unit of mass or volume;
- Life time, that is the expected life span of the storing device;
- Capital and operating cost;
- Storage capacity, or the total amount of energy stored in the device;
- Storage duration, that represents the amount of time the device can remain charged without starting a self-discharge process.
- Round trip efficiency, that represents the efficiency of the storage device during a single cycle of charge and discharge;
- Response time, that is the time span needed by the device to start releasing or absorbing energy;
- Maturity of the technology;

It is also important to remember that each conversion between different form of energy has a consequence that can be evaluated by an efficiency of the process.

Figure 2 shows the main features of some storage technologies [1].

Technology	Energy density Wh/kg(W h/L)	Power density W/kg(W/L)	Power rating	Discharge time	Suitable storage duration	Life time (years)	Cycle life (cycles)	Capital Cost			Round trip efficiency (%)	Technological maturity
								\$/kW	\$/kWh	\$/kWh-per cycle		
Flywheel	10-30(20-80)	400-1500(1000-2000)	0-250 kW	ms-15 min	s-min	~15	20,000+	250-350	1000-5000	3-25	85-95	Commercial
PHES	0.5-1.5(0.5-1.5)		100-5000 MW	1-24 h+	h-months	40-60		600-2000	5-100	0.1-1.4	65-87	Matured
CAES	30-60(3-6)		5-300 MW	1-24 h+	h-months	20-60		400-800	2-50	2-4	50-89	Developed
GES												
GPM	1.06(1.06)	3.13(3.13)	40-150 MW		h-months	30+		1000			75-80	Concept
ARES			100-3000 MW	34 s	h-months	40+		800			75-86	Concept
HES												
Fuel cell	800-10,000(500-3000)	500+(500+)	0-50 MW	s-24+h	h-months	5-15	1000	10,000+		6000-20,000	20-35	Developing
Gas engine	33,300(530-750)		0-50 MW	s-24+h	h-months						40-50	Developing
Super-capacitor	2.5-15	500-5000	0-300 kW	ms-60 min	s-h			100-300	300-2000	2-20	90-95	Developed
Batteries												Commercial
NaS	150-240(150-250)	150-230	50 kW-8 MW	s-h	s-h	10-15	2500	1000-3000	300-500	8-20	80-90	Commercial
NaNiCl	100-120(150-180)	150-200(220-300)	0-300 kW	s-h	s-h	10-14	2500+	150-300	100-200	5-10	85-90	Commercial
VRB	10-30		30 kW-3 MW	s-10 h	h-months	5-10	12,000+	600-1500	150-1000	5-80	85-90	Demonstration
FeCr	10-50	16-33	5-250 kW	s12+h	h-months				250		70-80	Commercial
ZnBr	30-50(30-60)		50 kW-2 MW	s-10 h	h-months	5-10	2000+	700-2500	150-1000	5-80	70-80	Demonstration
Zn-air	150-3000(500-10,000)	100	0-10 kW	s-24h+	h-months			100-250	10-60		50-55	Demonstration
Li-ion	75-200(200-500)	500-2000	0-100 kW	min-h	min-days			1200-4000	600-2500	15-100	85-90	Demonstration
SMES	0.5-5(0.2-2.5)	500-2000(1000-4000)	100 kW-10 MW	m-8 s	min-h	20+	100,000+	200-300	1000-10,000		95-98	Demonstration
LAES	97		350 kW-5 MW	1-24 h+	h-months	20+		1000-2000			50-70	Demonstration

Figure 2: main features of common energy storage technologies [1]

1.2. TES Characterization

TES are the most used type of energy storage, they can be classified [1] as low or high temperature TES depending on their maximum operating temperature in respect to ambient condition. Low-T TES operates in the range below 200 K over the ambient condition while High-T TES operates at higher temperatures. Low-T TES are mainly used for residential application like heating and cooling.

High-T TES are instead mainly used in industrial application like waste heat recovery, renewable energy technology and thermal power systems. The coupling of energy storages with renewable energy sources can be used to mitigate short fluctuations during transient weather condition or to shift the production in order to meet the energy demand but also to extend the generation period.

If we focus on CSP plants the main alternative as energy storage seems to be represented by TES as the use of batteries to store the produced electricity has not been proved to be economically viable [2]. Due to the large volume of storage media involved, the material price essentially relates to the bulk price. The energy storage alternatives by TES technologies for CSP are mainly of three different types [3],[4]. In figure 3 are listed the main characteristics of these three technologies.

	Sensible heat storage system	Latent heat storage system	Thermochemical storage system
Energy density			
Volumetric density	Small $\sim 50 \text{ kWh m}^{-3}$ of material	Medium $\sim 100 \text{ kWh m}^{-3}$ of material	High $\sim 500 \text{ kWh m}^{-3}$ of reactant
Gravimetric density	Small $\sim 0.02\text{--}0.03 \text{ kWh kg}^{-1}$ of material	Medium $\sim 0.05\text{--}0.1 \text{ kWh kg}^{-1}$ of material	High $\sim 0.5\text{--}1 \text{ kWh kg}^{-1}$ of reactant
Storage temperature	Charging step temperature	Charging step temperature	Ambient temperature
Storage period	Limited (thermal losses)	Limited (thermal losses)	Theoretically unlimited
Transport	Small distance	Small distance	Distance theoretically unlimited
Maturity	Industrial scale	Pilot scale	Laboratory scale
Technology	Simple	Medium	Complex

Figure 3: comparison of TES types [4]

From figure 3 we can see that TES system shows higher energy density and more permissive storage conditions but at the cost of having a more complex system. Another point that, for now, can be listed as a drawback is the low maturity level of this technology.

1.2.1. Sensible heat storage TES

Heat can be stored exploiting the specific heat capacity of any materials varying the temperature of the storage proportionally to the quantity of energy to be stored. It follows the next general equation:

Equation 1

$$Q = \Delta T * \bar{C}_p * M [J]$$

Where \bar{C}_p is the mean specific heat capacity of the mass M of the storage medium over the temperature variation ΔT that the system undergoes. The stored energy depends on the material medium characteristics, its total amount, and on the difference between its final and initial temperatures. During the process there is no phase change of the material. The main drawback is that the higher the storing temperature and the conductivity of the medium the higher will be the losses during the storing period without a proper insulation.

Currently all the TES installed in CSP plants are based on sensible heat storage materials like oil, molten salt, steam, ceramic and graphite. Storage media most desirable features can be summarized as follow: low freezing temperature, high maximum operational temperature, high heat capacity, high thermal conductivity and density, good thermal stability, low corrosion to the containment material and low cost. The state of the art for sensible TES is represented by molten salts TES. Figure 4 shows some of the most common HTF on the market with their main properties.

Salt	Composition (wt%)	Melting point (°C)	Maximum operation temperature (°C)	Cost, (USD \$/kg)	Cost, (USD\$/kW h)
Solar Salt	NaNO ₃ -KNO ₃ (60-40)	220	585	0.49	5.8 ($\Delta T=200$ K)
Hitec	NaNO ₃ -KNO ₃ -NaNO ₂ (7-53-40)	142	450-538 610-710 under different atmospheres	0.93	10.7 ($\Delta T=200$ K)
Hitec XL	NaNO ₃ -KNO ₃ -Ca(NO ₃) ₂ (7-45-48)	120	480-505	1.43	18.2 ($\Delta T=200$ K)
Therminol VP-1	-	-	400	3.96	57.5 ($\Delta T=100$ K)

Figure 4: properties and cost for common molten salts and Therminol VPI oil [3]

While the first three are molten salt the last one is a thermal oil. From the previous table we can see that molten salts show a quite high melting point from which rise some problem of solidification in the pipes when the system is not on duty.

Compared to other solutions molten salts bring to lower costs for the solar field and the storage. Furthermore, it leads to the possibility to work at a higher maximum temperature and so to have a higher efficiency in the power block.

Figure 5 show the HTF technical option that can be coupled to the different CSP technologies.

CSP technology	Technical options
Parabolic troughs (PT)	PT-oil: oil as HTF and molten salt storage PT-SHS: superheated steam as HTF PT-MS: molten salt as HTF and storage
Linear Fresnel systems (F)	Fresnel SaS: saturated steam as HTF Fresnel SHS: superheated steam as HTF
Towers (T)	T-SaS: saturated steam as HTF T-SHS: superheated steam as HTF T-MS: molten salt as HTF and storage T-AR: ambient pressure air as HTF and Rankine cycle T-GT: pressurised air as HTF and Brayton cycle T-SC: supercritical cycle T-CC: pressurised air as HTF and combined cycle
Parabolic dishes (DS)	DS: helium Stirling cycle

Figure 5: main CSP sensible TES technical options [3]

The main technical options as HTF for big scale plants are molten salts, solar oils, steam and air. Solar towers show the biggest range of HTF options already tested and confirmed.

As said before one of the main drawbacks about molten salts is the freezing point that is usually quite higher than ambient temperature. This characteristic of molten salts make necessary to have an anti-freeze system that has a not negligible impact on costs.

The research of fluids as HTF or storage medium is always looking for better solutions; between the newest development in this field there are many studies on ternary and quaternary molten salts composition [5] but also studies about new kind of fluid like Ionic liquids [6]. Another main technical problem on which research is trying to find valid long-lasting solution is related to the compatibility of containment materials with the storage medium.

In many cases the most commonly used storage technique in utility scale CSP plants is represented by the two-tank molten salt sensible storage. The available configurations of this technique are two: direct (a) and indirect (b) storage system, figure 6.

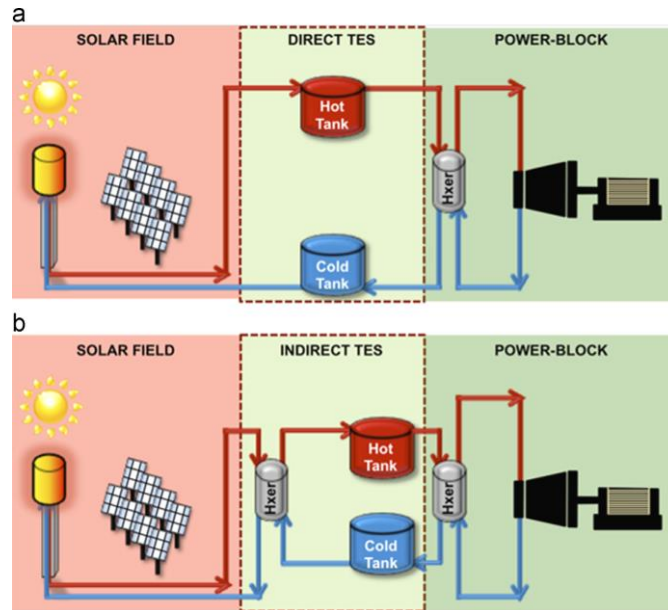


Figure 6: most common sensible TES configurations [3].

The indirect configuration permits to choose different material as storage medium and HTF fluid and is mainly used in parabolic through facilities with molten salt as storage medium and oil as HTF. The direct configuration has the advantages to not needing one of the heat exchangers and so it has higher efficiency and lower costs.

Other studies have proposed a single tank configuration with thermocline storage that allows to store the cold and the hot HTF in the same tank using an insulation baffle or thermal stratification as separation method.

To reduce the needed amount of relatively high-cost molten salt as storage medium some researches has been oriented to find low-cost filling solid materials to create a porous bed in the storage tank [7]. This kind of thermoclines are called dual-media or multi-media storage systems and requires an accurate choice of compatible filling material with the storage fluid by the chemical but also thermal and mechanical point of view.

1.2.2. Latent heat storage TES

The technologies based on latent heat storage exploit the large phase change heat of particular mediums, called PCM, to store energy. The most common PCM works between solid and liquid phase and the amount of energy that can be stored depends mainly on the phase change enthalpy but also on the specific heat capacity of the liquid and solid phases [3]:

Equation 2

$$Q = M * [C_{p,s} * (T_m - T_s) + h + C_{p,l} * (T_l - T_m)]$$

Where $C_{p,l}$ and $C_{p,s}$ are, respectively, the average specific heat of the PCM in liquid and solid phases. T_m is the temperature of phase change while T_s and T_l are the temperature of the solid and the liquid phases while M is the total mass amount of the PCM.

As the phase change for pure substances is an isothermal process, the latent TES can provide a big amount of heat at a constant level of temperatures; as consequence they also store heat at a fixed temperature and so the heat exchange during the charge step can be quite complex. PCM can be classified as organic or inorganic compound.

CSP systems have high temperature of functioning and so the most suitable PCM material are mainly inorganic salts/salt eutectics and metals/metal alloys. The exploitation of salts as PCM is the less expensive choice in relation to the material cost but usually they also have a low thermal conductivity and so the exploitation of this kind of medium needs the implementation of a system to enhance the heat transfer, particularly during the discharge mode, inside the storage medium.

There are many proposed solution to the poor salts heat conductivity: the use of fins [8], the introduction of higher heat transfer surface [9], the use of heat pipes or thermosiphons [10] and also the introduction of high thermal conducting material in the PCM medium [11]. The introduction of any of the previous methods to enhance the heat transfer means also a considerable increment in the system complexity. The exploitation of metal alloys shows higher cost but, they have a better thermal conductivity and so the system can be simpler.

1.2.3. Thermochemical heat storage TES

The thermochemical storage systems are based on the exploitation of reversible sorption process or of chemical reaction:

Equation 3



During the charging step the heat is used to drive an endothermic process that brings to the dissociation of the reactant AB; then, A and B, the product of the charging step, can be stored separately. The inverse exothermic process, between the stored chemicals A and B, will have as product the initial species AB and an amount of heat. The Heat involved in the charging and discharging steps can be defined as:

Equation 4

$$Q = a_r * M * \Delta H$$

Where a_r is the reacted fraction, ΔH is the specific heat of reaction and M is the mass of the reactant to which ΔH is referred. Thermochemical storage is still at an early stage of development and so most of the systems have been only tested at laboratory level.

The reversible reactions that are suitable for a TES system can be characterized by reactant family, reaction enthalpy and turning temperature. Figure 7 shows a list of the main reactant family that are feasible for thermochemical energy storage at medium and high temperatures also providing some example of the involved chemical species.

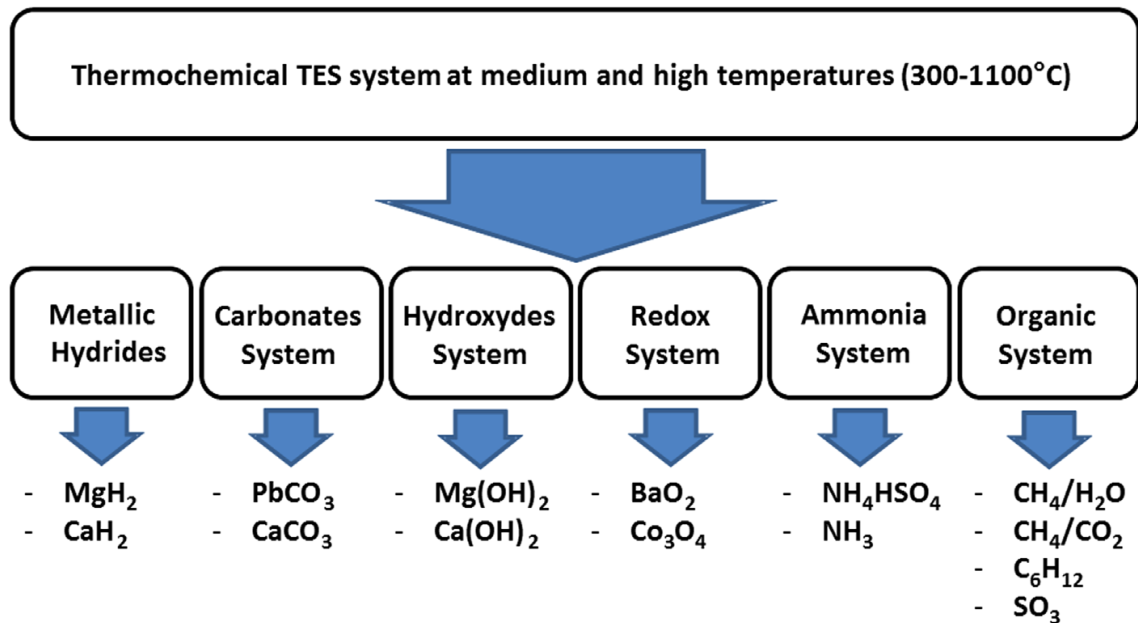


Figure 7: list of feasible reaction for thermochemical storage at medium-high T [3].

Turning temperature T^* can be defined as the temperature at which the reaction rate constant K is equal to 1; T^* can be approximated as:

Equation 5

$$T^* = \Delta H_r / \Delta S_r$$

Turning temperature can be useful to understand the temperature at which both the endothermic and exothermic reactions can be carried out.

In figure 8 is shown a comparison between many chemical species about their volumetric and mass energy density in relation to their turning temperature.

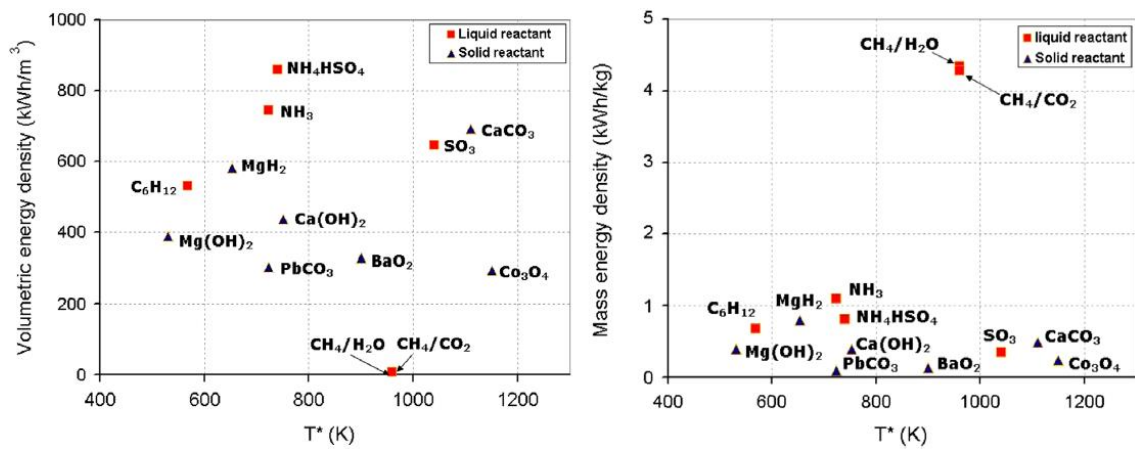


Figure 8: volumetric (a) and mass (b) energy density vs turning temperature for some reversible reactions [3].

The procedure needed to find a chemical loop suitable for a thermochemical storage usually start with the study of the chemical characteristics of the system: reversibility of the reaction, rate of reaction, operating conditions (p and T) and kinetic properties. Then other useful criteria that has to be followed to find the best candidate for TES applications are proposed by Wentworth and Chen [12]:

- The endothermic reaction used for heat storage should occur at a temperature lower than 1273 K
- The exothermic reaction used to recover heat should occur at a temperature higher than 773 K.
- Large enthalpies of reaction and a product of small molar volume are required to maximize the storage capacity (500 kWhm⁻³).

- Both reactions should be completely reversible, with no side reactions, and have high yields in order to use the materials over a long period of time.
- Both reactions should be fast enough so that the absorption of solar energy and heat release can be carried out rapidly.
- The chemical compounds of both reactions should be easily handleable.
- When stored, the chemical compounds should not react with their environment.
- Experiment feedback on the reaction is required to use a well- known chemical process.
- Low costs should be required.

In the field of TES system many of the solutions described in literature are only tested on laboratory scale until now. Pardo et al, in their work [4], report that in the range of temperature 573-1273 K the most promising chemical reactions because of the actual related development and cost are the following:

- $MgH_2 \leftrightarrow Mg + H_2$;
- $PbCO_3 \leftrightarrow PbO + CO_2$;
- $Ca(OH)_2 \leftrightarrow CaO + H_2O$;
- $NH_3 \leftrightarrow N_2 + H_2$;

Between them the ammonia dissociation and synthesis is the most mature technology for high temperature as it can relate on already 40 years of research and tests. The dehydration/hydration of the calcium hydroxide and the calcium oxide couple shows a high potential for TES applications but there is the need of further studies and tests.

In Figure 9 is shown a list with a comparison between the main characteristics of the chemical compounds studied by Pardo et al for the TES purpose [4]:

Reaction	Phase	Reaction enthalpy (kJ/mol _r)	Operating temperature conditions	Energetic density	Related works	Technology
Hydride system $MgH_2 + \Delta H_r \Leftrightarrow Mg + H_2$	Solid-gas	$\Delta H_r = 75$ kJ/mol	Heat Charge: 653 K Heat release: 503 K	- 580 kWh/m ³ _{MgH₂} - 0.80 kWh/kg _{MgH₂}	- Kinetic study - Reversibility study - Reactor design - heat exchanger design - Review	- Steam generator (3.6 kWh) - Packed bed reactor - Solar power station - Solar cooking and cooling device - Heat exchanger
Carbonate system $PbCO_3 + \Delta H_r \Leftrightarrow PbO + CO_2$	Solid-gas	$\Delta H_r = 88$ kJ/mol	- Heat charge: 723 K - Heat Release: 573 K	- 303 kWh/m ³ _{PbCO₃} - 0.09 kWh/kg	- Equilibrium relationship - Kinetics study	- TGA (thermogravimetric analysis)
$CaCO_3 + \Delta H_r \Leftrightarrow CaO + CO_2$	Solid-gas	$\Delta H_r = 178$ kJ/mol	- Heat charge: 1133 K - Heat release: 1153	- 692 kWh/m ³ _{CaCO₃} - 0.49 kWh/kg _{CaCO₃}	- Reversibility - Reactivity - Reactor design - Decarbonation reactor - CO ₂ capture - Review	- TGA - Fluidised bed reactor - Packed bed reactor - Chemical heat pump - Horizontal rotary reactor
Hydroxide system $Mg(OH)_2 + \Delta H_r \Leftrightarrow MgO + H_2O$	Solid-gas	$\Delta H_r = 81$ kJ/mol	- Heat charge: 423 K - Heat release: 373 K	- 388 kWh/m ³ _{Mg(OH)₂} - 0.39 kWh/kg _{Mg(OH)₂}	- Equilibrium relationship - Kinetic study - Reversibility - Reactor design	- TGA - Packed bed reactor - Chemical heat pump
$Ca(OH)_2 + \Delta H_r \Leftrightarrow CaO + H_2O$	Solid-gas	$\Delta H_r = 104$ kJ/mol	- Heat charge: 723 K - Heat release: 298–673 K	- 437 kWh/m ³ _{Ca(OH)₂} - 0.39 kWh/kg _{Ca(OH)₂}	- Equilibrium relationship - Kinetic study - Reversibility - Reactor design - Simulation - Heat transfer enhancement - Cost analysis	- TGA - Packed bed reactor - Chemical heat pump
Ammonium system $NH_4HSO_4 + \Delta H_r \Leftrightarrow NH_3 + H_2O + SO_3$	Liquid-gas	$\Delta H_r = 336$ kJ/mol	- Heat charge: 1200 K - Heat release: 700 K	- 860 kWh/m ³ _{NH₄HSO₄} - 0.81 kWh/kg _{NH₄HSO₄}	- Theoretical analysis - Thermodynamics analysis - Process simulation	[-]
$2NH_3(g) + \Delta H_r \Leftrightarrow N_2(g) + 2H_2(g)$	Gas	ΔH_r Heat Charge = 66.9 kJ/mol ΔH_r Heat Release = 53 kJ/mol	Heat charge: 723 K; P=9–150 bar Heat release: 723 K; P=10–300 bar	745 kWh/m ³ _{NH₃(l)} 1.09 kWh/kg _{NH₃(l)}	- Kinetic study - Process simulation - Technical and economical feasibility study - Reactor design study - Ammonia receiver design	- 1 kW _{chem.} Laboratory-scale ammonia dissociation and synthesis reactor - 10 kW _{chem.} Laboratory-scale ammonia dissociation and synthesis reactor - Ammonia receiver design for a 500 m ² dish
REDOX system $2Co_3O_4 + \Delta H_r \Leftrightarrow 6CoO + O_2$	Solid-gas	$\Delta H_r = 205$ kJ/mol	T=1143–1173 K	- 295 kWh/m ³ _{Co₃O₄} - 0.24 kWh/kg _{Co₃O₄}	- Equilibrium analysis - Kinetic study - Mixed oxide reaction - Thermodynamic analysis	- TGA - Packed bed reactor
$2BaO_2 + \Delta H_r \Leftrightarrow 2BaO + O_2$	Solid-gas	$\Delta H_r = 77$ kJ/mol	T=963–1053 K	- 328 kWh/m ³ _{Ba₂O₂} - 0.13 kWh/kg _{Ba₂O₂}	- Equilibrium analysis - Kinetic study	- TGA
Organic system $CH_4 + H_2O + \Delta H_r \Leftrightarrow 3H_2 + CO$	Gas	250 kJ/mol	- Heat charge: 1223 K - Heat release: 803 K	- 7.8 kWh/m ³ _{CH₄(g)} - 4.34 kg/kg _{CH₄(g)}	- Process simulation - Reactor design - Kinetic study - Energy transport	- Laboratory pilot plant - Industrial size pilot plant 300 kW _{transported} (EVA I/ADAM I)
$CH_4 + CO_2 + \Delta H_r \Leftrightarrow 2H_2 + 2CO$	Gas	247 kJ/mol	- Heat charge: 1223 K - Heat release: 803 K	- 7.7 kWh/m ³ _{CH₄(g)} - 4.28 kg/kg _{CH₄(g)}	- Technical and economical feasibility study - Reactor design - Energy transport	- Design of the receiver reactor 200–300 kW (DLR)
$C_6H_{12} + \Delta H_r \Leftrightarrow C_6H_6 + 3H_2$	Liquid-gas	$\Delta H_r = 206.7$ kJ/mol	Heat charge: T=590 K Heat release: T=670 K	530 kWh/m ³ _{C₆H₁₂(l)} 0.68 kWh/kg _{C₆H₁₂(l)}	- Process simulation analysis in chemical heat pump	[-]
SO₃ system $2SO_3 + \Delta H_r \Leftrightarrow 2SO_2 + O_2$	Liquid-Gas	$\Delta H_r = 98$ kJ/mol	Heat charge: 1073–1273 K Heat release: 773–873 K	646 kWh/m ³ _{O₃(l)} 0.34 kWh/kg _{O₃(l)}	- Process analysis to produce a continuous 100 MW electric power output	[-]

Figure 9: main information about different TES chemical systems [4]

2. Calcium Hydroxide Chemical Looping

2.1. Ca(OH)₂ / CaO Main Information

Calcium hydroxide is a strong base chemical which look like a white odourless powder. Its molecular weight is 74.08 g/mol. It has a low solubility in water that goes down further for high temperatures[13].

In the industrial field has a wide range of application from petrochemical, food and building industry to the pharmaceutical one. The interest for this molecule in the energy field is due to the reversible chemical reaction which can be exploited to store energy. If this molecule is heated up over a certain temperature, that depend on the steam partial pressure of the environment, its thermal decomposition in calcium oxide and water is obtained by means of an endothermic reaction. On the other side the resulting calcium oxide can react with water or steam by means of an exothermic reaction. The stoichiometric reaction is the following:



Where the absolute value of the heat of reaction at a temperature of 505 °C and 1 bar steam partial pressure is about 104.4 kJ/mol[14], figure 10.

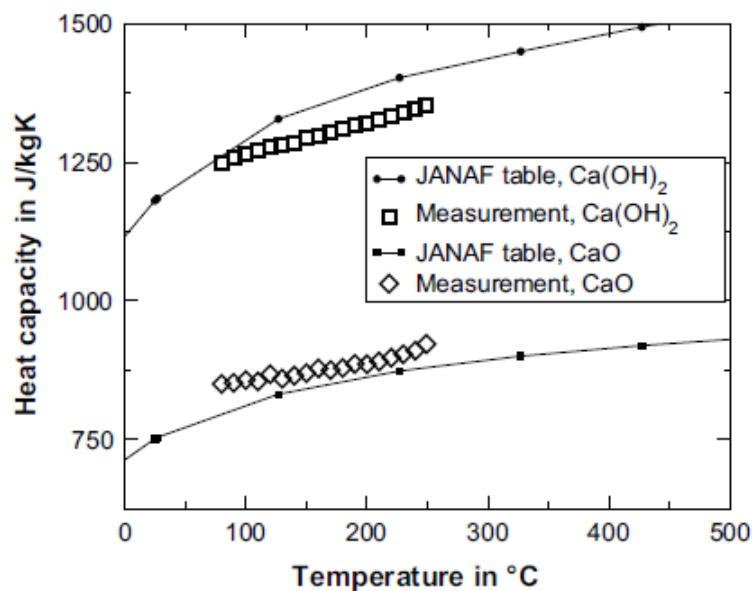


Figure 10: Pure CaO and Ca(OH)₂ heat capacity [14].

Calcium oxide has a molar weight of 56.08 g/mol and it is also a widely used chemical in many fields like agricultural, building and food industry. Its industrial production is done starting from calcium carbonate by calcination at high temperature with side production of carbon dioxide.

The data about the heat capacity of the two molecules is made experimentally by Schaube et al [14] and it is compared with the results reported by JANAF, figure 10. Calcium hydroxide shows a higher heat capacity in respect to its oxide with a slightly divergent behaviour for increasing temperatures. The calcium hydroxide shows, in the temperature range of interest, a not negligible increment of heat capacity for increasing temperature. Furthermore the $\text{Ca}(\text{OH})_2$ molar heat capacity is higher than the one of the calcium oxide and so, for a constant molar flow, a higher concentration of the calcium hydroxide means a higher amount of energy needed to preheat the stream.

Figure 11 shows the absolute value of the heat of reaction related to the CaO hydration/ $\text{Ca}(\text{OH})_2$ dehydration as a function of temperature. The graph is obtained for ambient pressure.

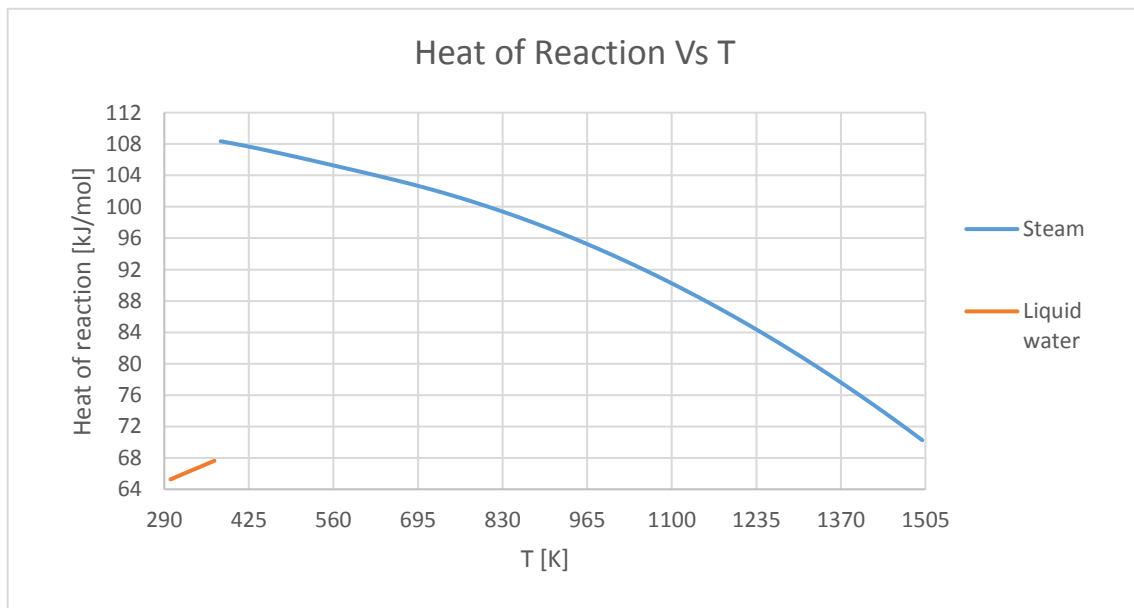


Figure 11: enthalpy of reaction vs temperature.

The orange curve is for temperature lower than the 100 °C so is related to liquid water. For this part of the chart the behaviour is quite linear and there is an increment with temperature.

The blue curve is related to temperature higher than 100 °C and so is referred to steam. In this case there is a decreasing trend for increasing temperatures.

For higher or lower pressure the orange curve will cover respectively a bigger or a lower range of temperature following the variation of the water evaporation temperature and showing always a linear trend.

The energy gap between the heat of reaction with liquid water and steam at 100 °C is the same as the heat of evaporation of water (40.8 kJ/mol).

For a TES system point of view the heat of reaction trend is not the best one as the best way to exploit the material characteristics would be a charge step at very high temperature and a discharge step at low temperature.

Calcium hydroxide is also a non-toxic cheap material and among metal hydroxides is the one that shows the highest enthalpy of dehydration and also the highest gravimetric energy density [15].

This material and its counterpart, CaO, have been already studied for energy applications like chemical heat pumps [16], preheating of engines [17], self-heating foods [18], and even power generation on the moon [19].

There are many preliminary studies about the exploitation of these molecules for TES application; the main advantages and drawbacks linked to them can be summarized as made in figure 12.

Advantages	Drawbacks
<ul style="list-style-type: none"> • No catalyst ++ • Material energy density (Experimental: 300 kWh m⁻³) +++ • Reversibility of the reaction (~100 cycles) ++ • No by-product ++ • Product separation (gas-solid) ++ • Operating pressure (1 bar) +++ • Availability and price of the product ++ • Nontoxic product + • Experimental feedback (10 years) + 	<ul style="list-style-type: none"> • Agglomeration and sintering ■■ • Change of volume (95%) ■ • Low conductivity ■

Figure 12: main advantages and drawbacks of Ca(OH)₂/CaO chemical looping [4].

2.2. Ca(OH)₂ Dehydration / CaO Hydration Reactions Kinetics

The first things that has to be taken into account when studying the reaction behavior is the equilibrium curve that shows the couple of steam partial pressure and temperature values for which the equilibrium between the reactant and the product is reached.

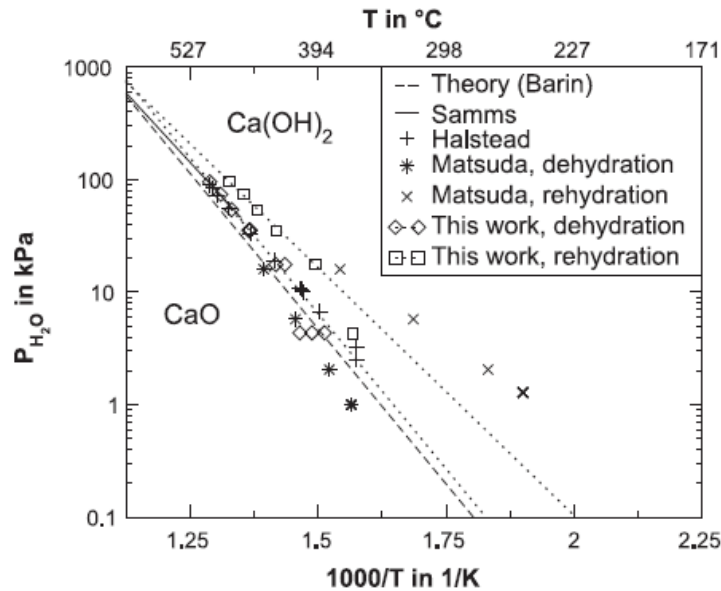


Figure 13: log-scale plot of the reaction equilibrium curve from different works

From figure 13 we can see that the reaction at a steam partial pressure of 1 atmosphere the equilibrium curve is around 520 °C. At this pressure the dehydration reaction occurs for temperatures higher than the equilibrium while the hydration reaction is favored for lower temperatures.

From a thermochemical energy storage point of view is obvious that the lower the charging step temperature the more convenient the process. On the other side the performance of the discharging step is higher for a higher temperature of the process.

Criado et al.[20] studied the effect of temperature between 400 and 560 °C and steam partial pressure between 0 and 100 kPa both for hydration and dehydration reactions having as results a good fitting with a shrinking core model. The total pressure is maintained at ambient level providing air as fluidizing gas. Their studies are focused on conditions that can be matched with fluidized bed reactors.

As can be seen in figure 14, the result of their studies shows a quite fast rate of reaction and resulting conversion for both hydration and dehydration process.

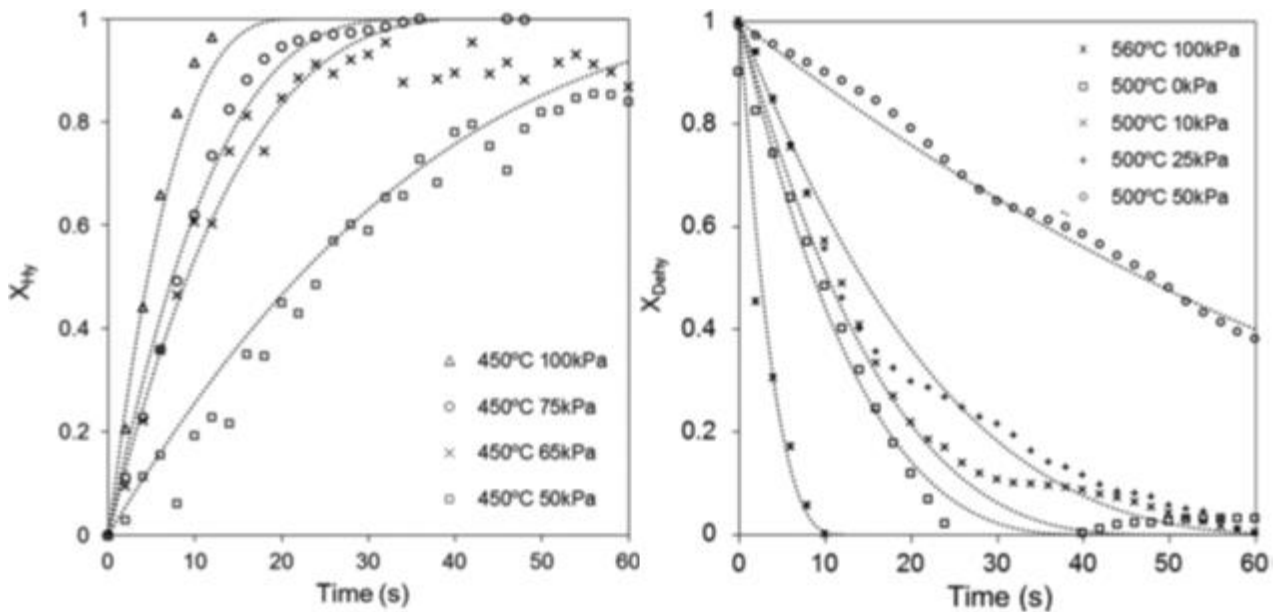


Figure 14: Hydration conversion vs time (left), Dehydration conversion vs time (right) [20].

The complete conversion of the active material during the hydration and dehydration steps are in the order of 10 to 60 s. At constant temperature the dehydration is faster for lower steam partial pressure. The dehydration rate of reaction is also faster for higher temperature at the same level of steam partial pressure.

For the hydration the rate of reaction behavior is the opposite, compared to dehydration, in respect to the partial pressure at constant temperature as for higher partial pressure the rate of reaction is higher.

The starting raw materials are the Compostilla and Imeco limestones, also called calcium carbonate, at different purity grade that are used to produce calcium oxide by calcination at 800 °C. to see the influence of the particle size on the reactions' behavior the authors made tests for four different particle sizes: 100-200 μm , 400-600 μm , 800-1000 μm , 1-2 mm.

Figure 15 shows the conversion reached by the different particle size samples after many cycles of consequent hydration and dehydration reactions.

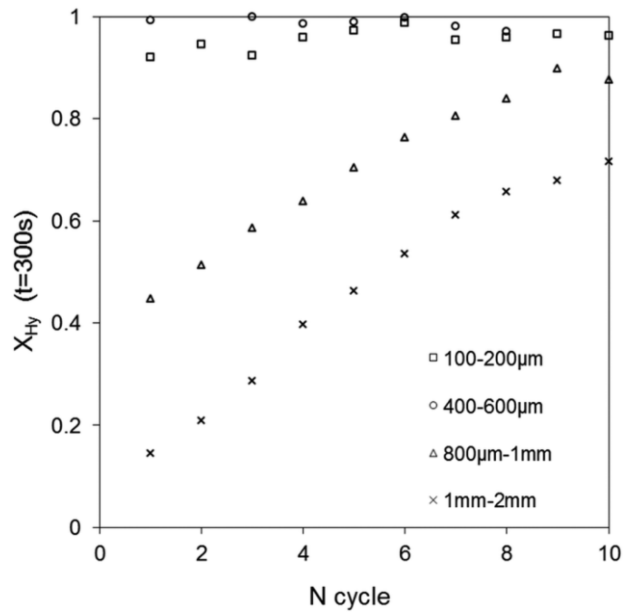


Figure 15: dehydration cycles and reached conversion at specified time [20].

As can be seen the sample of lower particle size reaches higher conversion for a few cycles while the samples with higher particle size need more time to reach the total conversion for a few numbers of cycles.

The observed behaviour is in accordance with the shrinking core model as the available surface is inversely proportional to the particle size and for a low available surface, bigger particles, only a reduced amount of the material can react with the steam during the hydration step. The increment of the conversion for an increasing number of hydration/dehydration cycles is related to the particle breakage that facilitates the diffusion of steam through the particle cracks and makes more CaO surface available for the reaction with steam. The consequence of the particle breakage is also the reduction of the particle size but at the same time reduce the particle size that can be a drawback as lower particle size are more difficult to be fluidized in FB reactor.

An interesting study is the one by Wang et al. [21] on the effect of higher than atmospheric steam partial pressure on CaO hydration reaction. From this study it can be assumed that for a certain temperature a higher difference between the steam partial pressure and the equilibrium one improves the reaction rate of the CaO hydration. This study also shows the influence that the porosity and the specific surface of the raw material have on the reaction's dynamics.

The samples used in the study have an equivalent particle diameter between 250 and 500 μm and belong to four different Ca-based sorbent that show different properties in respect to porosity and specific surface. Between the different samples the one with higher porosity and

specific surface has also the highest rate of reaction. This behaviour can be explained by the fact that during the reaction steam can reach easily the pores by diffusion but when all the external surfaces are already reacted to form calcium hydroxide the hydration process is slowed down due to the calcium hydroxides pores obstruction.

A study by Lin et al. [22] on the cyclical calcium hydroxide thermal decomposition and calcium oxide hydration show that both the molecules also after many cycles reach a complete conversion. In the case of calcium oxide hydration, the rate of reaction decreased with increasing number of cycles. Instead the calcium hydroxide dehydration rate of reaction seems to be not influenced by the increments of the cycle's number. In any case, as also reported by other authors, the chemical looping of calcium oxide and calcium hydroxide show a good reversibility and also a good rate of reaction that make their exploitation compatible with the requirement of a TES system.

3. Calcium Hydroxide TES System

3.1. Reactor Choice

The reversible reactions involved in the process are related to solid-gas chemical interactions. In this kind of process mass and heat transfer are determinant in order to have a fast and extensive reaction rate in a big plant size.

Fixed bed reactors, that are one of the most common reactor types available on the market and in many studies have been taken into account for this kind of application, show some important limitations mostly for their application at large scale level. One of the main drawbacks is the modest heat transfer capacity related to stationary solids that means a very large network of heat exchanger surface to manage the heat duty of a large-scale plant. Moreover, in a fixed bed reactor, the pressure drop would be very high in order to reach the required level of contact between solids particles and reacting gases [20].

As reported by Pardo et al. [23] other common available technologies for this kind of application are:

- Fluidized bed
- Free fall bed
- Rotary kiln
- Screw extruder

Rotary kiln and screw extruder show a complex operation behaviour, due to the needed mechanical system for the reactor rotation, other than a poor heat exchange between particles and reactor walls.

The free fall bed reactor could be an interesting solution, mainly for the dehydration step, in order to have a direct integration with a solar receiver as this kind of technology is already used for solar receiver in CSP applications. The main limitation linked to this technology is the too low residence time that are in the order of 1 to 10 seconds while the reaction times of calcium oxide hydration and calcium hydroxide dehydration, in order to reach a quite good reaction extent, are mainly above the minute [23].

For FB reactors the main drawbacks and advantages can be summarized as follows in figure 16.

Advantages	Drawbacks
<ul style="list-style-type: none"> - High heat transfer coefficient ($100\text{--}600\text{ W m}^{-2}\text{ K}^{-1}$) - High mass transfer coefficient between the solid and the gas - Heat exchanger/reactor experience feedback - Forward and backward reactions in the same reactor - Homogenous temperatures - Well-known industrial scale-up 	<ul style="list-style-type: none"> - Need of a fluidization gas - Particle attrition - Need of a separation unit - More expensive than a fixed bed reactor

Figure 16: FB reactor main features [23].

Considering the features offered by FB reactors, they seem to be best choice for this type of application.

In literature there are many references about the use of fluidized bed reactor as the best hypothesis for a TES system based on solid-gas reversible reaction [20],[24],[23],[25].

In the case of calcium hydroxide and calcium oxide the fluidized bed technology shows another drawbacks as these chemical species are in the group C of the Geldart classification [26]. This is related to the particle diameter of commercial calcium hydroxide that are generally close to 1-15 μm . This means that the fluidization of these particle is not easy to do since they appear as a very cohesive powder that during the fluidization process inside an FB reactor tend to create solid blocks instead of lending themselves to easy mixing. Furthermore, as reported before, the solid particles suffer a progressive fragmentation during consecutive hydration and dehydration cycles.

This problem can be overcome by the exploitation of different solutions [23]:

- Addition of an inert easy to fluidize particle (EFP);
- Addition of a fluidization additive (nanoparticles);
- Use of a mechanical agitation system;
- Use of vibration system;
- Shaping of the $\text{Ca}(\text{OH})_2$ on a support;

Mechanical agitation and vibration system introduce a higher level of complexity in the system and also an energy requirement to work.

The easiest solution is the addition of an inert EFP that consist in the introduction of large inert particles that behave as a mechanical agitator. The introduction of this inert material has two main drawbacks:

- EFP must be separated from the dehydration product to have a high energy density during the storage step;
- EFP sensible thermal energy must be recovered.

The separation of the EFP is the only way to keep a high storage energy density and it can be made at the outlet of the reactor in order to be recirculate the EFP to the reactor without being cooled down. In any case, if the storage is made at ambient temperature, the solid stream has to be cooled down before being stored and so there is however the need for a hex.

The study made by Pardo et al. [23] on this topic shows the best fluidization results for a mixture of Al_2O_3 70 % wt and 30% $\text{Ca}(\text{OH})_2$ wt. These values are indicative of how the EFP presence could affect storage energy density; the cited work, with EFP separation, evaluates energy density values of 60 kWh/m^3 without separation while EFP separation allows to reach energy density values of 156 kWh/m^3 .

A different solution is provided by the addition of a fluidization additive like nanoparticles; Roßkopf et al. [27] have investigated the exploitation of a small amount of SiO_2 (Aerosil) as additive to minimize channelling effect and also to enhance the cycling stability of the system.

The shaping on a support like pelletizing is really complex as the material undergoes a big volume change during the reaction that will means the breakage of the pellet.

3.2. Reference layout

The simulation of the $\text{CaO}/\text{Ca}(\text{OH})_2$ chemical looping at system level as thermochemical storage is made using the ASPEN PLUS V8.8 software. The conceptual process design [24] defined by Criado et al., shown in figure 17, is taken into account to define the reference layout for the Aspen model.

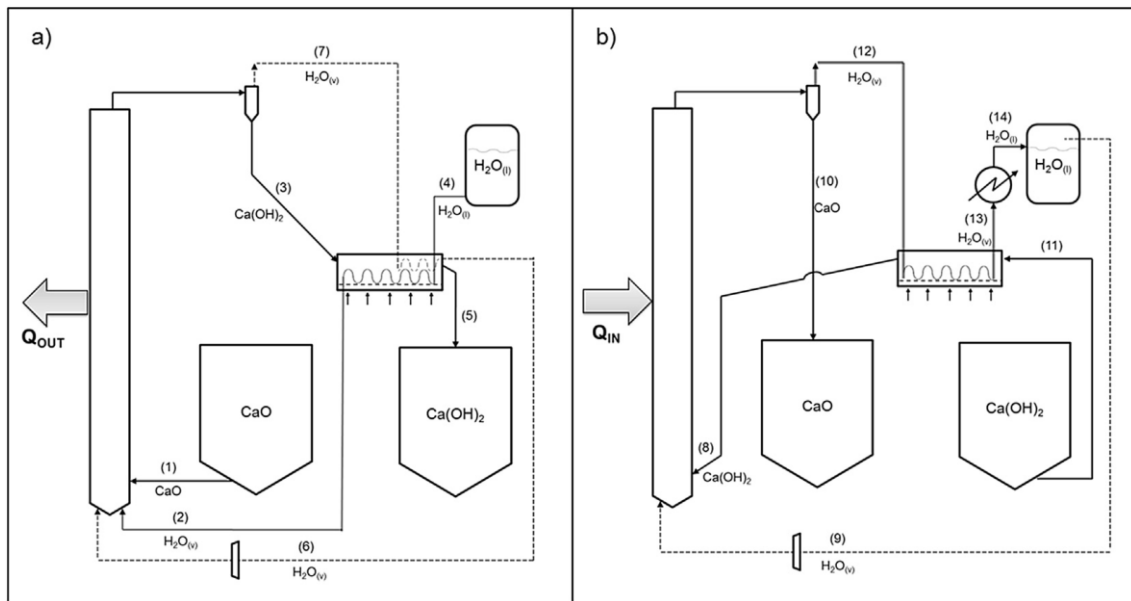


Figure 17: CaO hydration/dehydration conceptual process design [24].

Their study is focused on the definition of a layout for a large-scale energy storage system based on $\text{CaO}/\text{Ca}(\text{OH})_2$ reversible reactions. Their suggestion is to use the same reactor both for hydration and dehydration process in order to reduce the costs of the plant. This choice is justified if the charge and discharge process only happen, as they assumed, at different times. FB is the chosen reactor technology and it is made taking account of the solution available on the market and of the requirements of the system.

The storage of solids after the hydration step and the water storage after both the process are done at low temperature (about 373 K and liquid state for water) while the storage of the dehydration step is made at high temperature (same T of the dehydration reactor 813 K). As dehydration is the charging step of the chemical loop then the energy storage process is based both on chemical and sensible heat.

Their suggestion to recover waste heat in the plant is the exploitation of FBHX (fluidised bed heat exchanger) with a small flow of air to fluidize the HEX beds.

The operating conditions provided by [24], for both hydration and dehydration, are assumed to be at atmospheric pressure for the sake of simplicity and for similarity to already existing large scale thermal fluidized bed like circulating fluidized bed combustors (CFBCs). Atmospheric pressure for large scale application also means a high volumetric gas flow in the reactor and so; for this reason, the best FB reactor design seems to be the circulating one because they can be easily coupled with standard solid circulation elements like risers, cyclones, stand pipes, loop seals, etc.

Both hydration and dehydration steps are carried out using steam as fluidizing agent also if using steam as fluidizing agent in the dehydration is not the best choice as the steam presence shift the equilibrium of the reaction to the reactant side. While for the dehydration step the purpose of the steam is only the fluidization, for the hydration step the inlet flow of steam has to be enough also to fulfil the reaction needs in terms of chemical conversion. The calculated amount of steam needed to fluidize the hydration bed reactor is represented, in the reference case, by an excess of 50% in respect to the reaction stoichiometric value.

The reactor temperatures choice is made on the basis of the equilibrium thermochemical data provided by Barin [28]:

Equation 6

$$P_{eq} = 2.30 * 10^8 * e^{(-11607/T)}$$

Where P_{eq} is the equilibrium pressure of steam in kPa and T is the temperature in Kelvin. With this data the maximum operating temperature for hydration at a steam pressure of 1 atmospheres is 792 K.

Their suggestion on the hydration temperature choice is to remain in the range 700 to 750 K. As reference case they chose a temperature of 743 K for which they measured a rate of reaction consistently higher than $1.3 * 10^{-2}$ [s⁻¹] for an average particle size of $dp = 0.25$ mm[20]. The dehydration temperature, 813 K, is taken to have a rate of reaction of the same order ($1.6 * 10^{-2}$ [s⁻¹]) of the one occurring during the hydration step.

The conceptual design they have defined is built to provide a thermal output during the hydration process of 100 MW calculated as:

Equation 7

$$Q_{out} = (\Delta H_{743K} * F_{CaHy} * \Delta X) + (Q_1 + Q_2 + Q_6) - (Q_3 + Q_7) \text{ [kW]}$$

Where Q_i represent the sensible heat of the streams, ΔH_{743K} is the reaction enthalpy at 743 K, ΔX is the increment in conversion and F_{CaHy} is the molar flow of calcium.

ΔX , that is defined as the difference between the average value of the conversion of hydration and dehydration, is calculated as:

Equation 8

$$\Delta X = X_{ave Hy} - X_{ave Dehy} \text{ [-]}$$

For the reference case ΔX is 0.6. The average conversion is calculated as:

Equation 9

$$X_{ave} = \int_0^{\infty} (X(t)) * ((1/\tau) * \exp(-t/\tau)) * dt \text{ [-]}$$

Where τ is the average particle residence time and $X(t)$ is the conversion as function of time that can be written as described by equations 10 and 11.

Equation 10

$$X_{Hy}(t) = 1 - (1 - t * k_{Hy})^3 \text{ [-]}$$

Equation 11

$$X_{Dehy}(t) = (1 - t * k_{Dehy})^3 \text{ [-]}$$

The conversion values are calculated assuming a shrinking core model[29] and the already mentioned rate of reactions. Previous equation are valid only for $t < t^*$ that is the time needed to reach the complete conversion. After t^* the conversion as function of time is equal to zero

for dehydration and equal to 1 for hydration. Time t^* can be calculated as function of active fraction of Ca material f_a and τ as:

Equation 12

$$t^* = -\tau * \ln(1 - f_a) \quad [s]$$

The average residence time can be calculated as a function of the solids inventory W , the reactor free cross-sectional area A_{bed} , the total flow of calcium moles F_{Ca} that enters the reactor in each operation mode, the moles of inert material present in the solids per moles of Ca f_{inert} , and the molar mass of M the whole inlet flow:

Equation 13

$$\tau = \frac{(W * A_{bed})}{(F_{Ca} * (1 + f_{inert}) * M)} \quad [s]$$

Typical value for the solid inventory are between 100 and 1000 kg/m² with a typical range of solids circulating flow rates of 0.5 to 30 kg/(m²s) [30],[31]. f_{inert} is related to the necessity to have a certain fraction of inert material, like an inorganic binder or a stable porous support, to ensure the mechanical stability of the CaO/Ca(OH)₂ as natural CaO particles are known to be friable. The characterization of the inert material is not carried forward and f_{inert} is set to zero. To compensate the previous choice the authors have settled the conversion increment to a low value, their suggestion is to have $\Delta X = 0.6$.

To reach this value of increment in conversion they settled a solid inventory of 443 kg/m² for hydration and 373 kg/m² for dehydration with a cross sectional area of 34.4 m² and a residence time of 120 s for both the processes. For the reference case the gas velocity during hydration is between 5 m/s at the inlet and 1.7 m/s at the outlet, with a steam excess of 50% in respect to the stoichiometric value, while for dehydration the inlet velocity is 1.7 m/s and the exit velocity is 3.9 m/s. With these data the solids circulation flows are between 3.1 and 3.7 kg/sm², values that are in the typical range of other CFB reactors using similar material. These data are shown in figure 18 and are the streams specifications obtained by the papers' authors for the reference case of hydration.

Stream N°	(1)	(2)	(3)	(4)	(5)	(6)	(7)
m (kg/s)	106.9	20.1	127.0	20.1	127.0	17.3	17.3
<i>Composition (wt%)</i>							
CaO	90.0		26.5		26.5		
Ca(OH) ₂	10.0		73.5		73.5		
H ₂ O		100		100		100	100
T (K)	813	743	743	373	393	393	743
Q (MW _t)	55.1	19.1	77.2	6.7	15.6	3.4	16.7

Figure 18: hydration reference case streams specifications [24].

Figure 19 is instead referred to the dehydration streams specifications.

Stream N°	(8)	(9)	(10)	(11)	(12)	(13)	(14)
m (kg/s)	127.0	15.8	106.9	127.0	35.9	35.9	35.9
<i>Composition (wt%)</i>							
CaO	26.5		90.0	26.5			
Ca(OH) ₂	73.5		10.0	73.5			
H ₂ O		100			100	100	100
T (K)	597	373	813	393	813	413	373
Q (MW _t)	50.2	2.5	55.1	18.7	40.0	8.5	9.2

Figure 19: dehydration reference case streams specifications [24].

The data shown in figure 18 and 19 are rereferred to the layout in figure 17. The data about Q in MW_t are related only to the sensible heat of the streams and are taken by the author from literature [32], [28] with a reference temperature of 298 K [24].

In the proposed reference case the molar amount of CaO that is hydrated during the discharging step is around 65% while the molar amount of Ca(OH)₂ that is being dehydrated during the charging step is around 88.5%. These conversion values are only indicative, due to the fact that are only supposition based on study made at lab scale in conditions that maybe are not the best ones for a comparison with a large-scale system equipped with FB reactors. With the previous data and assumptions, the paper shows that the system thermal efficiency can be calculated with equation 14.

Equation 14

$$\eta_P = [(Q_{out} * t_{op,Hy}) / (Q_{in} * t_{op,Dehy})] * 100 \quad [\%]$$

The thermal efficiency obtained with the same operational time for charging and discharging steps is around 63% as the thermal input Q_{in} needed by the system is of 158.7 MW_{th} where only 116.2 MW_{th} are needed to run the dehydration while the remaining amount is needed to preheat the reactants.

Moreover, they have evaluated the effective energy storage density of the system by means of the following equation:

Equation 15

$$ESD_{eff} = \frac{Q_{out}}{\left(F_{CaHy} * (1 + f_{inert}) * \frac{M_{Hy}}{\rho_s} * 3.6 \right)} \left[\frac{kWh}{m^3} \right]$$

The conceptual layout in the reference case shown in the paper is able to reach an $ESD_{eff} = 260 \left[\frac{kWh}{m^3} \right]$; this result is obtained with $f_{inert} = 0$ and taking into account both the energy stored chemically by the reaction and the enthalpy related to the sensible heat of the stored solids. The storage volumes calculated for an hour of charging and discharging process are of 384 and 457 m³ respectively for CaO and Ca(OH)₂ assuming a bulk solids density ρ_s of 1000 kg/m³. We can say that the volumetric storage density is of the same magnitude of the expected one ($\approx 500 \frac{kWh}{m^3}$) for this type of technology, but we have to remember that also the sensible heat has a role in this calculation and so on a long time base the ESD_{eff} would be lower.

Another interesting result that is reported in this paper is the study of ΔX influence on the reactor solid flow circulation. The analysis shows that could be possible to produce the same amount of Q_{out} also with ΔX lower than 0.1 if the solid circulation in the reactor can be maintained close to those of existing large-scale CFBs that use similar solids [30]. This means that also solids with a low activity could be allowed in practical design if combined with large storage volumes. The main energy drawback of having an higher flow of solids for the same power output is that the thermal power required for the charging process would be higher because there will be an higher amount of solids to be preheated.

3.3. Base Layout

3.3.1. Description

On the base of the previous streams data, and the reactor working condition chosen in the cited papers, this master thesis has been developed a similar conceptual design for a hydration/dehydration process at medium temperature to be coupled with CSP facility as energy storage. The model has been implemented in ASPEN PLUS. The development of this concept has evolved from a simpler integration obviating a real heat exchanger network to a final design.

This initial conceptual layout works with the assumption of distinct period of charge and of the same duration under the conceptual design approach previously mentioned. Steady state conditions were assumed, with same time of charge and discharge, and equality condition between the molar flow of the solid streams entering the hydration and the dehydration reactors. Mass flow of the streams depends on their composition that change as a function of the conversion reached in the reactors to fulfil the mass balance of the system.

The main differences with respect to the design proposed by the aforementioned papers [24] are related to the storage temperatures and to the heat exchangers network. The water and the product of both the discharge and charge steps are stored at a more likely ambient temperature (298 K) although other temperatures are possible. The first modification of the heat exchange network is related to the water recycling to the reactors that now do not take part in the heat exchange process and so are reinjected to the reactors at the same temperature as they left them. Furthermore, the temperature reached by the solids before entering the dehydration reactor is modified as now is the same as the reactor.

Then the temperature of the fresh water inlet to the hydration reactor is modified in order to reach the reactor temperature too. Furthermore, the water recirculation and the fresh water inlet to the hydration reactor are mixed before entering and only the water fraction that is not being recirculated to the dehydration reactor is condensed and stored at ambient temperature.

The heat sources and sinks are not defined and as first assumption any coupling is made between the system mass flows to recover energy.

Then the thermal efficiency of the storage system can be calculated as:

Equation 16

$$\eta_P = [abs(Q_{Hy}) * t_{op,Hy} / (Q_{Dehy} + Q_{Hex1} + Q_{Hex2} + Q_{Hex4}) * t_{op,Dehy}] * 100 \quad [-]$$

The resulting thermal efficiency in the reference condition is about 36.88%; this is a lower value compared to the one reported in the reference paper, but, the main reasons of this difference are linked to the absence of the heat exchanger network and so the heat needed to preheat the streams has to be taken from outside the system. For the dehydration step the source could be sun as it works when this source is available while hydration side should have a different heat source, but this is not fundamental to be defined as the simulation of the system without a pinch analysis is only to see and to study the heat needs of the system.

If we evaluate the ESD_{eff} in the same way as before, and with the same assumption on the storage density, we obtain a value of 313.66 kWh/m^3 for the reference case. This value is higher because Q_{out} is affected by the enthalpy of the inlet flows to the reactor that, for the different working condition, are higher.

Figure 20 shows the system layout of the base case that has been developed for this master thesis.

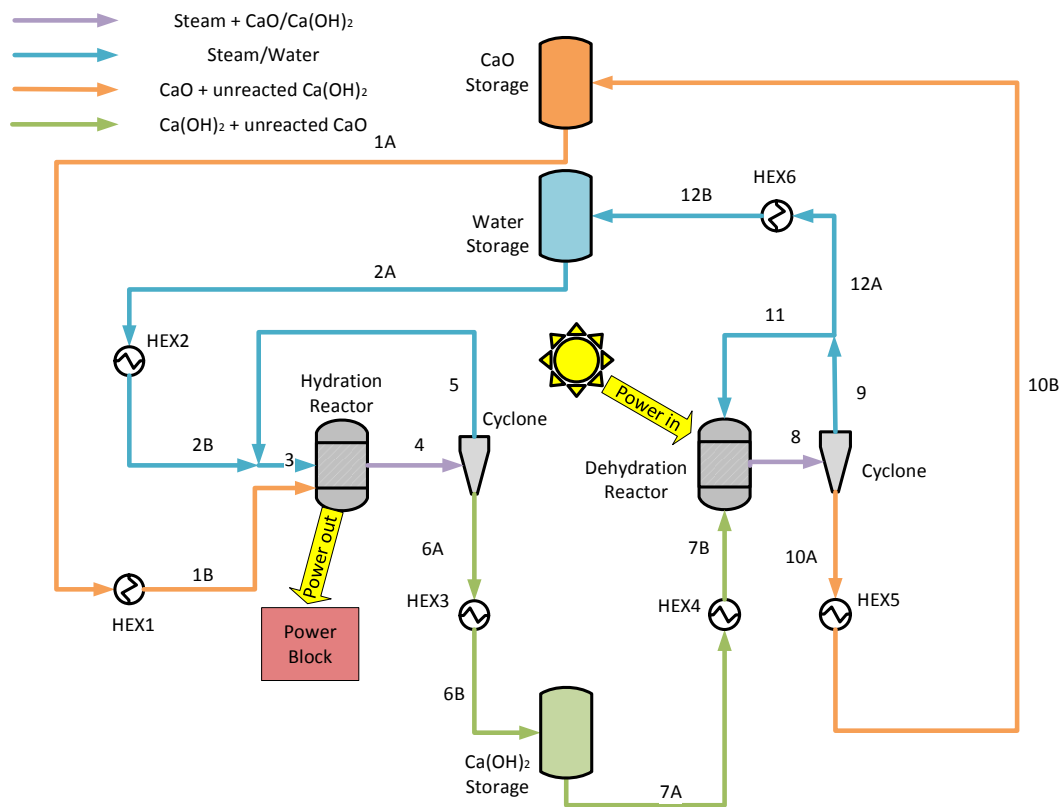


Figure 20: Base case system layout configuration.

In figure 20 we can see all the streams subdivided with different colours depending on which kind of substance are made of. In the layout are also included the storages of the solids and of the water needed by the process. Table 1 shows the main information about the reactors that are represented in figure 20.

Equipment name	Exchanged power	Pressure	T_{in}	T_{out}
[-]	[MW]	[bar]	[K]	[K]
HEX1	45,29	1,01	298	743
HEX2	66,71	1,01	298	743
HEX3	-71,38	1,01	743	298
HEX4	83,78	1,01	298	813
HEX5	-52,74	1,01	813	298
HEX6	-69,72	1,01	813	298
Hydration reactor	-113,26	1,01	743	743
Dehydration reactor	111,33	1,01	813	813
Water storage	0	1,01	298	298
CaO storage	0	1,01	298	298
Ca(OH)₂ storage	0	1,01	298	298

Table 1: figure 20 equipment characterization.

Table 2 shows the main data of the streams in figure 20.

Stream name	Total mass flow	CaO	Water	Ca(OH)₂	Temperature	Pressure
#	[kg/s]	[kg/s]	[kg/s]	[kg/s]	[K]	[bar]
1A	106,90	96,21	0,00	10,69	298,00	1,01
1B	106,90	96,21	0,00	10,69	743,00	1,01
2A	20,09	0,00	20,09	0,00	298,00	1,01
2B	20,09	0,00	20,09	0,00	743,00	1,01
3	37,38	0,00	37,38	0,00	743,00	1,01
4	144,28	33,67	17,29	93,32	743,00	1,01
6A	126,99	33,67	0,00	93,32	743,00	1,01
6B	126,99	33,67	0,00	93,32	298,00	1,01
5	17,29	0,00	17,29	0,00	743,00	1,01
7A	127,00	33,66	0,00	93,35	298,00	1,01
7B	127,00	33,66	0,00	93,35	813,00	1,01

Stream name	Total mass flow	CaO	Water	Ca(OH)2	Temperature	Pressure
#	[kg/s]	[kg/s]	[kg/s]	[kg/s]	[K]	[bar]
8	142,85	96,18	35,94	10,73	813,00	1,01
9	35,94	0,00	35,94	0,00	813,00	1,01
10A	106,91	96,18	0,00	10,73	813,00	1,01
10B	106,91	96,18	0,00	10,73	298,00	1,01
11	15,85	0,00	15,85	0,00	813,00	1,01
12A	20,09	0,00	20,09	0,00	813,00	1,01
12B	20,09	0,00	20,09	0,00	298,00	1,01

Table 2: Figure 20 streams characterizaton.

The data in tables 1 and 2 referred to streams and equipment are obtained with Aspen Plus and the boundary conditions and data mentioned above. All the system works at ambient pressure and so the reaction temperature of the two reactions are limited by this condition.

3.3.2. Parametric analysis 1

The system behaviour is therefore evaluated with a parametric analysis made varying the temperature and the conversion of both the hydration and dehydration reactions in order to cover ranges that are in the neighbourhood of the reference conditions.

This analysis is developed in order to identify how the proposed system works under different conditions. During the parametric analysis, as previously mentioned, the molar flows of solids that pass through the reactors are kept constant at the value extrapolated by the papers reference case. The resulting mass change in the streams, in respect to the reference case, are all in a range lower than $\pm 4\%$

Figure 21 shows the thermal efficiency of the storage system, calculated with equation 16, when the temperature and the conversion of hydration reaction are varied respectively between 700 and 760 K and between 0.5 and 0.7 while dehydration conditions are kept constant.

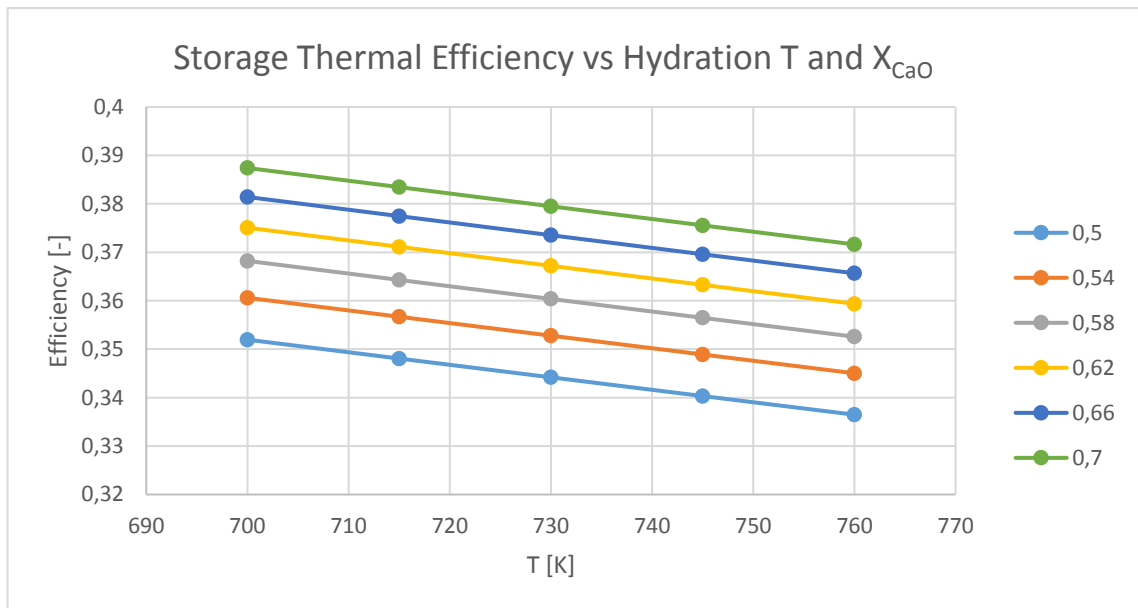


Figure 21: TES efficiency vs Hydration temperature and conversion.

As can be seen in figure 21, the efficiency shows an increment for higher conversion and lower temperature of the hydration reactor. The efficiency behaviour related to the temperature of hydration can be explained by the lower energy needed to heat up the reactant to the reactor temperature for lower temperature of reaction.

The efficiency variation related to the increment of the hydration temperature between 700 to 760 K is about -1.5 percentage points. The variation of the hydration conversion between 0.5

to 0.7 brings to an increment of about +3.5 percentage points. The conversion related behaviour can be explained as for higher conversion value at a fixed reaction temperature the energy released by the reaction is higher while the energy needed to heat up the reactant is almost constant.

Figure 22 shows the power output that the hydration reactor provides as a function of the temperature of reaction and the conversion of CaO.

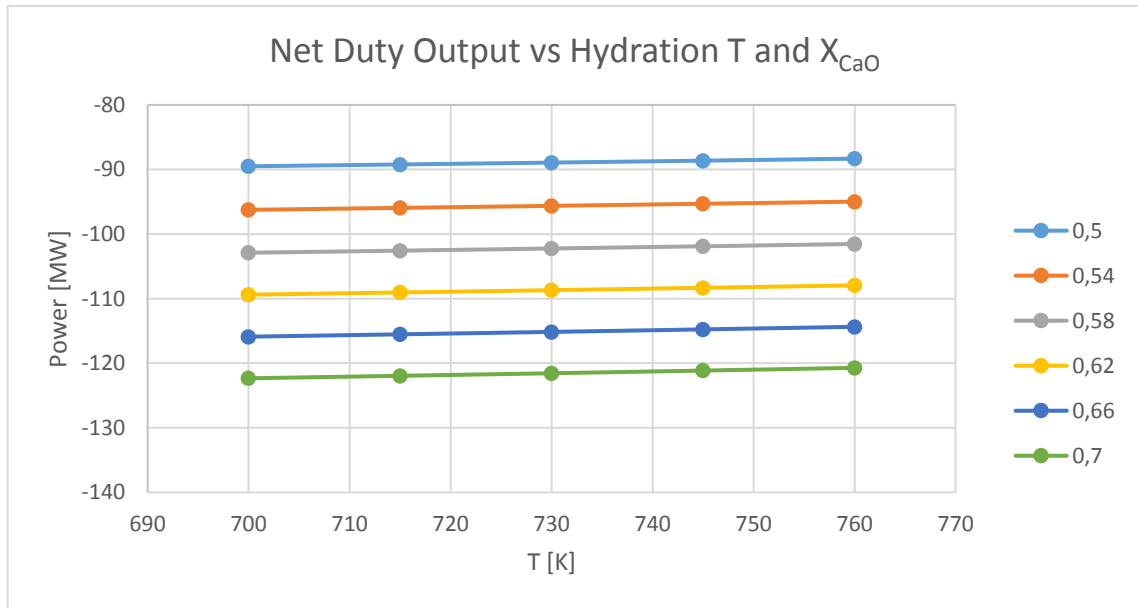


Figure 22: TES power output vs Hydration temperature and conversion.

In figure 22 the power output the hydration reactor is shown as negative in accordance to the first principle as it represents an output from the system. The power output trend is higher for lower temperature and higher conversion values. This behaviour is in accordance with the prevision as for higher conversion values the heat released has to be higher and as for higher temperature the reaction enthalpy is lower. The minimum value of power output is about -88.3 MW and is obtained for a conversion value of 0.5 and a temperature of 760 K. The highest value is obtained for a conversion of 0.7 and a temperature of 700 K and is about -122.3 MW.

In figure 23 is shown the relation between the power input to the TES system and both the conversion and the temperature of the hydration reaction.

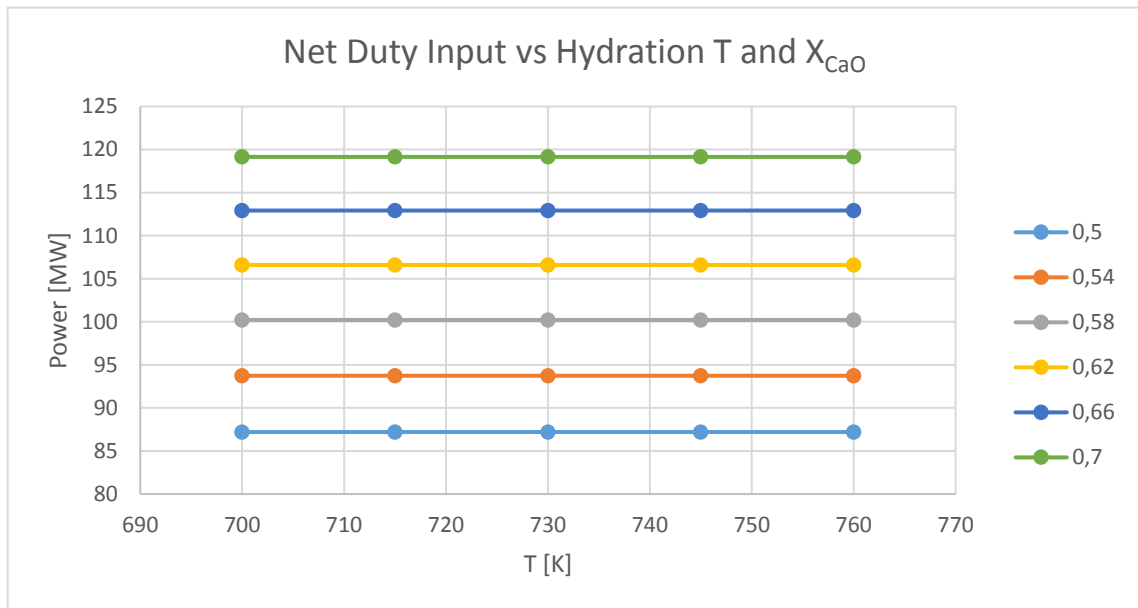


Figure 23: TES power input vs Hydration temperature and conversion

Figure 23 shows that only the conversion reached in the hydration reactor can have an influence on the dehydration net duty while hydration temperature is not important as the stream of solid that leave the hydration reactor is cooled at ambient condition before being stored and is then introduced in the dehydration reactor at the same reaction temperature.

Figure 24 shows the results of the same analysis made changing the value of X and T of the dehydration process. Here the temperature ranges between 800 and 860 K while the conversion of calcium hydroxide ranges between 0.75 to 0.95. Also in this case the parameters of the hydration reaction are kept constant at the reference levels.

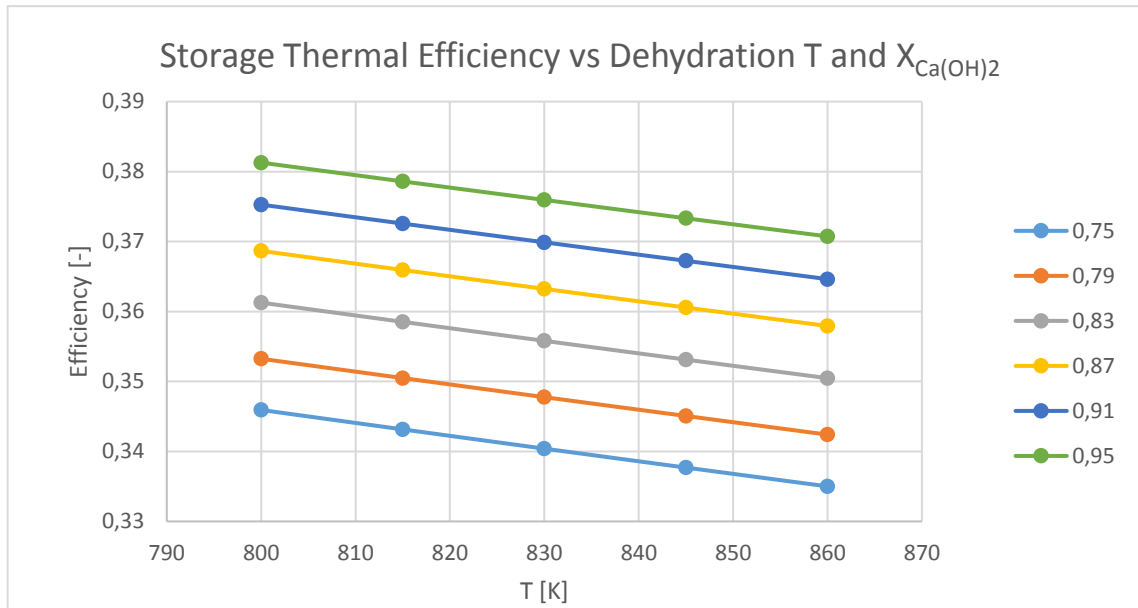


Figure 24: TES efficiency vs Dehydration temperature and conversion.

Figure 24 shows the dependency behaviour of the storage system thermal efficiency in respect to dehydration temperature and hydroxide conversion. As can be expected, the thermal efficiency reaches higher values for higher hydroxide dehydration conversion and for lower temperature of reaction. Lower temperature means lower preheating heat duty and so higher efficiency for a fixed conversion value.

Moreover, a higher dehydration conversion means higher amount of energy that can be stored at fixed temperature as the preheating duty remain almost the same. The dehydration temperature variation from 800 to 860 K brings to a decrement of the TES efficiency of about -1.1 percentage points while the increment of the dehydration conversion brings to an increment of about 1.5 percentage points.

Figure 25 shows the relation between the power input to the TES system and both the dehydration temperature and conversion.

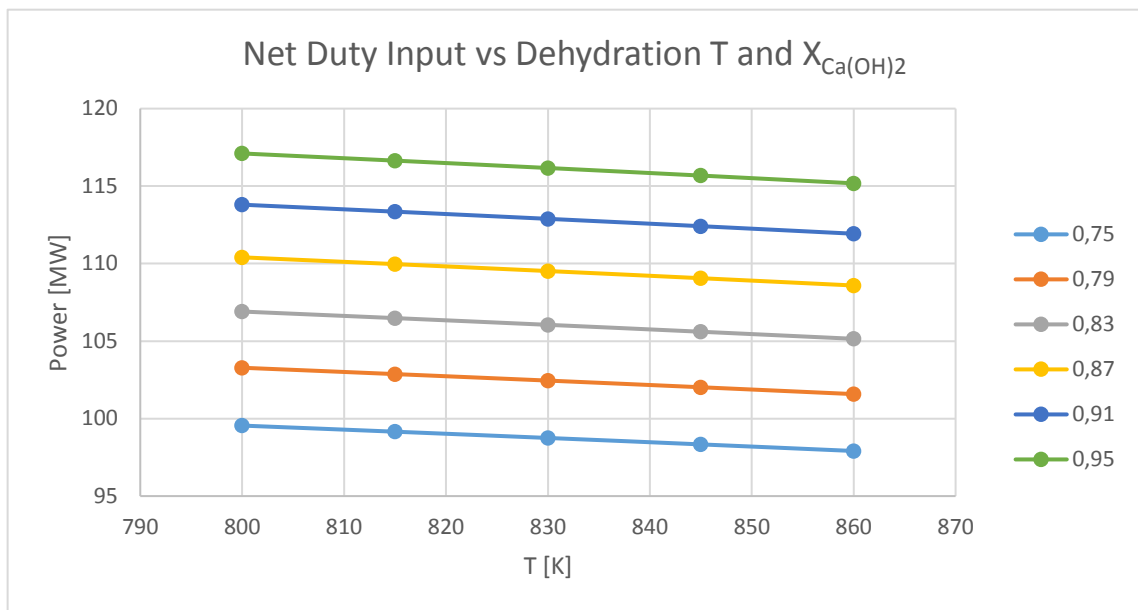


Figure 25: TES power input vs Dehydration temperature and conversion.

As can be seen in figure 25 the energy needs of the dehydration process are linked both to the temperature at which the reaction is run, as for high temperature the energy needs are lower due to the change in the enthalpy of reaction, and to the conversion, as higher conversion means more energy that can be stored. While the increment of the temperature brings to a decrement of the power input of few megawatts the increment in the conversion brings to an increment of about +17.5%.

Figure 26 is a confirmation that the temperature of the dehydration reactor doesn't affect the hydration reactor while higher hydroxide conversion means higher amount of energy that is stored and so that can be released.

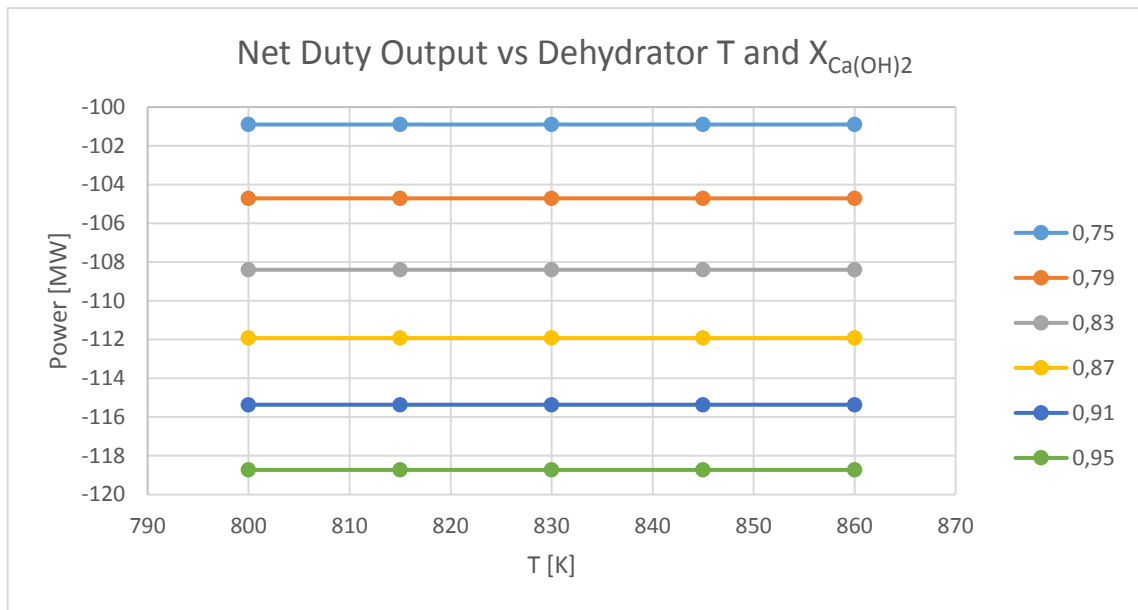


Figure 226: TES power output vs Dehydration temperature and conversion.

The previous results from the parametric analysis show mainly a linear behaviour; this is both correlated to the relatively simple reaction and also to the relatively simple structure of the system layout. While the dehydration temperature has no influence on the power output of the dehydration reactor a higher conversion in the dehydration reactor means also a higher power output of the hydration reactor. For the range of conversion reported in figure 26 the hydration power output shows a variation of about 18 MW that means a +18 % in respect to the lowest value.

3.3.3. Parametric analysis 2

Another potentially interesting parametric analysis that can be done on the base layout is to set a temperature in the two reactors and then vary the conversion value of both the reactions.

The chosen temperatures are always 743 K for hydration and 813 K for dehydration as for an atmospheric pressure working condition with only steam as gas the equilibrium curve and the purpose of the system impose to work in the neighbourhood of these temperatures. The evaluation of different conversion values is related to not knowing what the system's behaviour could be.

In figure 27 is shown the thermal efficiency of the storage system in respect to the variation of the conversion value between 0.1 and 1 in both the reactors. The simulation is done with a

constant molar flow rate and so the composition of the streams and their mass flow are changing in order to satisfy the mass balance of the system as in the previous case.

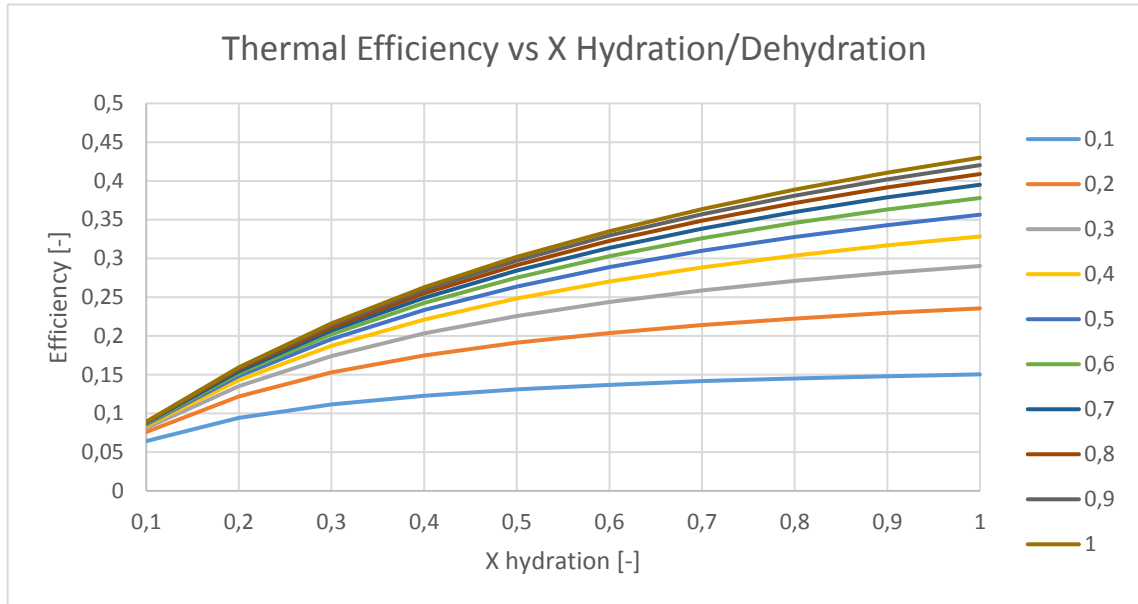


Figure 27: TES thermal efficiency vs hydration and dehydration conversion

The interesting results of the analysis shown in figure 27 is that as the conversion in the dehydration reactor rises the efficiency gain became lower and lower. Instead the hydration conversion affects more the efficiency for higher dehydration conversion value. In any case is important to have a quite good conversion in both the reactor otherwise the benefit of a higher conversion in one of the reactors would be penalized by the other one.

For a hydration conversion of 0.1 the efficiency ranges between 7.6% to 8.9% as consequence of the dehydration conversion. When the hydration conversion is 1 the maximum efficiency that can be obtained is with also a unitary dehydration conversion and is about 43% while if the dehydration conversion is 0.1 the efficiency is only about 15 %.

As can be seen in figure 28, the power output of the system is influenced by both the conversion values and it can be seen that for low dehydration conversion like 0.1 or 0.2 the power output tends to be linear when the hydration conversion is approaching to the unity. This happens as for low dehydration conversion also for high hydration conversion the chemical energy available in the mass flow is very low.

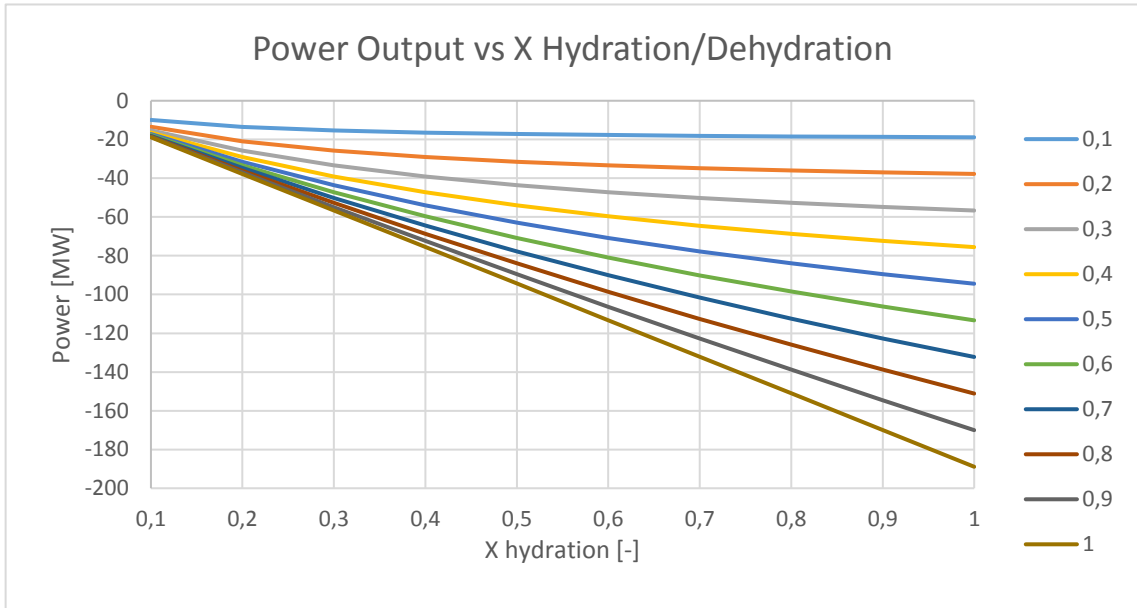


Figure 28: power output as function of hydration and dehydration conversion.

From figure 28 we can see that the power output ranges between -16.4 to -38 MW, depending on the dehydration conversion, for a hydration conversion of 0.1 while at a hydration conversion of 1 it ranges between -189 and -18.9 MW.

Figure number 29 shows the sum of the thermal power input needed to run the whole system.

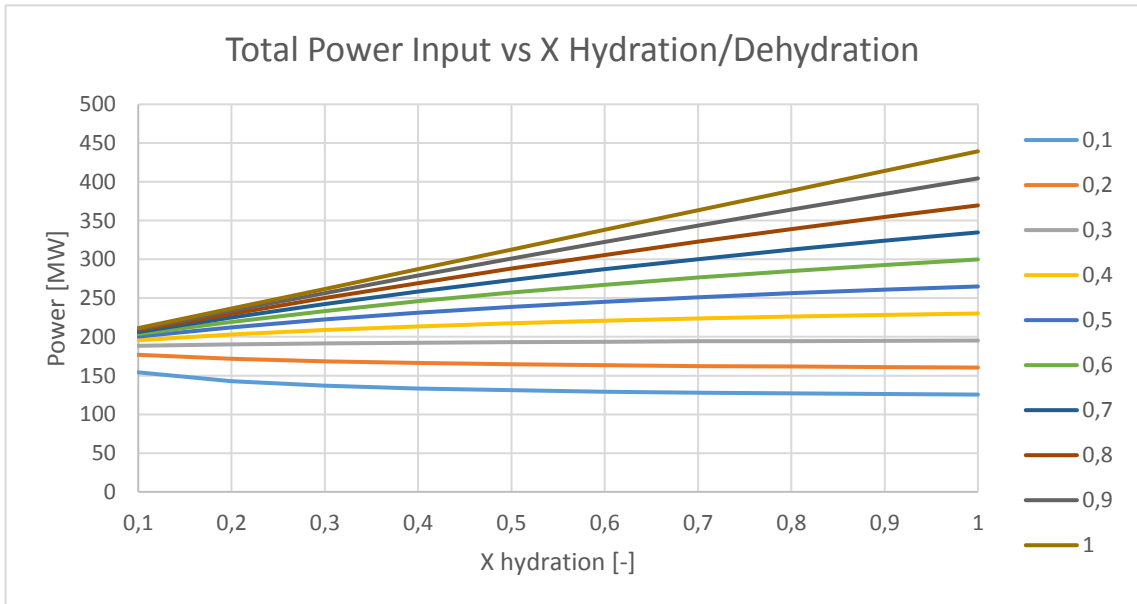


Figure 29: power output as function of hydration and dehydration conversion

It can be seen from figure 29 that, for constant conversion in the dehydration reactor, the conversion increment in the hydration reactor brings to a lower heat need and then, when the dehydration conversion is higher, a higher conversion in the hydration reactor means a higher power demand. For a hydration conversion of 0.1 the power input ranges between 154 and 211 MW while at a unitary hydration conversion the power input is between 125 and 440 MW depending on the dehydration conversion. It has to be reminded that the simulations are made on the assumption of same charge and discharge time in steady state condition and so the thermal efficiency of the system over a certain time-period can be expressed by the power instead than the energy.

3.3.4. Pinch analysis

The previous layout shows eight different streams that undergoes a heat exchange. In table 3, referring to the reference case only, we can summarize the available and the required heat flows.

Stream #/ source	Mass flow	T_{in}	T_{out}	C	C_p	C	Q	Cold/ Hot
[-]	[Kg/s]	[K]	[K]	[kJ/kg]	[kJ/kgK]	[kW/K]	[MW]	[-]
1	106,9	298	743	-	0,95	101,78	45,29	cold
2.1	20,1	298	373	-	4,20	84,42	6,33	cold
2.2	20,1	373	373	2260	-	-	45,43	cold
2.3	20,1	373	743	-	2,03	40,80	15,10	cold
6	127	743	298	-	1,26	160,40	-71,38	hot
HDRTN	-	743	743	-	-	-	-113,26	hot
7	127	298	813	-	1,28	162,68	83,78	cold
DEHDRTN	-	813	813	-	-	-	111,33	cold
10	106,9	813	298	-	0,96	102,41	-52,74	hot
12.1	20,1	813	373	-	2,05	41,21	-18,13	hot
12.2	20,1	373	373	-2260	-	-	-45,43	hot
12.3	20,1	373	298	-	4,20	84,42	-6,33	hot

Table 3: System hot and cold sources summary.

As the two reactor works at different time we can identify two distinct situations in which only some heat fluxes are available.

For the discharging step we have, as shown in table 4, the following hot streams:

Hot side							
Stream #/ source	Mass flow	T_{in}	T_{out}	C	C_p	C	Q
[-]	[Kg/s]	[K]	[K]	[kJ/kg]	[kJ/kgK]	[kW/K]	[MW]
6	127	743	298	-	1,263	160,404	-71,38
HDRTN	-	743	743	-	-	-	-113,26

Table 4: discharge step hot sources and streams.

And the cold ones in table 5:

Cold side							
Stream #/ source	Mass flow	T_{in}	T_{out}	C	C_p	C	Q
[-]	[Kg/s]	[K]	[K]	[kJ/kg]	[kJ/kgK]	[kW/K]	[MW]
1	106,9	298	743	-	0,952	101,775	45,29
2.1	20,1	298	373	-	4,20	84,420	6,33
2.2	20,1	373	373	2260	-	-	45,43
2.3	20,1	373	743	-	2,03	40,803	15,10

Table 5: discharging step cold sources and streams.

The chosen minimum temperature approach is of 15 K; as the system show the pinch point at the lowest temperature of the system the imposition of the minimum temperature approach will shift the cold curve to the right rising the necessity to dissipate 2.4 MW of heat at a temperature level near to the ambient temperature.

The minimum temperature approach value affects also the maximum temperature at which the streams entering in the reactor can be heated up. The heat needed by these streams to reach the reactor temperature is then provided inside the reactor by the reaction itself. So, the temperature reached by these streams outside of the reactor, is not anymore 743 K but only 728 K.

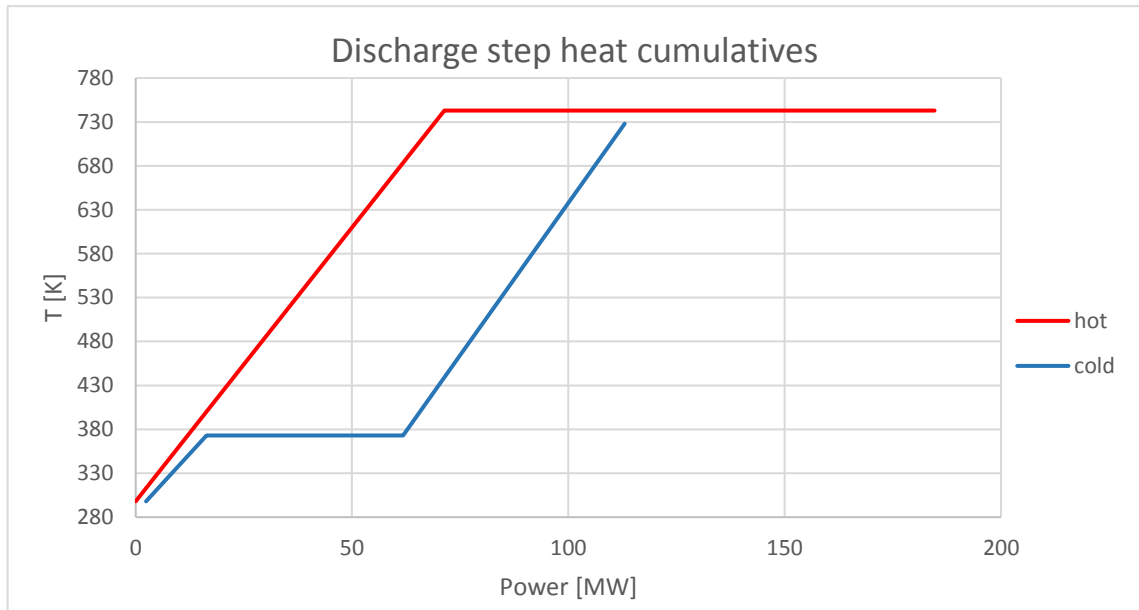


Figure 30: Discharge step heat cumulative.

The required heat to run the discharging step in this way can be brought to zero and the remaining amount of heat provided at 743 K, which is around 72.48 MW, can be used to run a Rankine power cycle.

The Hex network for the charging step is made dividing the outgoing stream of hot solids (#3) into two flows that can be matched well one with the solid inlet flow and one to the water inlet flow. Figure 31 shows the HEX network layout.

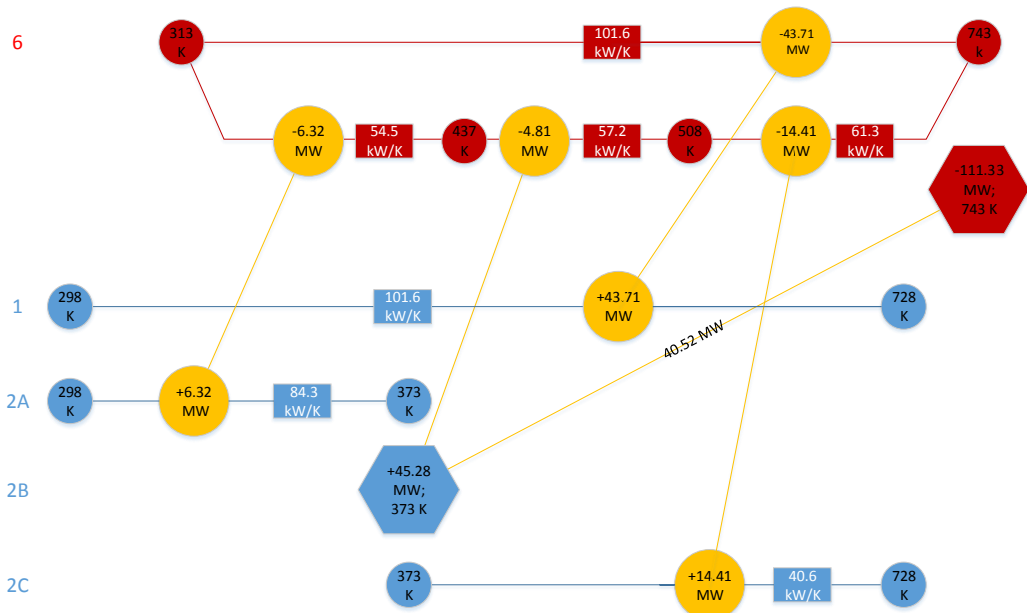


Figure 31: HEX network for the TES discharging step.

The choice for the HEX network shown in figure 31 to couple the streams was to split the stream number 6, of the outgoing solids, in stream 6A and 6B in order to have perfect matching with cold solids stream number 1. Stream number 6A has the same thermal capacity of stream 1 and is cooled down from 743 K to 313 K in order to heat up stream 1 from 293 K to 728 K. Stream number 6B is instead used to preheat and do the superheating of the inlet water stream number 4. The main amount of heat needed to evaporate the stream 4 is taken from the hydration reactor. Another solution could be to use stream 6B to heat stream 2 from its lower temperature to the highest possible and then using the heat from the reactor to reach the inlet reactor temperature. For the charging step we can summarize in table 6 the data about the available heat streams:

Hot side							
Stream	Mass flow	T_{in}	T_{out}	C	C_p	C	Q
#	[Kg/s]	[K]	[K]	[kJ/kg]	[kJ/kgK]	[kW/K]	[MW]
10	106,9	813	298	-	0,96	102,41	-52,74
12.1	20,1	813	373	-	2,05	41,21	-18,13
12.2	20,1	373	373	-2260	-	-	-45,43
12.3	20,1	373	298	-	4,20	84,42	-6,33

Table 6: charging step hot side streams and sources data.

And:

Cold side							
Stream	Mass flow	T_{in}	T_{out}	C	C_p	C	Q
#	[Kg/s]	[K]	[K]	[kJ/kg]	[kJ/kgK]	[kW/K]	[MW]
7	127	298	813	-	1,28	162,68	83,78
DEHDRTN	-	813	813	-	-	-	111,33

Table 7: charging step cold side streams and sources data.

In this case the pinch point is at 373 K for the hot side. With the same minimum temperature approach used for the discharge step the heat, from the hot side, that can't be recycled is about 49.7 MW. Figure 32 shows the heat cumulative of the charging step where can be seen the pinch point position.

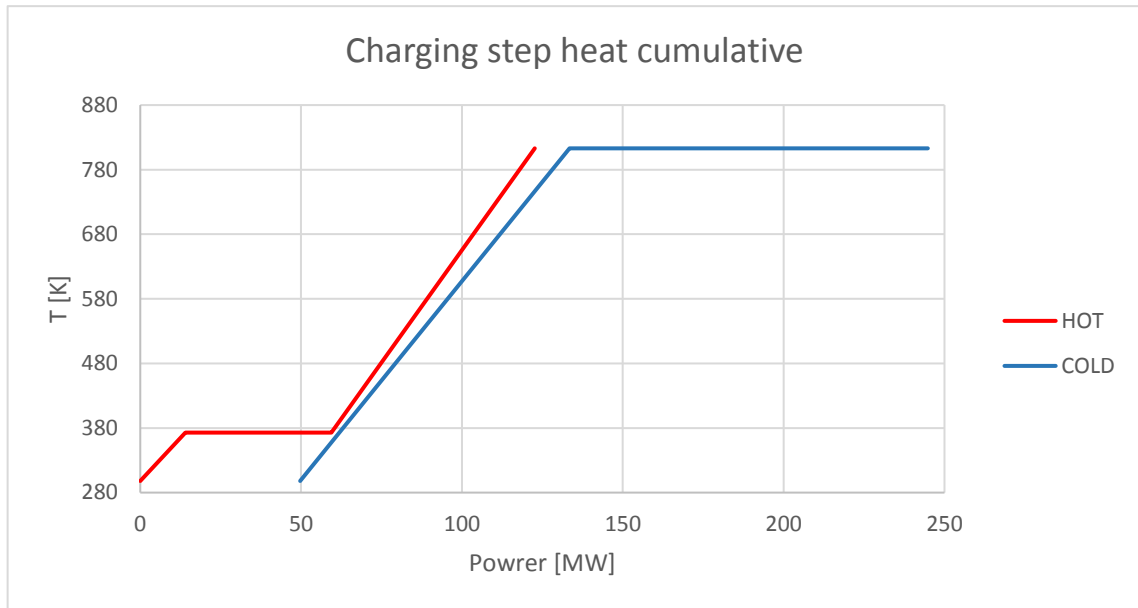


Figure 32: Charging step hot and cold cumulative curves.

In figure 32 is clear that the power needed by the dehydration reactor, that is represented by the flat curve at constant temperature, has to be taken from the solar plant. Moreover, as shown in the previous figure, also the cold streams need some energy from the sun to reach the reaction temperature of the dehydration reactor. This amount of energy is about 11.61 MW.

Referring to figure 33 we can see that the cold solid stream number 7 had to be split in order to heat it up using the available hot streams number 10 and 12. The splitting is made only above the pinch point in order to reach the highest possible temperature for stream 7, that is about 748 K, using the available two hot streams. From this temperature to the reaction temperature the needed heat has to be provided exploiting the same heat source used to run the charging step reaction.

Under the pinch point temperature, that is 373 for hot streams and 358 for cold ones, the stream 7 is heated exploiting a little amount of heat from the condensation of the water stream number 12. The other heat available under the pinch point is can't be used for useful purpose in this configuration. The heat needed by the dehydration reactor has to be provided entirely by the sun. In this way the heat need by the system during the charging step can be lowered to 122.94 MW.

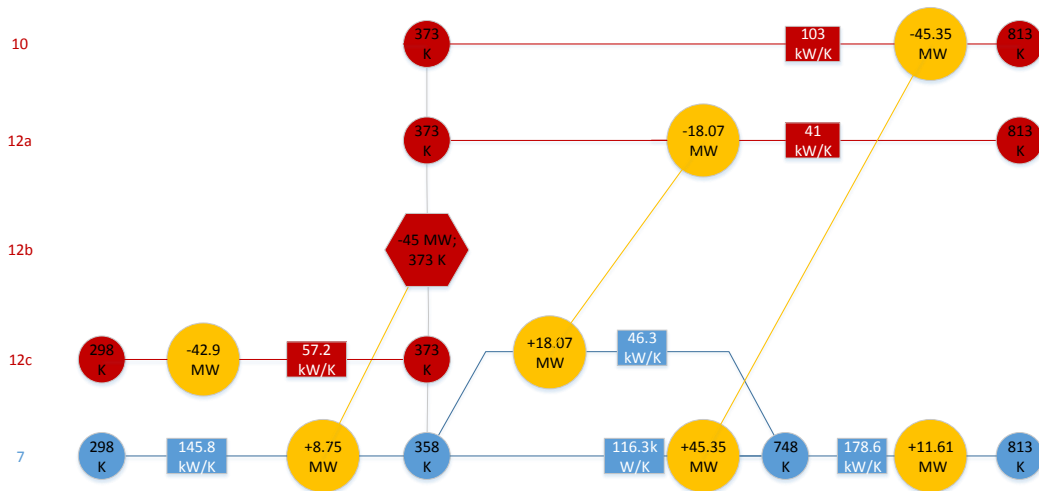


Figure 33: Charging step HEX network

The pinch analysis is made to see which is the thermal efficiency that the proposed system can reach in the paper reference condition. The thermal efficiency obtained with the proposed HEX network reach a value of about 58.95 %. A comparison with the conceptual design thermal efficiency provided by the reference case is not so easy to do as the paper layout doesn't show all the information needed to create a proper HEX network.

Anyway, the comparison shows that the layout developed in this thesis shows lower thermal efficiency of about 6 percentage points. This difference can be traced back to the different assumption made on the storage temperature of the solid outlet from the dehydration reactor. In the proposed layout the storage is at ambient temperature while the papers assume a storage at the same temperature of the dehydration reactor.

The choice to have an ambient temperature storage is taken in order to have a storage without insulation, and so less expensive, and also because is nearly impossible to store sensible heat at so high temperature for a useful time. This analysis shows that the system heat integration has a fundamental role to get higher thermal efficiency. The pinch analysis of the discharging step show that the outlet hot streams can provide only a portion of the heat needed to preheat the inlet cold stream, but, they are reused almost completely.

So, the reaction condition, are reached using also part of the power output of the reactor itself as during the discharging step the sun source is assumed to be not available. This fact has a high influence on the thermal efficiency of the system as part of the useful produced power has to be employed to ensure the self-reliance of the system. The charging step need heat from the

outside not only to run the reaction but also to bring the inlet streams at the reaction temperature as the outgoing stream has not enough heat to cover the inlet streams needs. The wasted heat, in this case, is higher than the one related to the charging step and moreover is always at a low temperature.

Table 8 shows a comparison of the system before and after the pinch analysis.

Parameter	Unit	Before	After
TES thermal efficiency	[%]	36.86	58.95
Power output	[MW]	113.26	72.48
Power input	[MW]	307.21	122.94

Table 8: before and after pinch analysis comparison

From table 8 we can see that the comparison of the system, with the same boundary conditions, before and after the pinch analysis has an increment in the thermal efficiency of about 20 percentage points due to a heavy reduction of the needed power input. The efficiency is calculated as the ratio of all the power output and all the power input of the system because, as assumption, the time of charge and discharge are the same.

To underline the influence of the storage temperature, figure 34 shows the influence on the TES thermal efficiency of the solid storage temperature.

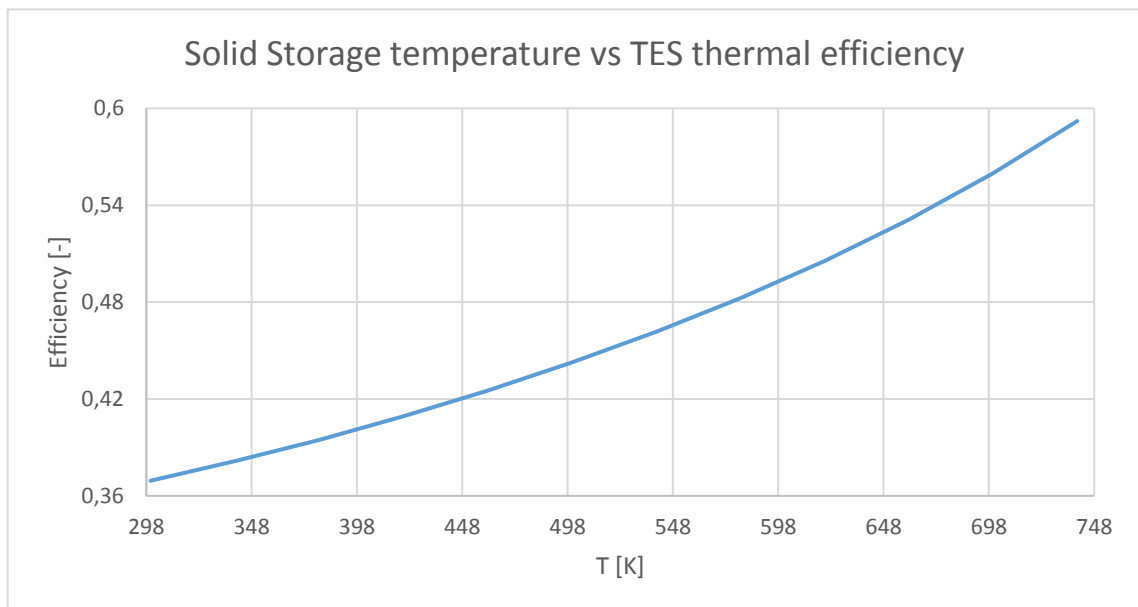


Figure 34: Solid storage temperature effect on TES thermal efficiency

As shown by figure 34 an increment of the temperature at which the solid medium is stored means an increment in the TEs thermal efficiency as the solid streams that are introduced in the system needs less energy to reach the requested temperature.

The simulation is made taking into account only the solid streams and not the water ones as water, over 100 °C, becomes steam and this means a very high increment in its specific volume, if not at high pressure, and so a steam storage won't be so interesting to be studied in this configuration. From figure 34 we can see that if the temperature of solid storage would be around the hydration temperature the efficiency increment would be of around 22 percentage points.

This parameter seems to have a very high influence on the system efficiency and, on short period, should be very important to have storage at the highest possible temperature. Instead if the storage has to work on very long period the effort needed to maintain a high solid storage temperature would be too high and not convenient.

4. Plant Configuration

4.1. Plant Size

If we want to make a preliminary sizing of the plant, we have to consider the energy inlet to the TES system that can be obtained from the solar plant.

We can take as reference the typical plant size of a CSP facility for power production. In literature there are some reference on this topic that gave an overall characterization of these kind of plants.

From Liu et al.[3] we have a comparison of the main CSP technologies, figure 35.

	Current trough	Current tower	Current linear Fresnel
Maturity	High, commercially proven	Medium, recently commercially proven	Medium, pilot plants, commercial projects under construction
Typical plant capacity	100 (MW)	50–100 (MW)	50 (MW)
Operating temperature of solar field (°C)	290–390	290–565	250–390
Plant peak efficiency (%)	14–20	23–35	18
Annual average conversion efficiency (%)	13–15	14–18	9–13
Collector concentration (suns)	70–80	> 1000	> 60 (depends on secondary reflector)
Power block cycle and fluid conditions	Superheated steam Rankine, steam @380 °C/100 bar	Superheated steam Rankine, steam @ 540 °C/100–160 bar	Saturated steam Rankine (steam @ 270 °C/55 bar), superheated steam Rankine (steam @ 380 °C/50 bar)
Power cycle efficiency (%)	37.7	41.6	–
Heat transfer fluid	Synthetic oil, water/steam (DSG), molten salt (demonstration), air (demonstration)	Water/steam, molten salt, air (demonstration)	Water/steam
Annual capacity factor (%)	20–25 (no TES) 40–53 (6 h TES)	40–45 (6–7.5 h TES) 65–80 (12–15 h TES)	22–24
Storage system	Indirect two-tank molten salt storage (293–393 °C)	Direct two-tank molten salt storage (290–565 °C),	Short-term pressurized water storage (Ruths tank)

Figure 35: efficiency and technical aspects comparison of different CSP technologies [3].

The previous summary in figure 35 shows that typically the peak power output is about 100 MW for parabolic trough and 50 to 100 MW for tower receiver and 50 MW for linear Fresnel facilities. Considering the power cycle efficiencies reported in figure 35 we can find that the thermal power provided to the power cycle are between 100 to 250 MW_{th} for central tower and less than 270 MW_{th} for parabolic trough.

On the bases of the previous data we can consider the hypothesis to set the power inlet to the TES charging step to a thermal power level of about 100 MW_{th} in order to have also a resulting power production of a few tens of MW_e when the TES is the only energy source available. In

this way the energy destined to the TES, if compared to the typical ranges of this kind of systems, is at least equal to a solar multiple unit.

If we take into account the minimum temperature needed for the dehydration of the calcium hydroxide at a steam partial pressure of 1 atmosphere we can see that the CSP technology that can be better matched for a large-scale power plant is the central tower receiver that, due to the higher concentration factor, can provide also higher temperatures.

Instead for small scale power plant the most interesting technology is represented by solar dish for their high concentration power and the resulting high temperature (550 -750 °C) [3].

On the bases of the data reported in the previous table about the capacity factor of a solar tower power plant we can assume that the annual amount of hour that a system like that can work at nominal power without a TES system is about 1350 hours every year.

This can be calculated making the mean value of the results obtained with the equation 17 for the extreme values of the range reported in figure 35.

Equation 17

$$h_{sun} = 8760 * C_f - 365 * h_{TES} \quad [h/year]$$

Where 8760 are the hours in a year, 365 are the days in a year, h_{sun} are the equivalent number of hours in a year for which the system can work at nominal power without the TES supply and h_{TES} is the number of hours at nominal power provided by the TES. Considering 365 days in a year the number of hours at full power for each day is about 3.7 [h/day].

This calculation is made considering a capacity factor between 40 and 45 % with a TES daily contribution respectively between 6 to 7 hours. This data is only an approximation to have a starting point to make a rough evaluation of other parameters. With this data and a nominal input power to the dehydration reactor of 100 MW, the mean value of energy that can be stored each day is about 370 MWh/day.

Figure 36 shows the amount of solid composed by calcium hydroxide and calcium oxide, considering a dehydration conversion of 0.88 and a hydration conversion of 0.65, that is needed to store the energy that the TES has to manage each day vs different level of energy provided daily to the TES from the solar field.

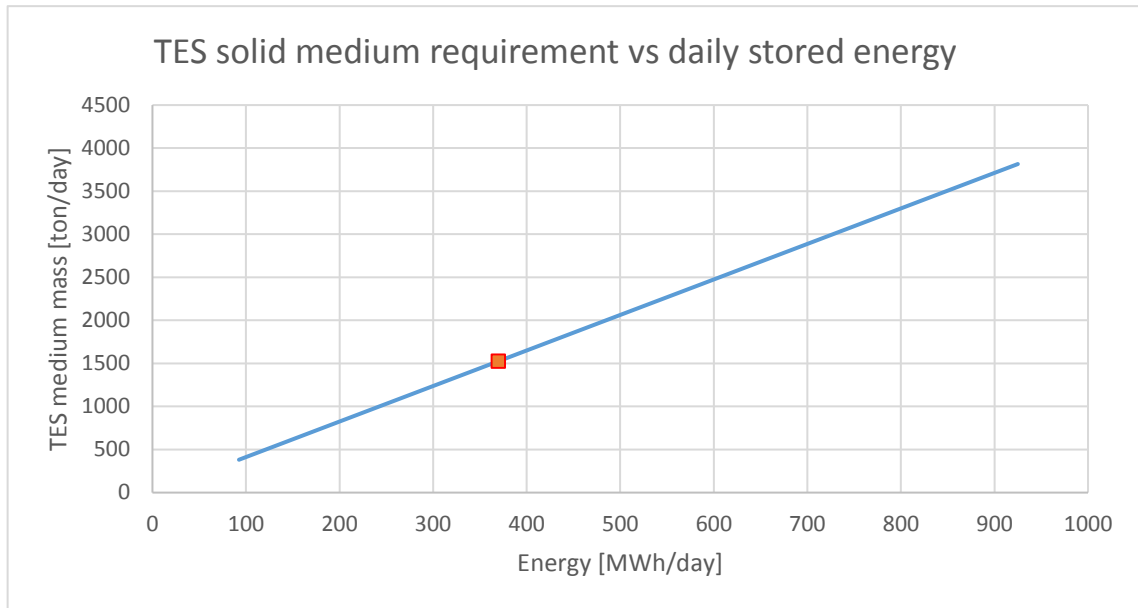


Figure 36: tons per day of solid medium as function of the stored chemical energy.

As can be seen in figure 36 the amount of chemical compound needed to store the energy is linearly dependant from the amount of energy that is stored each day. The molar composition of the solid medium used for the calculation is around 90 % of calcium hydroxide while the rest is calcium oxide.

The red point is referred to the case in which the nominal thermal power from the solar plant is 100 MW which means that during a day the amount of calcium hydroxide and calcium oxide mixture needed to store it is about 1530 tons. The trend shown in the graph is linear and, the curve slope, that is about 4,124, is related to the mass energy density of the TES medium that is equal to 242 kWh/kg. This value is in accordance to the hypothetical range related to thermochemical heat storage as is of the same magnitude.

If we consider a mass density of this mixture equal to 2525 kg/m³ we can also evaluate the storage volume needed for the solid medium in respect to the stored amount of energy. The following figure, number 37, shows the needed volume in respect to the amount of stored energy.

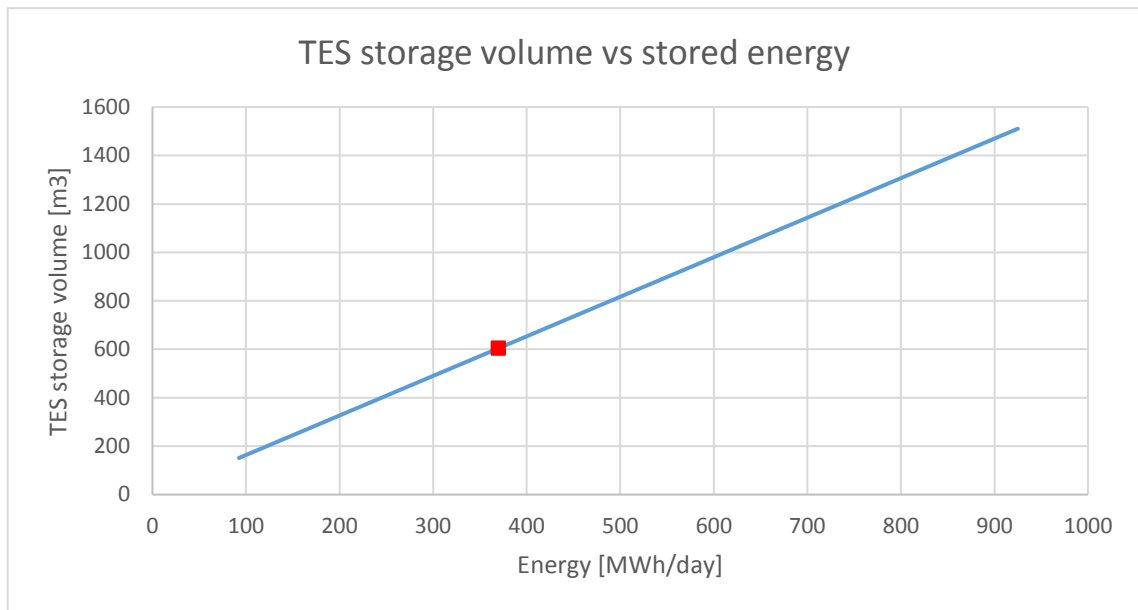


Figure 37: solid storage volume as function of the energy stored in one cycle of charge/day.

The red point in figure 37 is related to the case with 100 MW as inlet power to the TES system; for that case the storage volume should be around 600 m³. The trend is linear also in this case and, the curve slope, that is about 1.633, is related to the volume energy density of the TES that is equal to 612 kWh/m³.

As reference for the power block we can say that usually this kind of systems are coupled with Rankine-Hirn steam cycle that works at pressure between 100 and 160 bar and with temperatures around 540 °C (813 K) or 380 °C (653 K) depending on the maximum temperature that the employed CSP technology can provide.

4.2. Direct and Indirect Dehydration Reactor Integration

The fluidized bed reactor technology is usually linked to the exploitation of an HTF to match the heating and cooling demand of the process. On the other side the majority of the CSP plant configuration contemplate the exploitation of an HTF to absorb the concentrated sun radiation and so the match between the two technologies seems be easy.

If we consider the typical HTF maximum temperature of the CSP plants already made or under construction, we see that in many cases the temperature needed to run the thermal decomposition of calcium hydroxide is comparable or above them. The fact that the dehydration process is at a constant temperature also means that it is not easy to combine with an HTF. If we consider one of the most common solar HTF that is called Solar Salt and is composed by 40% wt KNO_3 and 60% wt NaNO_3 , the maximum allowed temperature to not incur in thermal decomposition and instabilities is around $565\text{ }^\circ\text{C}$ (838 K) and so the difference with the dehydration reactor is only of 25 K.

Figure 38 shows the equilibrium curve of the reaction with the point at which the TES system works the charge and discharge steps and also the maximum temperature that the solar salt can reach.

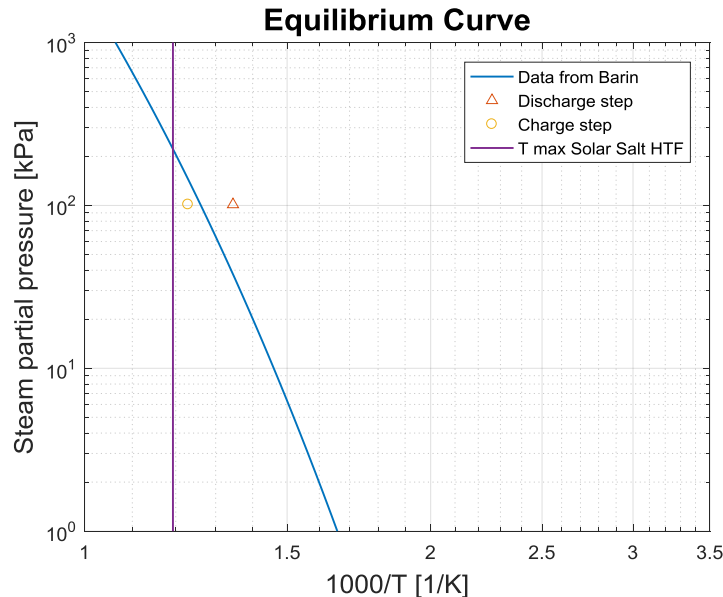


Figure 38: Base charge and discharge conditions with solar salt max temperature reference.

As can be seen in figure 38 the maximum available temperature of this common HTF is not compatible with the charging step of the TES under investigation.

Figure 39 shows the mass flow needed to cover the heat requirement of the TES charging step if solar salt is used as HTF.

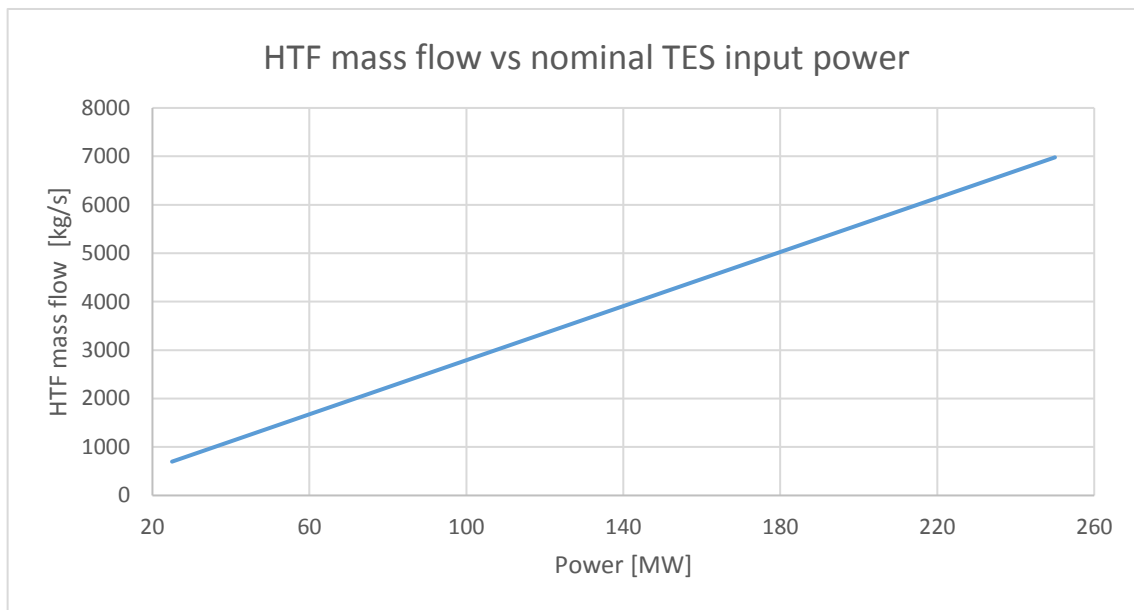


Figure 39: solar salt mas flow vs Power.

Figure 39 is made considering a minimum temperature approach of 15 K and an HTF maximum temperature of 565 °C. The corresponding HTF mass flow appear to be very high already for low nominal power. The relation between the two variables is linear and so, as the nominal power ranges between 25 to 250 MW, the HTF mass flow ranges between 700 to 7000 kg/s. As the maximum temperature is so near to the reaction temperature the temperature gap useful for the heat transfer is very narrow and so it has to be compensated by a high mass flow. If we take into account the solar salt volumetric flow, we have values, for the same range of power shown in figure 39, included between 1.81 m³/s and 18.11 m³/s as the mass density of solar salt is about 385 kg/m³. From the data previously shown is clear that this configuration is not applicable as it involves a too high mass and volumetric HTF flow in relation to the transferred power.

In the case of HTF that have a maximum working temperature comparable to the one of the charging step the only way to exploit them in a proper way is to have another user at temperatures immediately below those of the TES reactor during the charging step. In this way the HTF could be used on a wider temperature difference like 100 or 200 K. The first heat user that can be coupled with the HTF at temperature lower than the ones of the dehydration reactor is the stream that is introduced in the rector, because, as we have seen from the pinch analysis,

the charging step needs energy from the outside to preheat completely that stream. Another heat user that can be coupled could be a power block that works with maximum temperatures lower than 813 K (540 °C) and so also a steam Rankine-Hirn power block could be feasible. In any case the introduction of another thermal user at lower temperature won't solve the problem of having a very high mass or volumetric HTF flow in comparison to the TES nominal power.

Between the HTF shown in figure 4 is reported that Hitec salt, if it works in some kind of atmosphere, as also reported by Olivares [33], can be used at a higher maximum temperature. Hitec is a solar salt, composed in weight by: 7% of NaNO₃, 53 % of KNO₃ and 40 % of NaNO₂ [3], that shows a lower freezing point (142 °C versus 220 °C [3]) and a higher specific heat (compared to solar salt. In the cited work the reported maximum temperatures are 710 °C under pure oxygen and 650 °C under air and 610 °C under nitrogen or argon [33]. Taking into account the pure oxygen atmosphere, and so a maximum temperature of 710 °C (983 K), we can have a HTF that works with a temperature difference of 150 K thermally coupled with the dehydration reactor at 813 K respecting a minimum temperature approach of 15 K. Figure 40 shows the HTF mass flow needed by the TES as function of the transferred power working for temperature difference of 100, between 828 and 928 K, or 150 K, between 828 and 978 K.

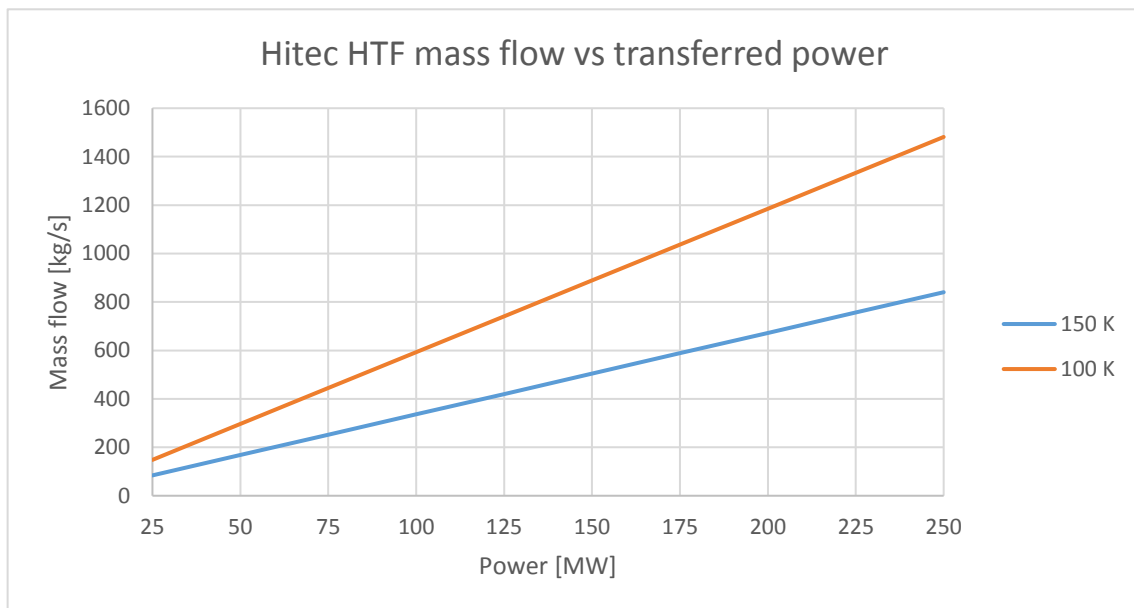


Figure 40: needed Hitec mass flow vs transferred power.

As can be seen in figure 40 the mass flow of Hitec as HTF needed in the same power range is drastically lower already with only an exploited temperature difference of 100 K if compared to the solar salt case. With a mass density of about 285 kg/m³ the volumetric flow ranges

between 0.3 and 3 m³/s with 150 K of exploitable temperature difference and between 0.51 to 5.1 m³/s for the case with 100 K as exploitable temperature difference.

Due to the high temperature required also air could be used as HTF but it would be needed a high mass flow and, if not pressurized, also high volumetric flow. In the case of air, the pressure choice would be fundamental to have an acceptable volumetric flow.

Another issue related to the maximum temperature of the solar plant is the heat losses due to radiation that are directly proportional to the cube of the body absolute temperature. So, a lower maximum temperature, will mean also a higher thermal efficiency of the solar plant.

On the other side the dehydration reactor could be also directly integrated in the solar plant and so it would be heated up directly without the exploitation of an HTF. In literature are reported some studies about fluidized bed reactor directly heated by solar source [34], [35], [36], [37], [38]. The exploitation of a directly heated FB reactor would eliminate all the problems and the loss related to the HTF system but would also mean to introduce another level of complexity to a component that is already very complex.

For the dehydration temperature that can be reached at atmospheric pressure both the solution of direct or indirect heating could be studied in the future as both can be matched. For lower dehydration temperature the exploitation of HTF would be easier as HTF are already used in many real applications while the direct integration should be deeply investigated.

4.3. Pinch analysis

In order to have a better view of the system thermal efficiency and a starting point for comparison in respect to further modifications in the following paragraph is carried out a pinch analysis of the system. The analysis is made for a case in which the input power to the dehydration reactor is 100 MW. This amount of power is supposed to cover only the reaction needs and so is related to the amount of energy directly stored during the charging step of the process. The hydration and dehydration temperatures are respectively 743 and 813 K while the conversion factors are 0.88 for dehydration and 0.65 for hydration. The system is studied considering an equal time for charge and discharge steps with the assumption that the two phases take place separately.

Table 8 shows the hot and cold streams, sources and sinks that are present in the system.

Stream/ Source	Mass flow	Tin	Tout	Cp	C	Q	Cold/ Hot
 [#]	 [Kg/s]	 [K]	 [K]	 [kJ/kgK]	 [kW/K]	 [MW]	 [-]
6	114,50	743	313	1,27	145,30	-62,48	hot
Hydration	-	743	743	-	-	-101,72	hot
1	96,50	298	743	0,95	40,97	40,97	cold
2a	18,00	298	373	4,30	77,33	5,80	Cold
2b	18,00	373	373	-	-	40,30	Cold
2c	18,00	373	743	2,07	37,32	13,81	cold
10	98,50	813	313	0,94	92,82	-46,41	hot
12a	18,00	813	373	2,05	36,95	-16,26	hot
12b	18,00	373	373	-	-	-40,70	hot
12c	18,00	373	313	42,97	773,50	-46,41	hot
7	114,60	298	813	1,28	146,83	75,62	cold
Dehydration	-	813	813	-	-	100,00	cold

Table 9: system heat sources and streams characterization.

The water streams, number 2 and number 12, are divided in three parts following the phase change: liquid water, evaporation and superheated steam. The reported streams inlet and outlet temperatures are referred to the temperature changes that are important for the system and that would happen in the HEX network, for example all the hot streams outlet temperatures are reported to be 313 as this temperature is the minimum that can be obtained in a HEX referring to the external environment or to the cold streams of the system.

During the hydration step the streams and heat sources/sinks that are available are reported below, divided between hot and cold side, respectively in table 9 and 10.

Hot side						
Stream/ Source	Mass flow	Tin	Tout	Cp	C	Q
 [#]	 [Kg/s]	 [K]	 [K]	 [kJ/kgK]	 [kW/K]	 [MW]
Hydration	-	854	854	-	-	-101,72
6	114,5	854	313	1,30	148,59	-80,39

Table 10: hydration step hot side available streams and sources.

Cold side						
Stream/ Source	Mass flow	T _{in}	T _{out}	C _p	C	Q
[#]	[Kg/s]	[K]	[K]	[kJ/kgK]	[kW/K]	[MW]
1	96,5	298	743	0,95	40,97	41,04
2a	18	298	373	4,30	77,33	5,8
2b	18	373	373	-	-	40,3
2c	18	373	743	2,07	37,32	13,81

Table 11: hydration step available cold streams and sources.

The cold streams outlet temperatures are now modified in order to respect the minimum temperature approach in respect to the reaction temperature. The gap of the 15 k of the minimum temperature approach is supposed to be covered directly inside the reactor itself. With the previous data it can be done the heat cumulative of the discharge step, figure 41.

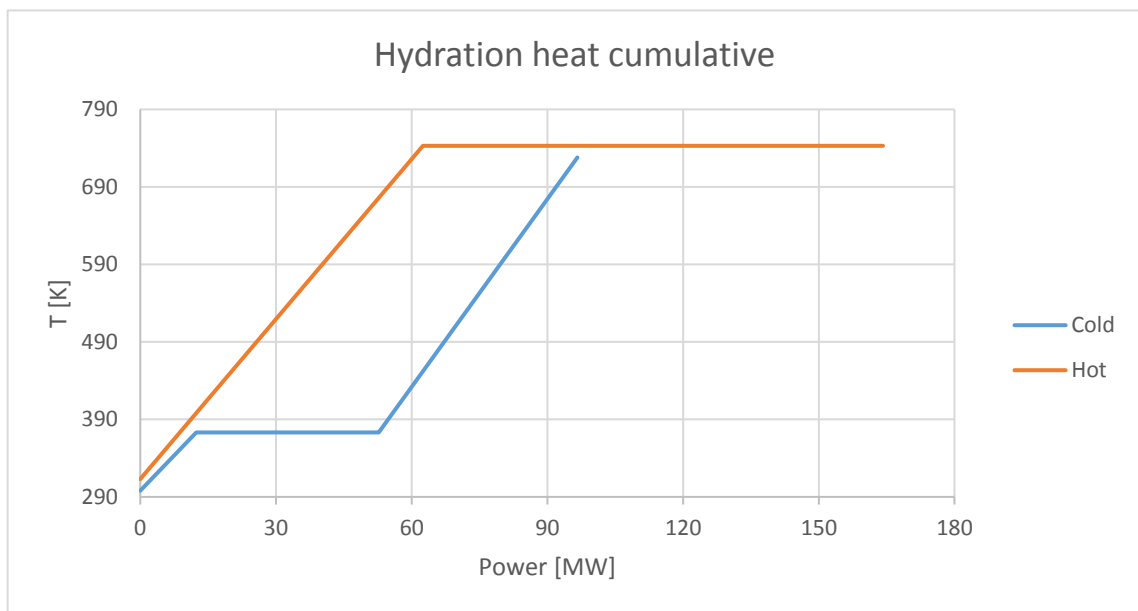


Figure 41: Hydration heat cumulative.23

As can be seen from figure 41 the pinch point is at 298 K for the cold side and at 313 K for the hot side. So, there is anything that has to be heated up or cooled down under the pinch point more than the heat related to the minimum temperature approach between hot streams and the environment that is not covered by the HEX network. To cover all the preheating needs of the cold streams is clear that a certain amount of heat has to be taken from the hydration process and so the useful output of the reaction will be lower than the previously obtained. On the other

side all the heat from the hot stream can be reused to heat up the cold ones. Figure 42 shows the HEX network of the discharge step.

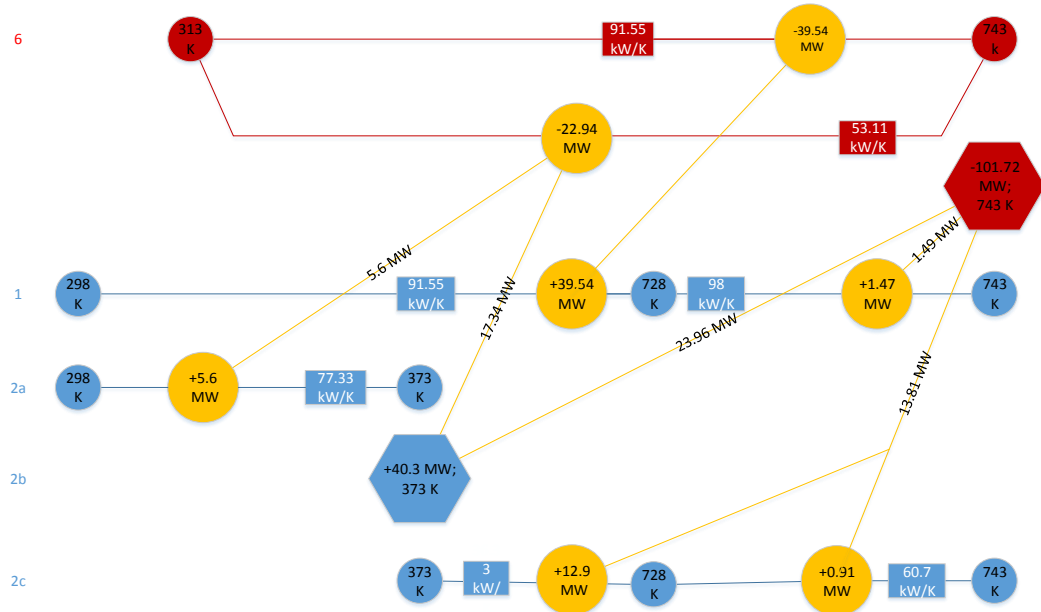


Figure 42: HEX network of the discharge step.

From figure 42 we can see that the amount of heat that the hydration reactor has to give back to sustain the process is about 26.34 MW and so the available power that can be used for other purpose is about 75.38 MW. Stream number 6 is cooled down only to 313 K and the remaining sensible energy due to the temperature difference with the environment is then lost during the storage.

The dehydration reactor has two outlet streams that can be cooled down and only one inlet stream that needs to be heated up. In the following tables, number 11 and 12, are reported the data of these streams and of the dehydration reactor taking into account the minimum temperature approach gap as in the other case.

Hot side						
Stream/ Source	Mass flow	Tin	Tout	Cp	C	Q
[#]	[Kg/s]	[K]	[K]	[kJ/kgK]	[kW/K]	[MW]
12a	18	813	373	2,05	36,95	-16,26
12b	18	373	373	-	-	-40,7
12c	18	373	313	42,97	773,5	-46,41
10	98,5	813	313	0,94	92,82	-46,41

Table 12: dehydration hot streams and sources.

Cold side						
Stream/ Source	Mass flow	T _{in}	T _{out}	C _p	C	Q
[#]	[Kg/s]	[K]	[K]	[kJ/kgK]	[kW/K]	[MW]
7	114,6	298	813	1,28	146,83	75,62
Dehydration	-	813	813	-	-	100

Table 13: dehydration cold streams and sources.

In the following figure, number 43, is shown the HEX network made with the previous data and assumptions.

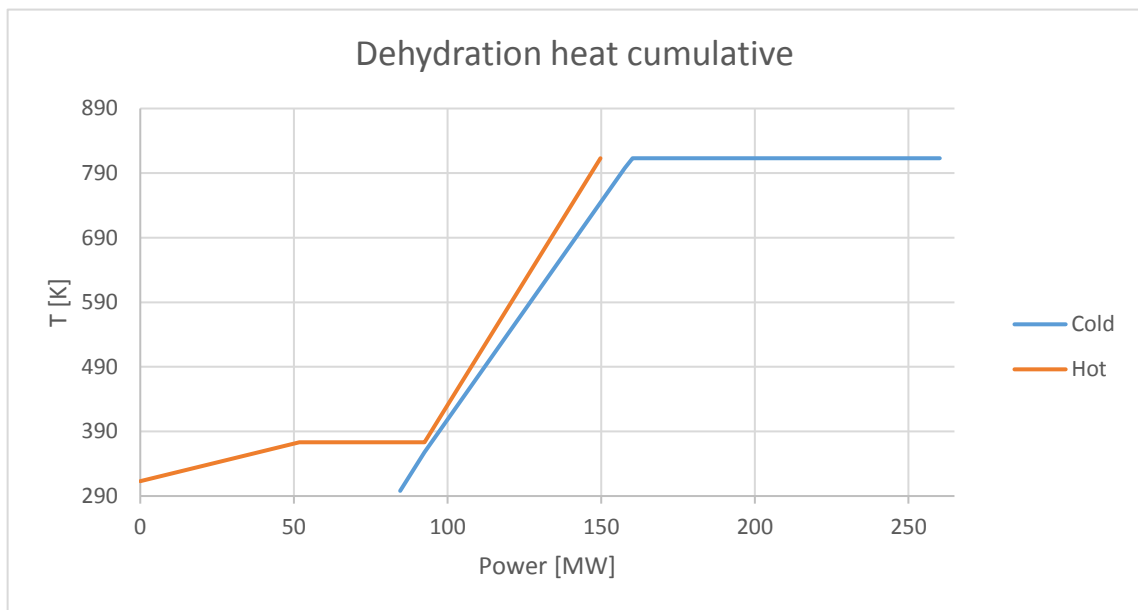


Figure 43: dehydration heat cumulative.

In this case the pinch point is at the start of the condensation at 373 K for the hot side and at 358 K for the cold side. As the hot streams can cover only a portion of the cold side heat demand the remaining part of the needed heat has to be provided by the sun. The heat needed to run the reaction, 100 MW, is already assumed to be covered by the sun. In addition to that there is the need of about 10.43 MW to completely heat up the cold stream to the reaction temperature. Due to the position of the pinch point the hot streams have certain quantity of heat that can't be used for any purpose in the charging step. This heat is about 42.73 MW and is available at temperatures lower than 373 K as can be seen also in figure 44.

Figure 44 shows the HEX network needed to reach the thermal coupling shown in figure 44.

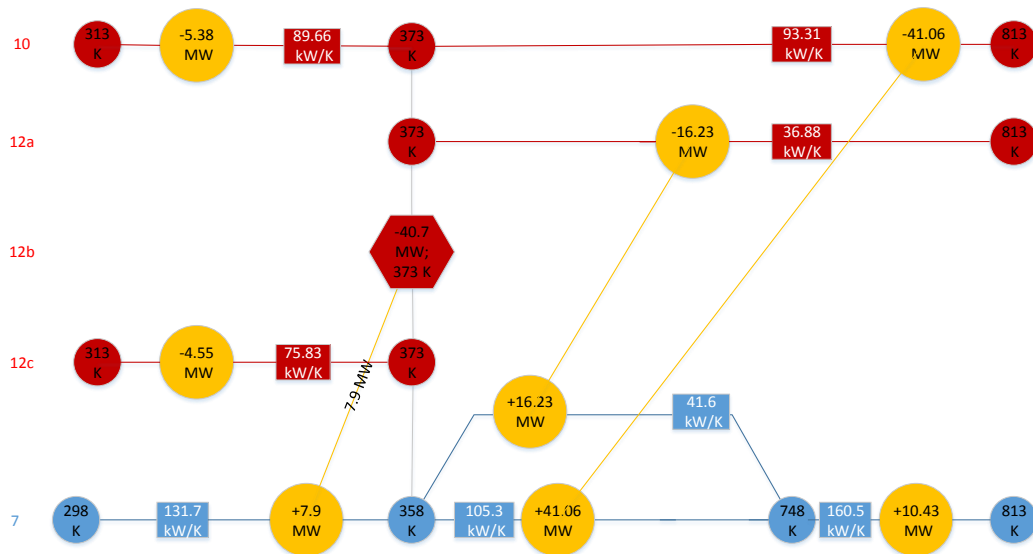


Figure 44: HEX network for the dehydration step.

Taking into account all the heat needed from the sun to run the dehydration reaction, 110.43 MW, and the net heat that the hydration reaction can provide to other process, 75.38 MW, the TES thermal efficiency after the pinch analysis is about 68.26 %.

Table14 shows a comparison of the system before and after the pinch analysis.

Parameter	Unit	Before	After
TES thermal efficiency	[%]	36.78	57.34
Power output	[MW]	101.72	63.32
Power input	[MW]	276.5	110.43

Table 14: before and after pinch analysis comparison.

After the pinch analysis the system has gained 20.5 percentage point in its thermal efficiency thanks to a reduction of the needed power input of 166.07 MW. The evaluation of the TES thermal efficiency is made using the ratio of the power values instead of the energy values because the operational time of the charging and discharging steps are equal.

5. TES System Modification

The following chapter contains some modifications to the base case TES system, described in chapter 4, made in order to see how the efficiency could be improved changing the working conditions of the reactors. The following summary reports, as a guide, the cases studied below:

- Dehydration steam partial pressure reduction, section 5.2, page 67. This is made introducing nitrogen in the dehydration reactor as a fluidizing agent in order to dilute the steam partial pressure and consequently the dehydration temperature;
- Series of dehydration reactors, section 5.3, page 85. This change is always made to have a higher dilution of the steam in order to reduce the dehydration temperature;
- Hydration pressure modification, section 5.4, page 97. In this case the hydration pressure is increased in order to work at higher discharge temperatures.

5.1. System Pressure Modification

For the previous simulations the system was working at ambient pressure with no other gasses besides steam. This assumption has a consequence on the reactor temperatures as the pressure of the steam define the equilibrium temperature of the reaction. So, in atmospheric condition, the hydration reaction is counteracted at temperature higher than 792 K while the dehydration can happen only above this temperature. Figure 45 shows the working point of the base case and Barins' equilibrium curve as reference.

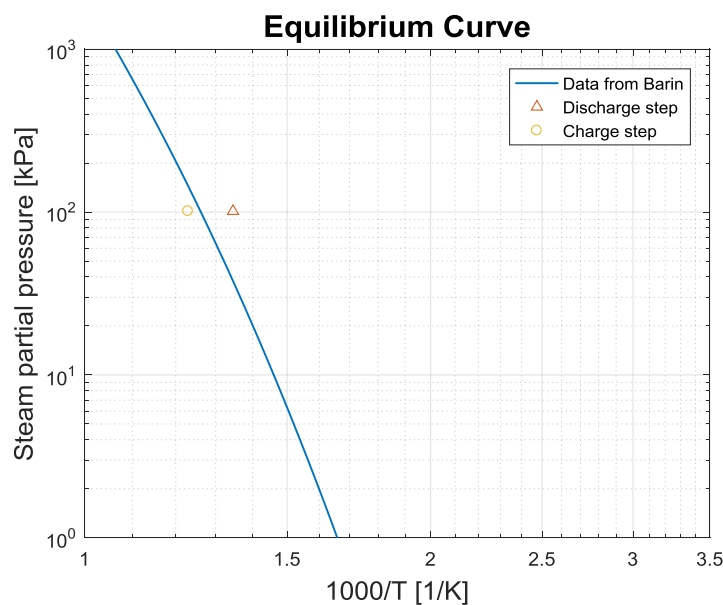


Figure 45: working point of the TES in the base case configuration.

A different working pressure could allow to have more advantageous temperatures during the charging and discharging steps and also a better match with both the power cycle and the CSP plant because during the charging step a lower steam pressure would mean also a lower temperature while during discharge step a higher pressure would mean a higher temperature.

5.2. Dehydration Steam Partial Pressure Reduction

The goal to have a lower dehydration temperature is linked to many things:

- A low temperature in the dehydration reactor would mean a low heat demand for the preheating of the streams entering the dehydration reactor and so it could mean a better thermal performance of the TES system;
- A lower maximum temperature is easier to reach and so it means a less sophisticated CSP plant.
- In the case of an indirect integration the HTF management would be easier as the temperature involved in the dehydration reaction are quite high and comparable or even higher than the higher limit of the common CSP HTF as Solar Salt or Terminol VP-1. Moreover, it could also mean a lower heat loss for irradiation and convection.
- A lower temperature could open interesting scenarios in the integration field with other type of heat sources.

The simple way to reduce the steam partial pressure but working at ambient pressure is the introduction of another gas that is employed to fluidize the reactor bed. Then the steam partial pressure is only dependent on the steam production related to the calcium hydroxide thermal decomposition. The reduction of the steam partial pressure could mean also a higher rate of reaction.

Air seems not to be the best choice for this reaction as the CO₂ content is quite high and in this range of temperature is over the equilibrium and so it will react with CaO to produce CaCO₃ inhibiting part of the active solids[24]. Unless the air flow would be decarbonized nitrogen could be an interesting alternative as fluidizing agent for the dehydration step.

In literature there are many studies where nitrogen is employed in reactors at different conditions where hydration and dehydration reaction are run. On this basis the chosen alternative fluidizing agent is nitrogen as there are no data about drawbacks on the reaction kinetics or effectiveness.

With the introduction of a different fluidizing agent, the nitrogen, in the dehydration reactor rises the necessity to separate it from the steam released by the reaction. The separation process can be obtained with the condensation of the steam and then the two phases can be separated. The main problem of the separation between nitrogen and steam is that the condensation temperatures of the water is not anymore at constant temperature if the stream is a mixture of steam and nitrogen. Then the separation of the two molecules is not so easy and the separation may not reach the completeness leaving some water traces in the recirculated nitrogen stream.

Another direct consequence is that the cooled nitrogen stream, after being separated from the steam, has to be reheated before being recirculated inside the dehydration reactor. This means the introduction of another heat exchanger at the outlet of the dehydration reactor.

The amount of nitrogen introduced is always calculated as a ratio in respect to the solid inlet molar flow but also considering the amount of steam that is not condensed and is then recirculated with the nitrogen.

The steam mixed with nitrogen can be totally condensed and separated only if the stream is cooled down at temperature below zero. In order not to introduce a device able to refrigerate the stream at temperature lower than 0 °C the condensation could be only partial. Considering an ambient temperature of 298 K the minimum temperature at which the mixture can be reasonably cooled is 313 K. At ambient pressure this would mean a separation of the two substances with in any case a quite high efficiency.

The following graph shows the behaviour of the gaseous fraction inside the stream of nitrogen and steam. The so-called vapour fraction in the following graph is comprehensive of both water and nitrogen in gaseous form. When the curve reaches the plateau for low temperature it means that no more water is present in the form of steam but, the only gaseous species is nitrogen.

To have a complete steam condensation the temperature has to be lowered to less than 270 K and so under the water freezing point. To cool down the stream at temperature lower than ambient condition is necessary to introduce a refrigerant cycle with significant consequence on the system efficiency.

Instead if the temperature of the stream is cooled down to temperature only some grades higher than the ambient condition the amount of vapour that can be separated is already very high so the introduction of a refrigerant cycle would make no sense.

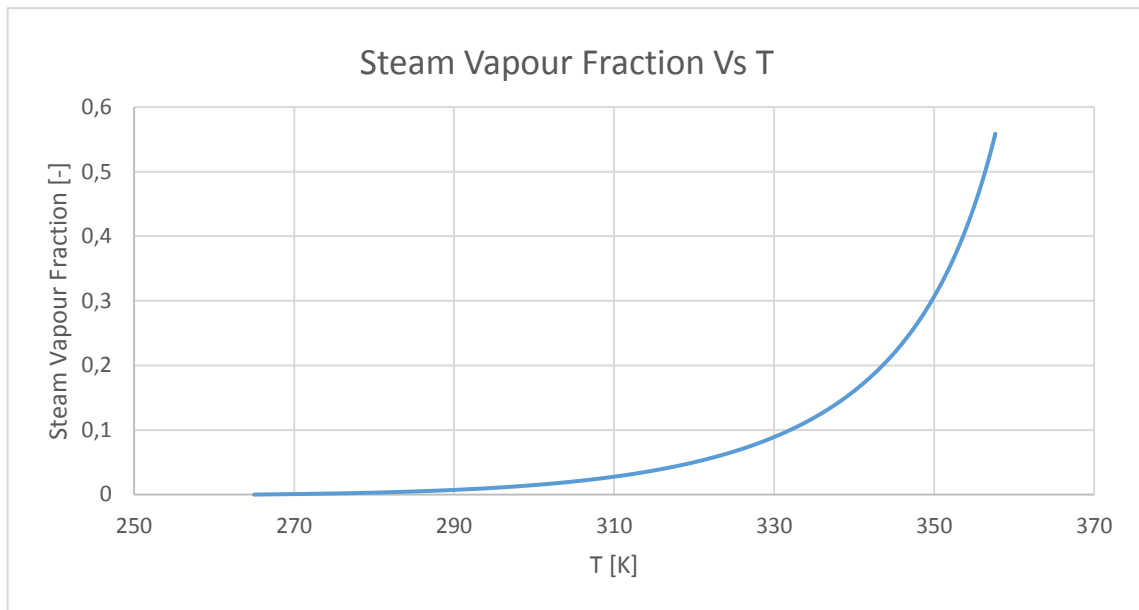


Figure 46: vapour fraction vs temperature during condensation at ambient pressure in presence of nitrogen.

he separation efficiency of the steam from the stream is plotted in the following graphic and it can be seen that the main gain is obtained between for temperature higher than 310 K as more than the 90 % of the steam can be condensed reaching this temperature. The condensation of steam at ambient pressure start not anymore at 373.15 K but at 357.65 K.

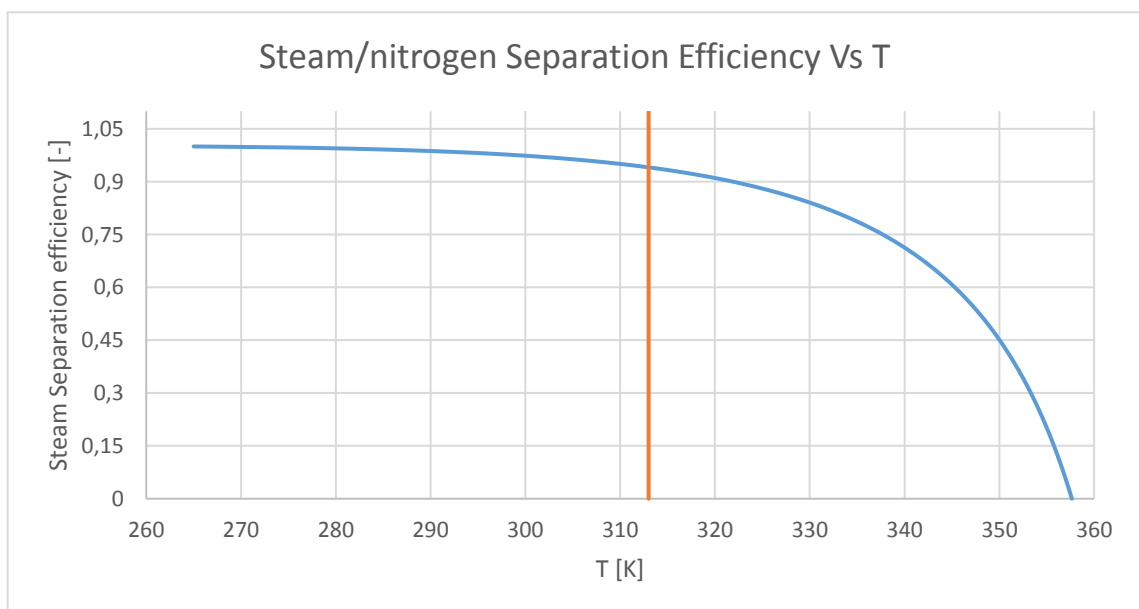


Figure 47: separation efficiency of steam from nitrogen by condensation vs temperature.

If we cool the stream to a temperature of 313 K, that means having a minimum temperature approach to the ambient condition of 15 K, the amount of steam that can be condensed and separated is about 95%.

Next figure, number 48, shows the temperature versus the heat power exchanged by the condensation process of the nitrogen/steam stream.

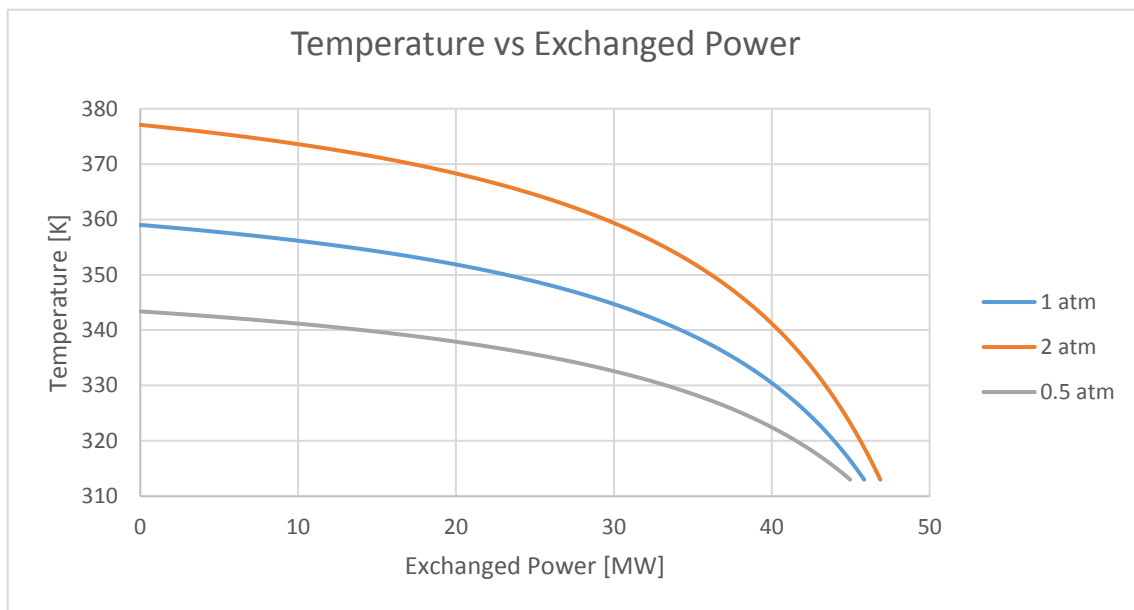


Figure 48: temperature profile during steam and nitrogen flow condensation vs exchanged power.

Figure 48 shows a comparison between three different pressure levels: 0.5, 1 and 2 atmospheres in order to show how the pressure can modify the process. In the studied layout the pressure level is 1 atmosphere. At 1 atmosphere the main part of the heat is available in the temperature range between 358 K and 313 K. This is the same temperature range in which the main part of the steam can be separated. In this temperature range the heat released is around 85 % while the separated heat is around 95 %; the difference is related to the sensible heat exchanged by the nitrogen.

Another way to reach a complete condensation of the steam and so a complete separation of the two substances is to work at higher pressure thus increasing the temperature of complete condensation

The best working temperature at a different pressure will be in any case different from the equilibrium one. The temperature should be chosen also depending on the resulting rate of

reaction achieved in the new working condition as it is affected by the distance from the working condition in respect to the equilibrium.

As the dehydration process seems to be faster than hydration one the temperature of dehydration could be nearer to the equilibrium curve than the hydration one. In the reference case, for an equilibrium temperature at ambient pressure of 792 K, the chosen hydration temperature was 743 and 813 for the dehydration. So, the dehydration was settled at a temperature of 21 K higher than the equilibrium while the hydration at a temperature of 49 K lower than the equilibrium.

Figure 49 shows the system layout with the nitrogen as fluidizing agent in the dehydration process.

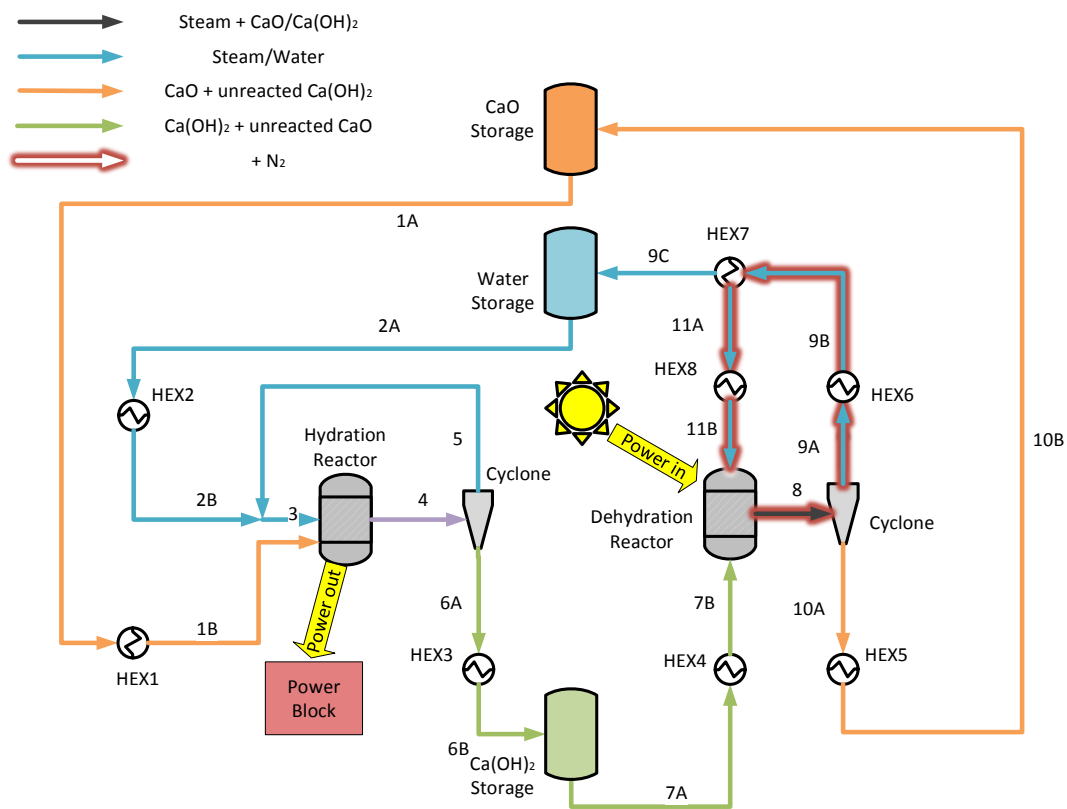


Figure 49: system layout with N_2 as dehydration fluidizing agent.

In figure 49 the HEX number 7 is where the separation of steam and nitrogen is carried out by condensation. Nitrogen flow is only present where the arrows in figure 49 are labelled with red colour. Due to the not unitary efficiency of separation from steam some traces of nitrogen are also present in stream 9 to the water storage where it can be separated by decantation.

Table 13 is referred to the characterization of the equipment shown in figure 48.

Equipment	Q	p	T_{in}	T_{out}
[name]	[MW]	[bar]	[K]	[K]
HEX1	40,78	1,01	298	743
HEX2	59,62	1,01	298	743
HEX3	-82,21	1,01	743	298
HEX4	72,36	1,01	298	795
HEX5	-44,45	1,01	795	313
HEX6	-26,21	1,01	795	359
HEX7	-45,85	1,01	359	313
HEX8	11,57	1,01	313	743
Hydration reactor	-101,23	1,01	743	743
Dehydration reactor	100	1,01	795	795
CaO storage	0	1,01	298	298
Ca(OH)₂ storage	0	1,01	298	298
Water storage	0	1,01	298	298

Table 15: equipment characterization.

All the storages are assumed to be at ambient temperature. Streams 9C leaves the system to enter the water storage at a temperature higher than the environment (313 K) but the energy related to this stream is neglected as it is at low temperature.

Table 14 contains the information about the streams shown in figure 48.

Stream	Total flow	CaO	Water	Ca(OH)₂	N₂	Temperature	Pressure
[name]	[kg/s]	[kg/s]	[kg/s]	[kg/s]	[kg/s]	[K]	[bar]
1A	96,07	85,99	0,00	10,08	0,00	298,00	1,01
1B	96,07	85,99	0,00	10,08	0,00	743,00	1,01
2A	17,96	0,00	17,96	0,00	0,00	298,00	1,01
2B	17,96	0,00	17,96	0,00	0,00	743,00	1,01
3	33,48	0,00	33,48	0,00	0,00	743,00	1,01
4	129,56	30,10	15,52	83,93	0,00	743,00	1,01
5	114,03	30,10	0,00	83,93	0,00	743,00	1,01
6A	15,52	0,00	15,52	0,00	0,00	743,00	1,01

Stream	Total flow	CaO	Water	Ca(OH) ₂	N ₂	Temperature	Pressure
[name]	[kg/s]	[kg/s]	[kg/s]	[kg/s]	[kg/s]	[K]	[bar]
6B	15,52	0,00	15,52	0,00	0,00	743,00	1,01
7A	114,02	30,10	0,00	83,93	0,00	298,00	1,01
7B	114,02	30,10	0,00	83,93	0,00	795,00	1,01
8	135,58	86,00	18,98	10,07	20,53	795,00	1,01
9A	39,51	0,00	18,98	0,00	20,53	795,00	1,01
9B	39,51	0,00	18,98	0,00	20,53	359,00	1,01
9C	17,98	0,00	17,96	0,00	0,02	313,00	1,01
10A	96,07	86,00	0,00	10,07	0,00	795,00	1,01
10B	96,07	86,00	0,00	10,07	0,00	313,00	1,01
11A	21,53	0,00	1,03	0,00	20,51	313,00	1,01
11B	21,53	0,00	1,03	0,00	20,51	795,00	1,01

Table 16: streams characterization.

An interesting work on the influence of the pressure on the charging step has been made by Schmidt et al [39]. In that work are studied different dehydration steam partial pressure in an experimental batch reactor. The studied steam partial pressure range goes from 1.4 kPa to 19.9 kPa at different temperature. Figure 50 show the results of the cited work and is related to a steam partial pressure of 10 kPa at different temperature.

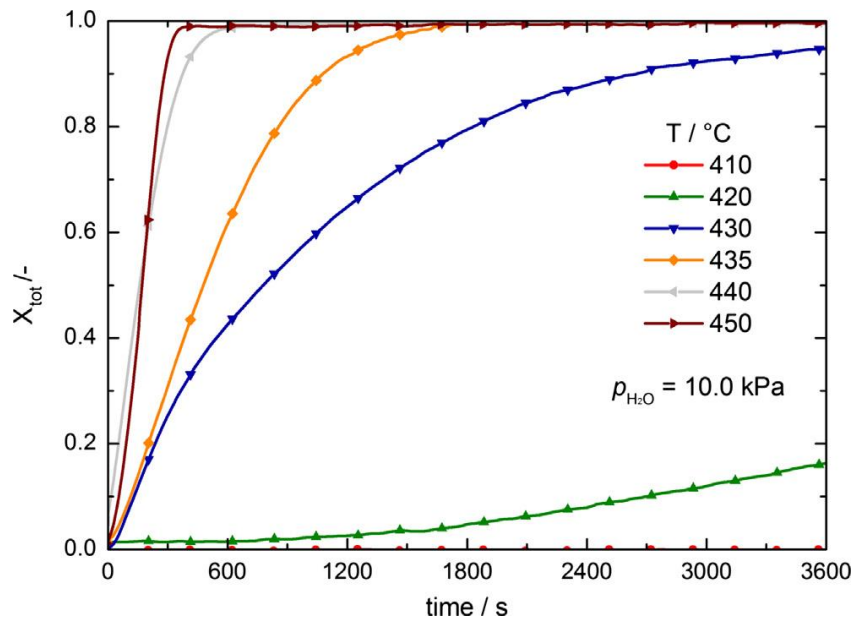


Figure 50: dehydration conversion at different steam temperatures [39].

In figure 50 it can be seen that with a temperature higher than 713 K (440°C) the rate of conversion becomes very high. At this pressure the equilibrium temperature evaluated with Barin equation is 685 K (412 °C) and so the temperature difference from the equilibrium is of 28 K.

It is plausible that for higher temperature difference in respect to the equilibrium the rate of reaction would be also higher and already at this temperature the conversion approach to 1 in about 300 seconds. As reported also by Criado et al. [20] the dehydration reaction developed under low steam partial pressure continues to show rates of reactions fast enough. So it could be assumed that for dehydration at different partial pressure the temperature difference from the equilibrium to have a rate of reaction high enough could be between 40 and 20 K.

It should be intended that for higher temperature the difference of the working condition in respect to the equilibrium temperature could be lower with the same rate of reaction. The following simulation is made setting a constant level of power input to the dehydration reactor that is fully absorbed by the reaction and considering a temperature difference of 30 K in respect to the reactor working condition from the equilibrium curve at the same steam partial pressure. The assumption on the fixed temperature difference from the equilibrium is set to have a rate of reaction that should be fast enough to have a good conversion value of the calcium hydroxide.

The molar and mass conservation principle are respected imposing the match between the inlet and outlet streams of the system.

The conversion value in the hydration reactor is kept constant at 0.65 as in the reference case. In the dehydration reactor the conversion value is changed with the temperature of reaction in order to simulate different scenarios that show different steam partial pressure at the outlet of the dehydration reactor.

The inlet molar amount of the calcium hydroxide to the dehydration reactor is changed time by time to meet both the power input boundary condition but also the one on the dehydration conversion values

Figure 51 shows the working point to which the system can work without any limitation and respecting the previous assumptions.

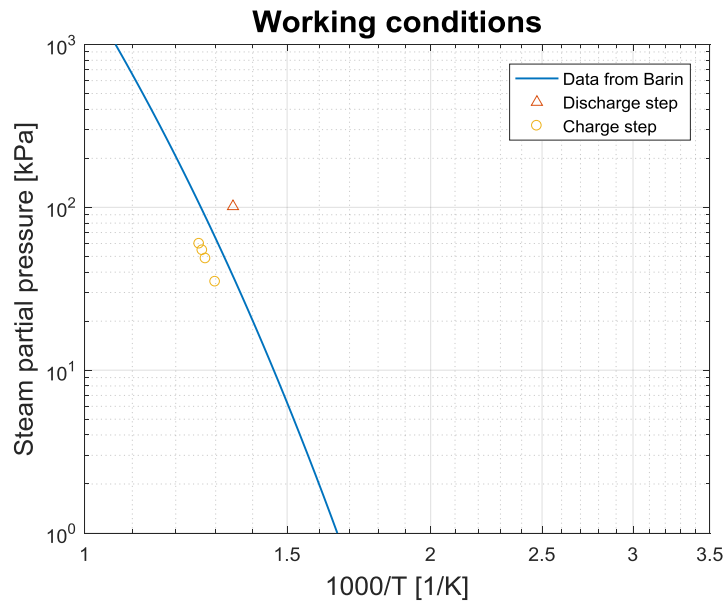


Figure 51: system working point with different steam pressures for the charging step.

The shown working points are the following:

Pressure [kPa]	Temperature [K]	$X_{\text{Dehydration}}$ [-]
34,92	770	0,22
48,48	785	0,46
54,47	790	0,64
59,75	795	0,88

Table 17: main data about the result of the dehydration step carried out at low steam pressure.

At lower temperature the steam partial pressure in the dehydration reactor that can be reached is so low that the dehydration conversion can be only lower than 22 % with a hydration conversion of 65 %.

As the dehydration conversion and the partial pressure are directly correlated the lowering of the temperature is directly linked to a lower conversion in order to have steam partial pressure under the equilibrium curve.

With the introduction of the nitrogen if the other parameters are kept constant the dehydration temperature can be lowered only of about 20 to 25 K.

The only way to overcome the limitation linked to the direct dependence between dehydration conversion and steam partial pressure is to have a higher nitrogen molar flow in order to have a higher dilution of the steam and so also a lower partial pressure. This could be the way to lower the dehydration temperature in a more consistent way.

Figure 52 shows the thermal efficiency of the system with N₂ as fluidizing agent when the dehydration conversion value is varied between 0.22 and 0.88. The blue line in figure 52 is made with a N₂ ratio in respect to the steam at the inlet of the dehydration reactor of 95.21%, in weight on gaseous species base, while at the outlet is, always in weight on gaseous species base, 51.96 %. The yellow and the grey line are made considering respectively a double and a half N₂ mass flow at the inlet of the reactor. For all the lines the trend is quite linear with a steeper behaviour for conversion lower than 0.5. In this case the thermal efficiency is evaluated considering any type of heat exchanger network and so all the heat correlated to the outgoing streams is considered as a loss.

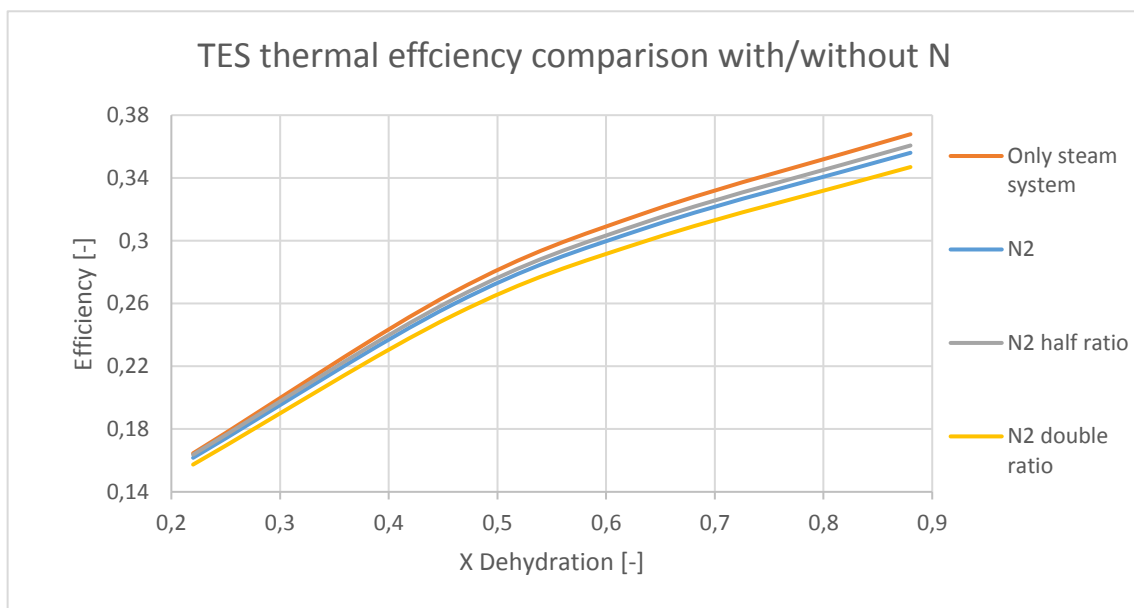


Figure 52: TES efficiency with or without N₂ as fluidizing agent at different N₂/steam ratio.

In the same figure, number 52, is also shown, for a comparison, the TES thermal efficiency for the system without N₂ as fluidizing gas. The comparison is made for the same dehydration conversion values. For the dehydration with only steam the reaction temperature is kept constant at 813 K with atmospheric pressure. The thermal efficiency of the cases referred to the TES system with N₂ shown in figure 52 are calculated as:

Equation 18

$$\eta = \frac{abs(Q_{hydration}) * t_{op}}{(Q_{Hex1} + Q_{Hex3} + Q_{Hex4} + Q_{Hex8} + Q_{Dehy}) * t_{op}}$$

As already said in principle the system is built only to see its energetic needs and so the source of the heat that have to be delivered as input to the heat exchanger for the preheating of the cold streams is not defined.

From figure 52 is clear that a high conversion in the dehydration reactor is very important to have a good efficiency of the system. From the comparison between the two system, with or without N₂ ass dehydration fluidizing agent, is underlined as, for the same dehydration conversion the TES thermal efficiency is not so different. The N₂ system show a slightly lower efficiency in each case and for higher conversion also the efficiency gap is higher. In any case the gap is at least around 1 percentage point. This means that introduction of the nitrogen is not a so high penalty for the TES system thermal efficiency. If the nitrogen stream is doubled or halved the efficiency is respectively lower or higher for a certain value of dehydration conversion.

Figure 53 shows a comparison of the dehydration temperatures at which the system works for the different N₂ mass flow in respect to the fixed dehydration conversion.

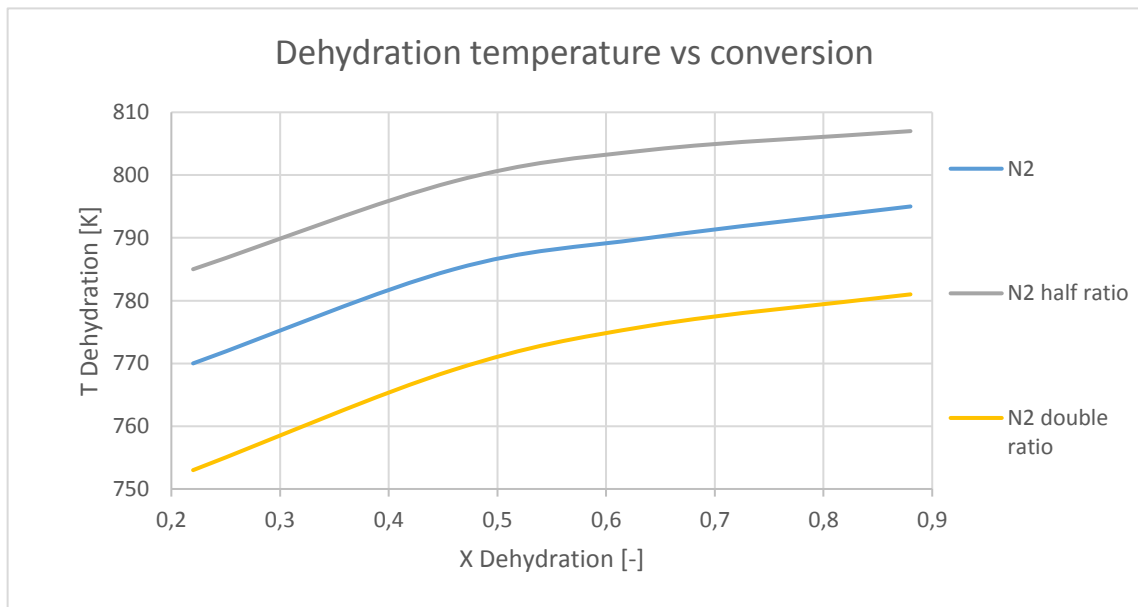


Figure 53: dehydration working temperatures for different N₂ ratio.

From figure 53 is clear that the incrementation of the nitrogen flow would lead to a reduction of the dehydration temperature for the same dehydration conversion value as a higher flow of nitrogen would mean a lower steam partial pressure, as it would be diluted more, and so the temperature of the reaction could be reduced more. If the nitrogen flow is instead reduced the result is the opposite.

5.2.1. Pinch Analysis

To make a comparison with the other configurations and to see if the layout changes have brought some benefit to the system is necessary to make a pinch analysis in order to have the less possible waste of heat from the hot available streams. The chosen case is the one where the nitrogen is simply substituted to steam using the same ratio to the solid mass flow input of stream 7 of figure 49.

The pinch analysis study is made taking as reference the energy input to the dehydration reactor. The choice is to have a constant power input to the dehydration reactor in order to have the analysis done for a case that can be easily compared with other situations. The fixed energy inlet to the dehydration reactor is then kept constant to 100 MW and is only used to run the reaction at the chosen temperature.

So, this amount of energy is completely absorbed by the reaction. If the inlet stream preheating needs heat from the outside to reach the reaction temperature, because the available hot streams are not able to do that, the designed source are the sun during dehydration and the hydration reactor during the discharge step.

The focus of this analysis is also the comparison between the comparison of the results that can be obtained with or without the employment of the nitrogen as fluidizing gas considering a full HEX network in order to reuse all the available heat sources. The other parameter that are kept constant are the conversion in the hydration and dehydration reactors that are respectively 0.65 and 0.88.

For the case with nitrogen as fluidizing agent in the charging step the pinch analysis is made for the case that has a dehydration temperature of 795 K and a partial pressure of 59.75 kPa that correspond to the case in which the nitrogen is simply added to the system.

Table 16 summarize the heat sources and sinks present in the system with their characteristics.

Stream/ Source	Mass flow	Tin	Tout	Cp	C	Q	Cold/ Hot
 [#]	 [Kg/s]	 [K]	 [K]	 [kJ/kgK]	 [kW/K]	 [MW]	 [-]
1	96,1	298	743	0,95	91,69	40,8	cold
2a	18	298	373	4,19	75,33	5,65	cold
2b	18	373	373	-	-	39,39	cold
2c	18	373	743	1,88	33,89	12,54	cold
6	114	743	313	1,269074	144,6744	-62,21	hot
Hydration	-	743	743	-	-	-100,86	hot
7	110,90	298	795	1,27	613,71	70,46	cold
11	20,90	313	795	1,12	521,05	11,19	cold
Dehydration	-	795	795	-	-	100,00	cold
9	38,40	795	313	3,79	1826,04	-70,12	hot
10	93,50	795	313	0,96	462,57	-43,25	hot

Table 18: system hot and cold streams and sources.

During the discharge step the system shows only the following streams and heat sources subdivided between hot and cold side as shown respectively in tables 17 and 18.

Hot side						
Stream/ Source	Mass flow	Tin	Tout	Cp	C	Q
 [#]	 [Kg/s]	 [K]	 [K]	 [kJ/kgK]	 [kW/K]	 [MW]
6	114	743	313	1,269074	144,6744	-62,21
Hydration	-	743	743	-	-	-100,86

Table 19: dehydration step available heat sources.

Cold side						
Stream/ Source	Mass flow	Tin	Tout	Cp	C	Q
 [#]	 [Kg/s]	 [K]	 [K]	 [kJ/kgK]	 [kW/K]	 [MW]
1	96,1	298	743	0,95	91,69	40,8
2a	18	298	373	4,19	75,33	5,65
2b	18	373	373	-	-	39,39
2c	18	373	743	1,88	33,89	12,54

Table 20: dehydration step available cold streams.

The system layout under study during the discharge step doesn't show any big difference from the base case as the introduction of the nitrogen affects only the charging step system layout. Figure 54 shows the heat cumulative of the discharge step.

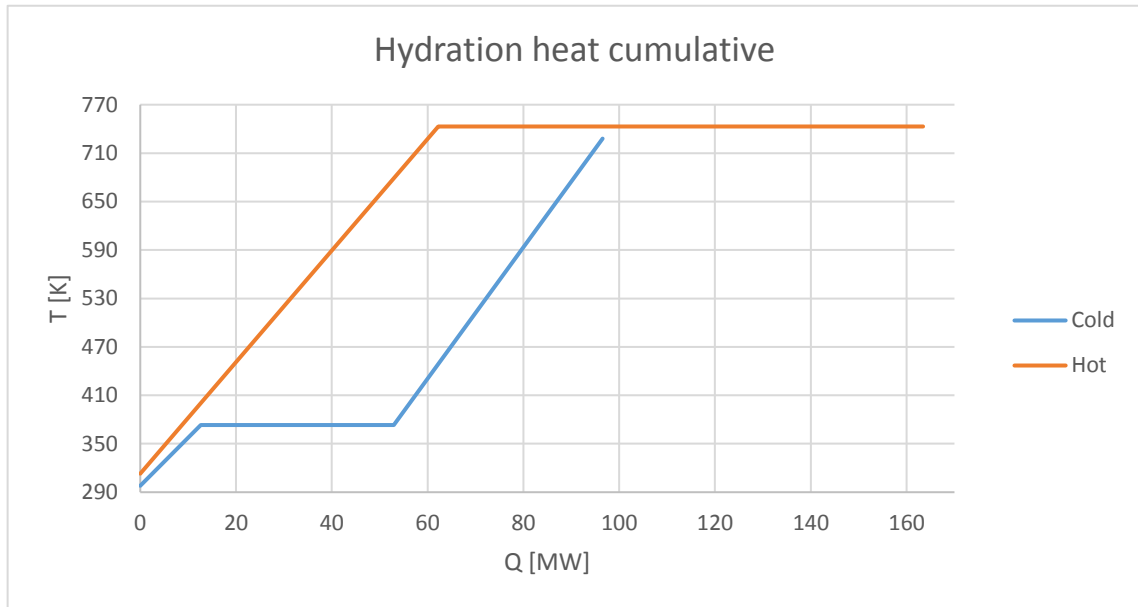


Figure 54: discharging step heat cumulative.

As can be seen by figures 54 and 55 the situation is the same with the pinch point temperature at 313 K for the hot side and at 298 K for the cold side of the discharge step that are linked to the steam condensation temperature. It can be seen that the required heat by the cold side can be provided only by exploiting part of the heat released during the hydration reaction. The amount of heat that the hydration reactor has to cover is about 37.29 MW and so the remaining heat for other application is about 63.67 MW.

In figure 55 is shown the Hex network configuration for the discharge step system with all the heat coupling underlined.

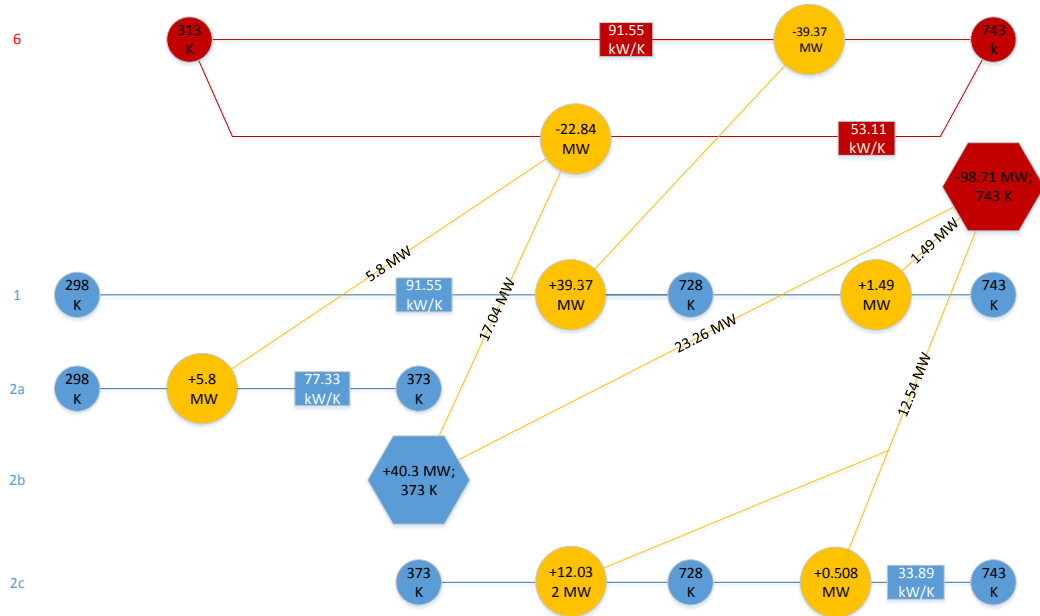


Figure 55: Hydration HEX network configuration.

During the charging step the system works only with the following list of streams and heat source or sink subdivided between hot and cold side:

Hot side						
Stream/ Source	Mass flow	Tin	Tout	Cp	C	Q
[#]	[Kg/s]	[K]	[K]	[kJ/kgK]	[kW/K]	[MW]
9	38,40	795	313	1,52	664,06	-70,12
10	93,50	795	313	0,96	462,57	-43,25

Table 21: charging step available hot streams and sources.

Cold side						
Stream/ Source	Mass flow	Tin	Tout	Cp	C	Q
[#]	[Kg/s]	[K]	[K]	[kJ/kgK]	[kW/K]	[MW]
7	110,90	298	795	1,27	613,71	70,46
11	20,90	313	795	1,12	521,05	11,19
Dehydration	-	795	795	-	-	100,00

Table 22: charging step available cold streams and sources.

Figure 56 shows the heat cumulative for the hot and the cold sides during the charging step.

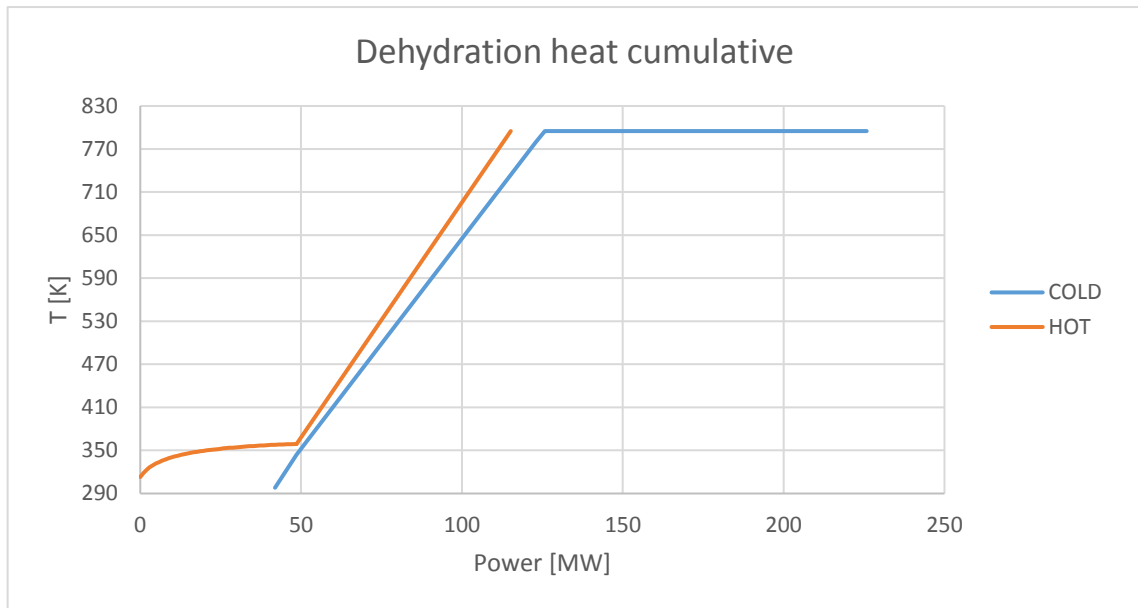


Figure 56: dehydration heat cumulative.

In this case the hot cumulative is different from the other case due to the behaviour of the steam condensation in the mixed stream with nitrogen. In the cold one there is also the presence of the nitrogen stream that has to be reheated before entering the dehydration reactor. In this case the pinch point is at 359 K that is the temperature at which starts the steam condensation of the stream mixed with nitrogen.

Figure 57 shows the HEX network for the charging step.

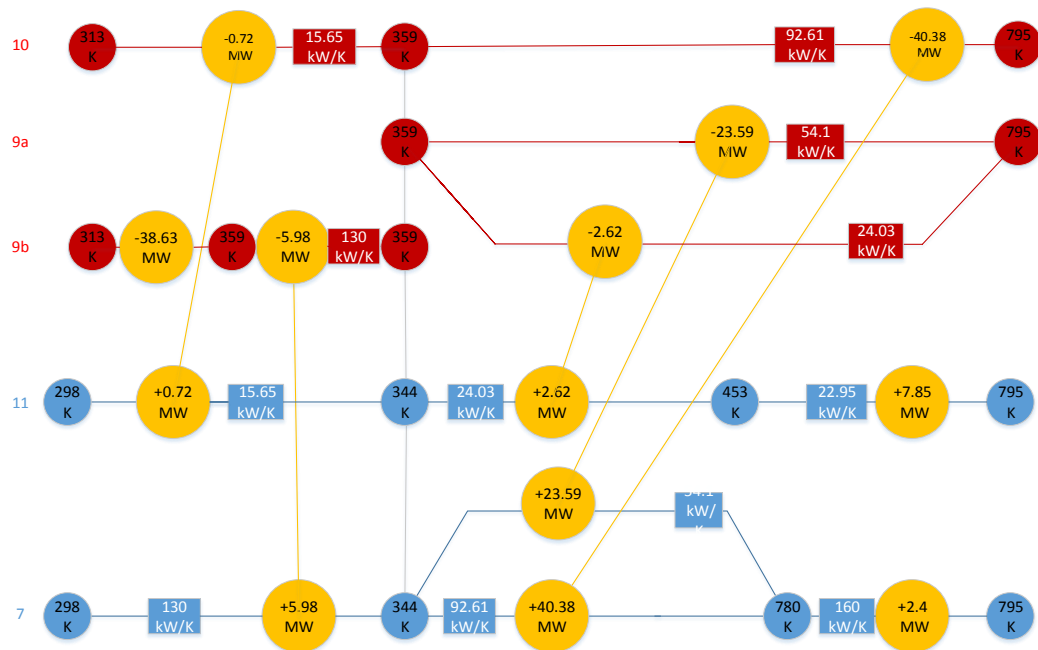


Figure 57: Charging step HEX network configuration.

As can be seen in figure 56 and 57 the hot side can cover only a part of the heat demand of the cold side required for the preheating of the streams at the inlet of the dehydration reactor. Due to that the amount of heat that has to be provided by the sun should be higher than the 100 MW used to run the reaction. This amount of heat, as can be clearly seen in figure 56, is about 10.25 MW. Most of the heat released during the condensation of the steam, also in this case, is released in the environment as it can be used to preheat some cold streams during the charging step. Considering the amount of power that the hydration reactor can provide for other applications, 63.67 MW, and the total amount of heat that is needed from the sun to run the dehydration process, 110.25 MW, the TES efficiency after the pinch analysis reach a value of 57.75 %.

From figure 57 we can also see that during the charging step there is about 39.35 MW of thermal power available at temperatures lower than 359 K that are not used by the process and that are then released to the environment. Potentially this heat can be stored and reused during the hydration process.

Table 23 shows a comparison of the TES before and after the pinch analysis.

Parameter	Unit	Before	After
TES thermal efficiency	[%]	36.01	57.75
Power output	[MW]	100.86	63.67
Power input	[MW]	280.03	110.25

Table 23: before and after pinch analysis comparison

In this case the pinch analysis has reduced the needed power input of 169.78 MW increasing the TES thermal efficiency of 21.74 percentage points in respect to the system with the same initial boundary conditions. As already said in the previous case the TES energy efficiency is calculated making the ratio of the power output and input values because the operational time of the charging and discharging steps are considered equal.

5.3. Series of Dehydration Reactors

The only way to have a greater reduction in the dehydration temperature is to have a higher steam dilution. In order to maintain also the same overall conversion of the calcium hydroxide during the dehydration step, and so of the produced steam, the solution could be the introduction of more nitrogen. This could be made ensuring that the reaction takes place in several reactors put in series, instead of only one, so that the flow of solids passing through them always find a stream of nitrogen not yet saturated by the Steam.

With this system configuration the steam production in any reactor would be low, and so the resulting partial pressure, and then the temperature of each reactor could be lowered in a stronger way. The number of the reactor putted in series and the working condition inside them can be changed in order to have the same overall conversion at the end of the process.

This new system layout has been tested for different configurations with a number of dehydration reactors between two and five. In table 21 are reported the main data referred to the different system layout configurations.

# of Dehydration Reactors	1	2	3	4	5
Temperature [K]	795	780	770	762	756
Steam Partial Pressure [kPa]	59,75	43,71	35,14	29,85	26,34
Efficiency [%]	35,60	34,53	33	32,50	31,58
HEX8 [MW]	11,57	22,31	33,06	42,64	52,51
HEX7 [MW]	-45,85	-46,11	-46,11	-46,55	-46,72
HEX6 [MW]	-44,45	-42,84	-42,33	-40,95	-40,35
HEX5 [MW]	-26,21	-35,88	-46,08	-54,84	-64,24
HEX4 [MW]	72,36	69,68	68,62	66,55	65,55
HEX3 [MW]	-62,21	-61,96	-61,9	-61,72	-61,65
HEX2 [MW]	59,62	59,4	59,33	59,12	59,14
HEX1 [MW]	40,8	40,64	40,6	40,49	40,43
Qin [MW]	100	100	100	100	100
Qout [MW]	-101,23	-100,85	-100,65	-100,41	-100,31
Mass flow stream #11 [kg/s]	114	113,6	113,5	113,1	113
Molar flow stream #11 [kmol/s]	1,67	1,66	1,66	1,66	1,65

Table 24: results and data of the TES system with different steam partial pressure in the dehydration process.

We can see that the evolution of the temperature that the dehydration reactors can reach with an increasing number of reactors putted in series is not so fast and also with a series of 5 reactor the temperature is lowered only of about 60 Kelvin. The relation between the number of reactors and the temperature is similar to the one between temperature and partial pressure as these factors are all correlated. Adding more reactors would means have step by step a lower benefit with a more and more complex system. Figure 58 shows the behaviour of the dehydration temperature in respect to the number of reactors putted in series

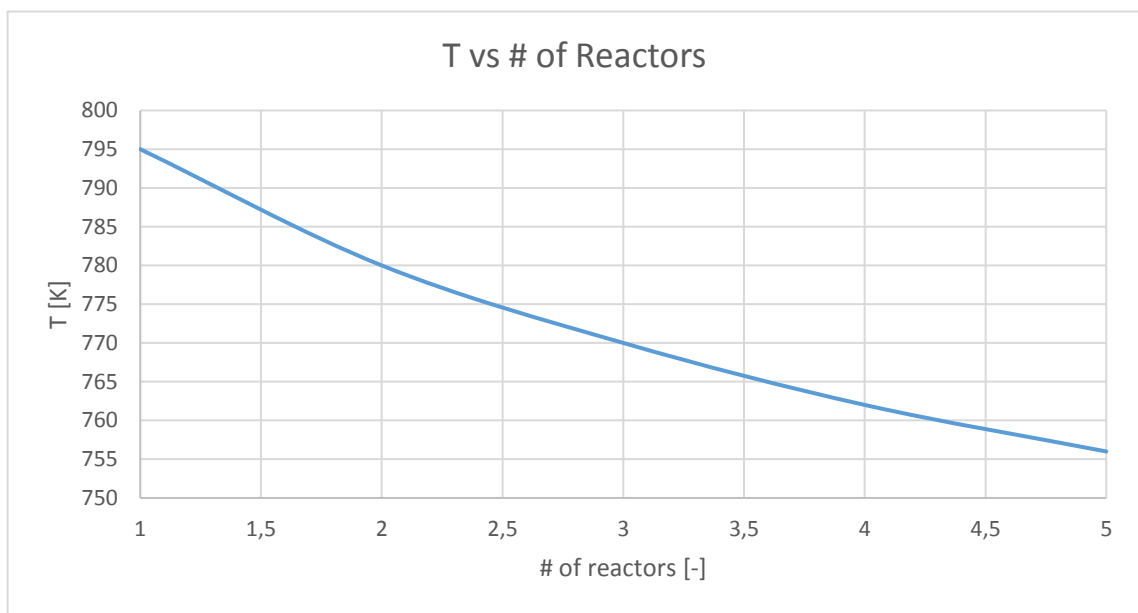


Figure 58: Dehydration temperature as function of reactors number.

The temperatures shown in figure 58 are the lowest that can be obtained using the specified number of reactors keeping the overall conversion of the dehydration process always constant. With five reactors in series the temperature decrement is only a 5 % in respect to the initial value.

As the trend of the curve becomes flatter with the increment of the reactors number is clear that adding more reactors will brings to lower and lower benefits.

As can be seen in figure 59 the efficiency shows a decreasing linear behaviour as the number of reactors putted in series is increased.

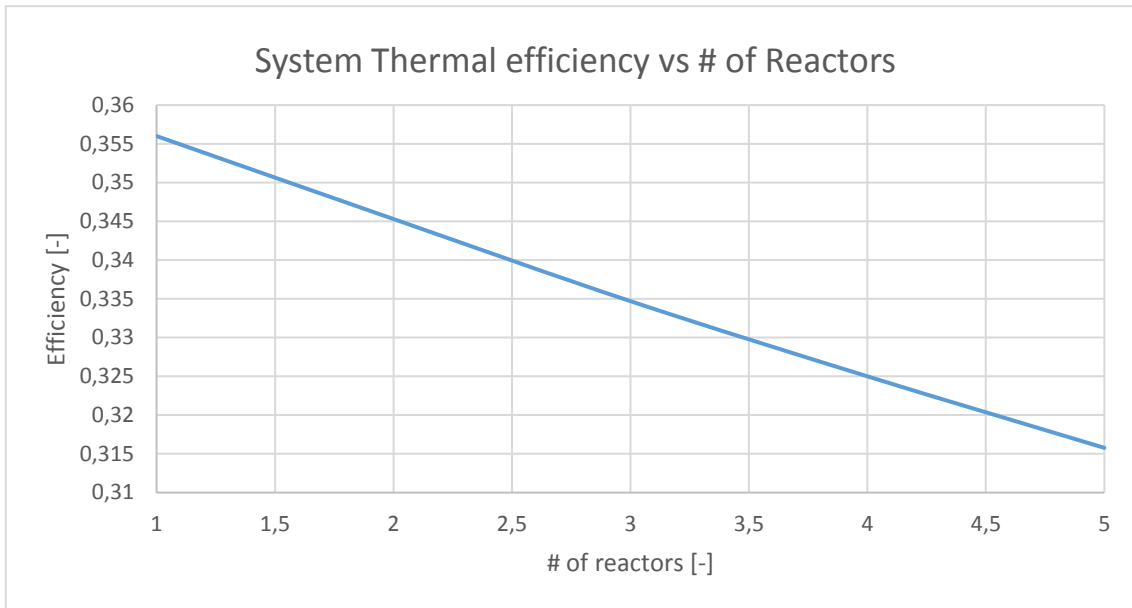


Figure 59: TES thermal efficiency vs number of dehydration reactors.

In figure 59 we can see that with 5 reactors the TES thermal efficiency is lowered of 4 percentage points that means a reduction of 0.75 percentage points for each added reactor.

Figure 60a shows the hydration process.

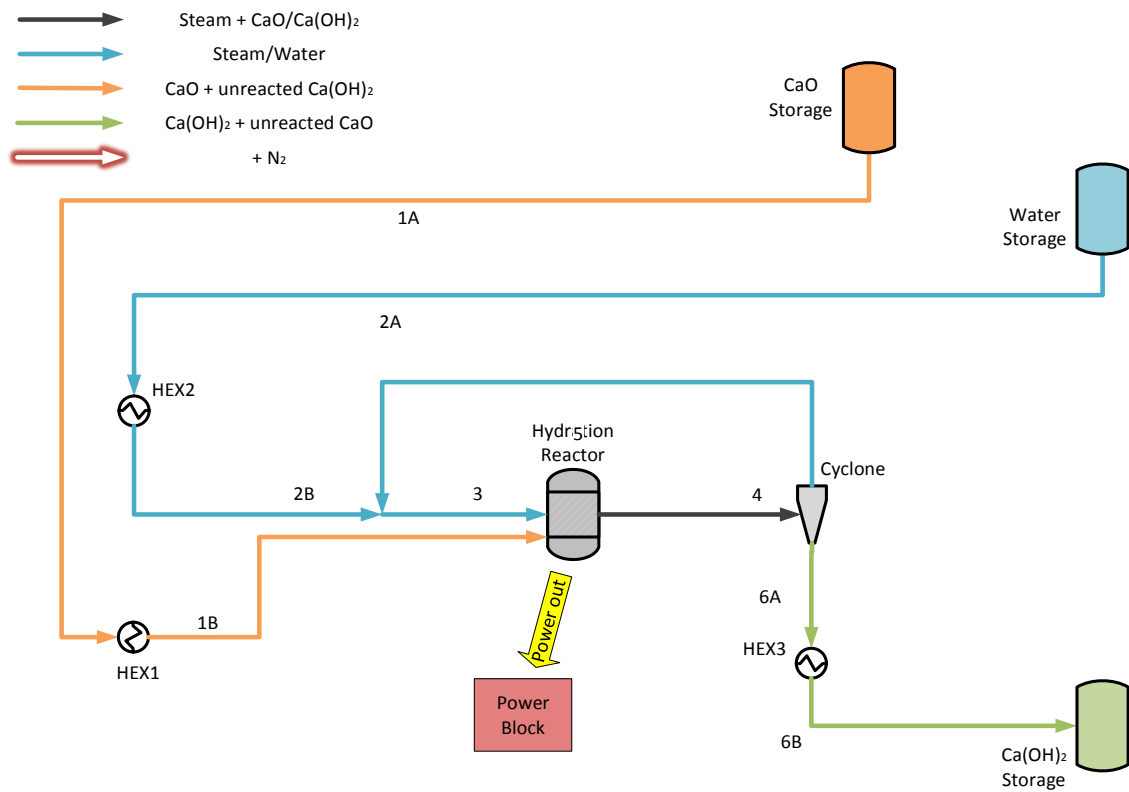


Figure 60a: Hydration step system layout

Figure 60b shows the dehydration process with 3 reactors in series.

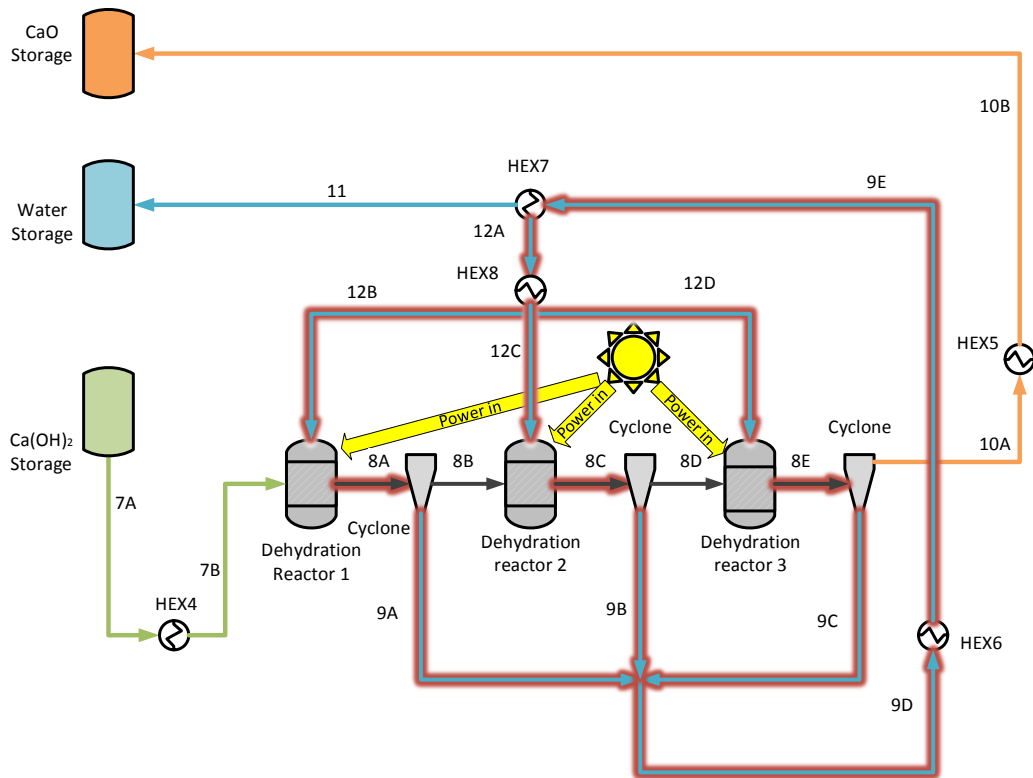


Figure 60b: Dehydration step with 3 reactors system layout.

Table 25 shows the main data of the equipment in figures 60a and 60b.

Equipment	Q	Pressure	Tin	Tout
Name	[MW]	[bar]	[K]	[K]
HEX1	40,55	1,01	298	743
HEX2	59,25	1,01	298	743
HEX3	-61,83	1,01	743	313
HEX4	67,95	1,01	298	770
HEX5	-41,8	1,01	770	313
HEX6	-45,46	1,01	770	346
HEX7	-46,35	1,01	346	313
HEX8	32,64	1,01	313	770
Hydration reactor	-100,6	1,01	743	743
Dehydration R1	33,33	1,01	770	770
Dehydration R2	33,33	1,01	770	770
Dehydration R3	33,33	1,01	770	770

Equipment	Q	Pressure	T_{in}	T_{out}
Name	[MW]	[bar]	[K]	[K]
Water storage	0	1,01	298	298
CaO storage	0	1,01	298	298
Ca(OH)₂ storage	0	1,01	298	298

Table 25: equipment data of the system .

Table 26 shows the main data about the streams of figures 60a and 60b.

Stream	Total flow	CaO	Water	Ca(OH)₂	N₂	Pressure	Temperature
Name	[kg/s]	[kg/s]	[kg/s]	[kg/s]	[kg/s]	[bar]	[K]
1A	95,48	85,46	0,00	10,02	0,00	1,01	298,00
1B	95,48	85,46	0,00	10,02	0,00	1,01	743,00
2A	17,85	0,00	17,85	0,00	0,00	1,01	298,00
2C	17,85	0,00	17,85	0,00	0,00	1,01	743,00
3	33,27	0,00	33,27	0,00	0,00	1,01	743,00
4	128,75	29,91	15,43	83,41	0,00	1,01	743,00
5A	15,43	0,00	15,43	0,00	0,00	1,01	743,00
5B	15,43	0,00	15,43	0,00	0,00	1,01	743,00
6A	113,32	29,91	0,00	83,41	0,00	1,01	743,00
6B	113,32	29,91	0,00	83,41	0,00	1,01	313,00
7A	113,32	29,91	0,00	83,41	0,00	1,01	298,00
7B	113,32	29,91	0,00	83,41	0,00	1,01	770,00
8A	134,74	48,43	6,97	58,95	20,40	1,01	770,00
8B	107,37	48,43	0,00	58,95	0,00	1,01	770,00
8C	128,80	66,94	6,97	34,48	20,40	1,01	770,00
8D	101,43	66,94	0,00	34,48	0,00	1,01	770,00
8E	122,85	85,46	6,97	10,02	20,40	1,01	770,00
9A	27,37	0,00	6,97	0,00	20,40	1,01	770,00
9B	27,37	0,00	6,97	0,00	20,40	1,01	770,00
9C	27,37	0,00	6,97	0,00	20,40	1,01	770,00
9D	82,11	0,00	20,91	0,00	61,20	1,01	770,00
9E	82,11	0,00	20,91	0,00	61,20	1,01	345,96
10A	95,48	85,46	0,00	10,02	0,00	1,01	770,00

Stream	Total flow	CaO	Water	Ca(OH) ₂	N ₂	Pressure	Temperature
Name	[kg/s]	[kg/s]	[kg/s]	[kg/s]	[kg/s]	[bar]	[K]
10B	95,48	85,46	0,00	10,02	0,00	1,01	313,00
11	17,87	0,00	17,85	0,00	0,02	1,01	313,00
12A	64,25	0,00	3,06	0,00	61,18	1,01	313,00
12B	21,42	0,00	1,02	0,00	20,40	1,01	770,00
12C	21,42	0,00	1,02	0,00	20,40	1,01	770,00
12D	21,42	0,00	1,02	0,00	20,40	1,01	770,00

Table 26: streams data of the system.

The mass and the molar flow that enters in the dehydration reactor remains almost constant in respect to the number of reactors putted in series; we can only see a very small reduction related to the change with temperature of the specific heath of reaction.

As the reaction temperature is decreasing for higher number of reactor then the specific heat of reaction is increasing a little bit and so the amount of calcium hydroxide needed to absorb at constant temperature the same power input became lower.

The dehydration working point tested with the previous layouts are shown in figure 61:

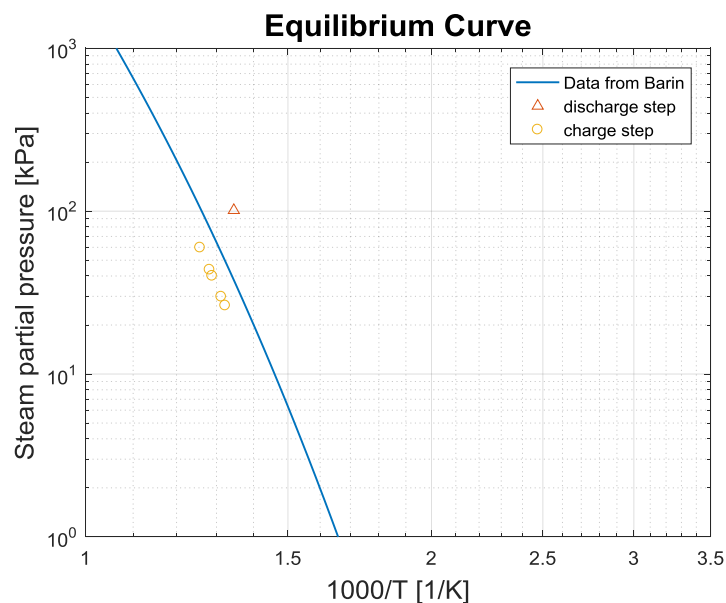


Figure 61: working points with series of dehydration reactors.

The amount of fluidizing agent increases almost linearly with the number of reactors putted in series. This fact can have a important consequence on the electrical overall system efficiency

as an higher nitrogen flow for the same power output means higher electricity consumption to run the fans. The hypothesis to reuse the same nitrogen flow for all the series reactors could be better from an efficiency point of view but it would mean a much more complex system because the nitrogen stream would have to be cooled down and then reheated many more times.

The introduction of the nitrogen as fluidizing agent in order to reduce the dehydration working temperature has a not so high influence on this parameter and to have a significant change the complexity of the system has to be augmented very much introducing more and more reactors in series.

The modifications introduced in the system bring to a reduction of the thermal efficiency of the system. This is mainly due to the facts that the reduction of the heat needed to preheat the inlet stream to the dehydration reactor is not so much and the reduction of the heat of reaction due to the temperature reduction overcome the positive effects.

Moreover, the steam separation from the nitrogen link to the necessity to reheat the fluidizing agent and so it brings to a higher heat demand during the charging step. These needs can be satisfied by a thermal coupling with other system streams to make a heat recover but, in any case, it would mean a more complicated system. The lower temperature at which the system can work could be enough to make an indirect coupling with the solar plant easier also with common HTF.

5.3.1. Pinch Analysis

The pinch analysis in this case is carried out for the layout with three dehydration reactors in series and is made to see how the increment of the nitrogen mass flow affect the heat balance of the system.

The boundary conditions are the same of the previous analysis on the system so the total power input to the three reactors is equal to 100 MW, the overall conversion is 0.65 and 0.88 respectively for hydration and dehydration step and a minimum temperature approach equal to 15 K. Charging and discharging steps work at different times. The hydration and the dehydration temperature are respectively 743 and 770 K, as reported in table 24, for the case with three reactors.

Table 27 shows the hot and cold streams and sources available in the system.

Stream/ Source	Mass flow	T_{in}	T_{out}	C_p	C	Q	Cold/ Hot
 [#]	 [Kg/s]	 [K]	 [K]	 [kJ/kgK]	 [kW/K]	 [MW]	 [-]
1	95,5	298	743	0,95	91,12	40,55	cold
2a	17,8	298	373	4,20	74,80	5,61	cold
2b	17,8	373	373	-	-	40,27	cold
2c	17,8	373	743	2,03	36,14	13,37	cold
6	113,3	743	313	1,269115	143,7907	-61,83	hot
Hydration	-	743	743	-	-	-101,23	hot
7	110,90	298	770	1,34	613,71	67,96	cold
12	20,90	313	770	1,18	521,05	32,65	cold
Dehydration	-	770	770	-	-	100,00	cold
9	82,10	770	313	2,45	1118,27	-91,81	hot
10	95,50	770	313	0,99	452,88	-43,25	hot

Table 27: hot and cold streams and sources of the system.

During hydration the hydration step we have the following hot and cold available streams shown in table 28 and 29.

Hot side						
Stream/ Source	Mass flow	T _{in}	T _{out}	C _p	C	Q
[#]	[Kg/s]	[K]	[K]	[kJ/kgK]	[kW/K]	[MW]
6	113,3	743	313	1,269115	143,7907	-61,83
Hydration	-	743	743	-	-	-101,23

Table 28: hot streams and sources of the hydration step.

Cold side						
Stream/ Source	Mass flow	T _{in}	T _{out}	C _p	C	Q
[#]	[Kg/s]	[K]	[K]	[kJ/kgK]	[kW/K]	[MW]
1	95,5	298	743	0,95	91,12	40,55
2a	17,8	298	373	4,20	74,80	5,61
2b	17,8	373	373	-	-	40,27
2c	17,8	373	743	2,03	36,14	13,37

Table 29: cold streams and sources of the hydration step

In figure 62 is shown the heat cumulative obtained with the previous data.

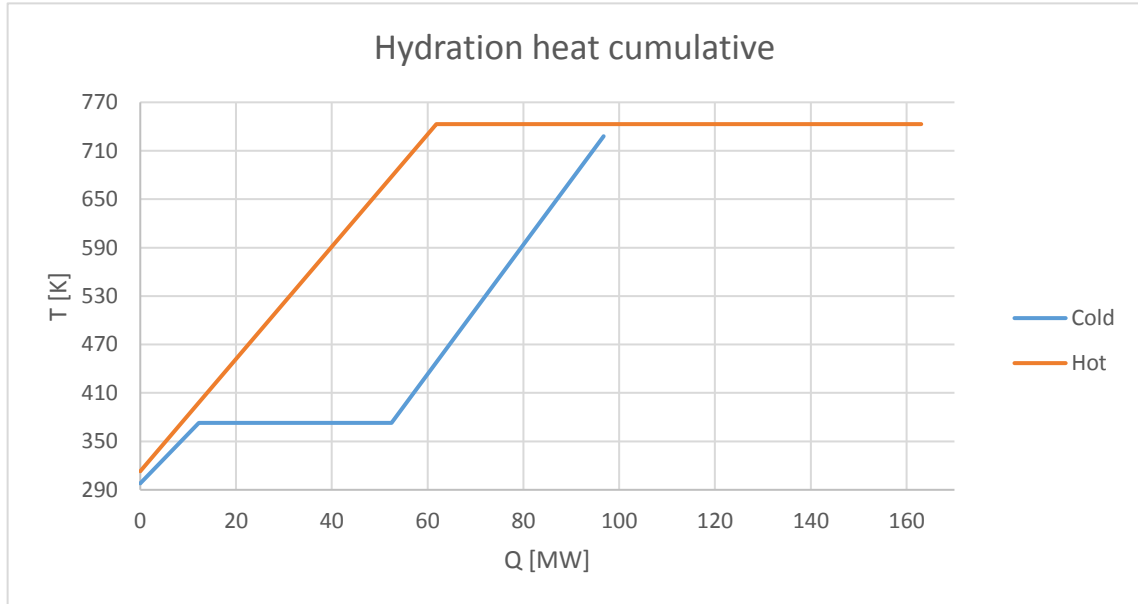


Figure 62: hydration step heat cumulative.

The hydration step is the same of the previous case, there are only some minor variation in the exchanged heat and in the mass flows and so the HEX network that can be used is the same as

before. Also in this case, the pinch point is at 313 K for the hot side and at 298 K for the cold side.

Figure 63 shows the Hex network for the hydration step.

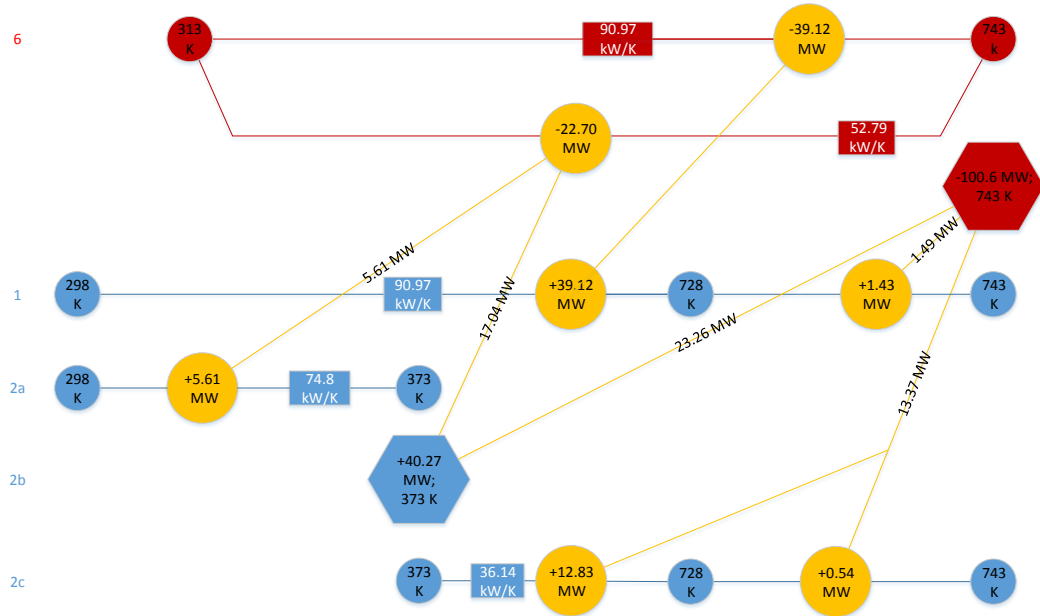


Figure 63: HEX network of the discharge step.

As can be seen from figures 63 and 62 the hydration reactor has to provide a power of about 38.06 MW to sustain the process and so the amount of power that is available for other purposes is about 62.54 MW. From the hydration step all the heat related to the hot streams is reused to preheat the cold streams until the temperature of 313 K. The remaining heat is then released to the environment.

For the dehydration step the available streams and sources are the following that are shown in tables 30 and 31.

Hot side						
Stream/ Source	Mass flow	T _{in}	T _{out}	C _p	C	Q
[#]	[Kg/s]	[K]	[K]	[kJ/kgK]	[kW/K]	[MW]
9a	82,10	770	359	1,35	553,71	-45,46
9b	82,10	359	313	12,27	564,56	-46,35
10	95,50	770	313	0,99	452,88	-43,25

Table 30: dehydration hot streams and sources.

Cold side						
Stream/ Source	Mass flow	T _{in}	T _{out}	C _p	C	Q
[#]	[Kg/s]	[K]	[K]	[kJ/kgK]	[kW/K]	[MW]
7	110,90	298	770	1,34	613,71	67,96
12	20,90	298	770	1,27	521,05	32,65
Dehydration	-	770	770	-	-	100,00

Table 31: dehydration cold streams and sources.

Figure 64 shows the heat cumulative of the dehydration step.

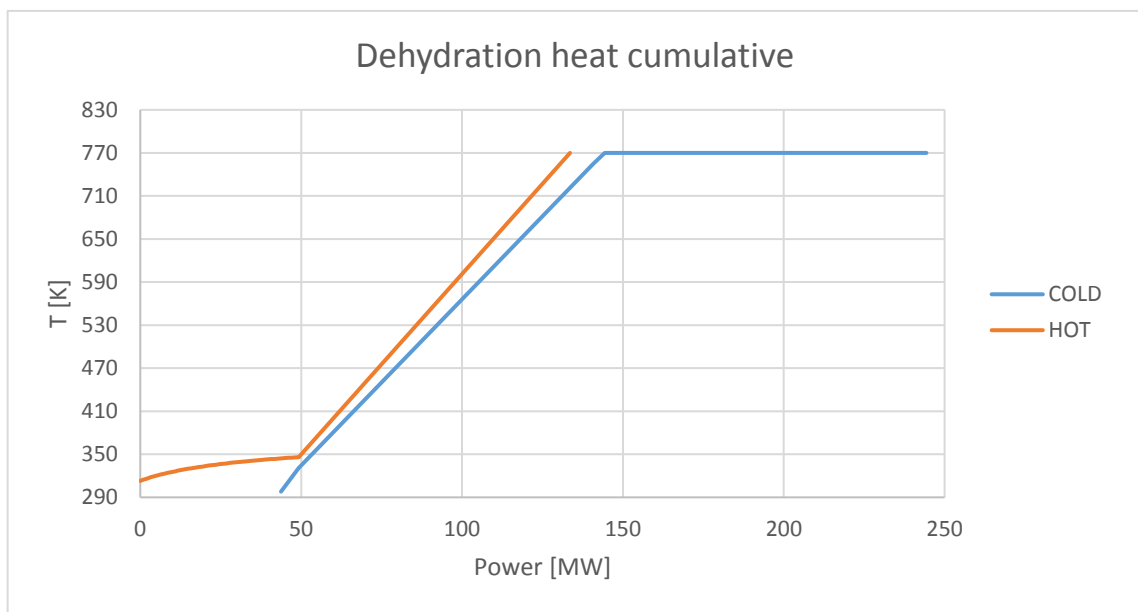


Figure 64: dehydration step heat cumulative

The trend of the cold and hot cumulative in figure 64 is similar to the one shown in figure 55 for the case with only one dehydration reactor and nitrogen as fluidizing agent but in this case the amount of heat and its distribution along the curves is different. This is due to the fact that the heat needed to heat up the nitrogen stream is higher as its flow is also higher.

The reduction of the temperature at which this stream has to be heated up has less influence on the amount of heat needed than the mass flow increment because the flow is triplicated while the temperature is decreased of 15 K. The pinch point is at 346 K for the hot side and at 331 K for the cold one.

Figure 65 shows the HEX network for the dehydration step with 3 reactors in series.

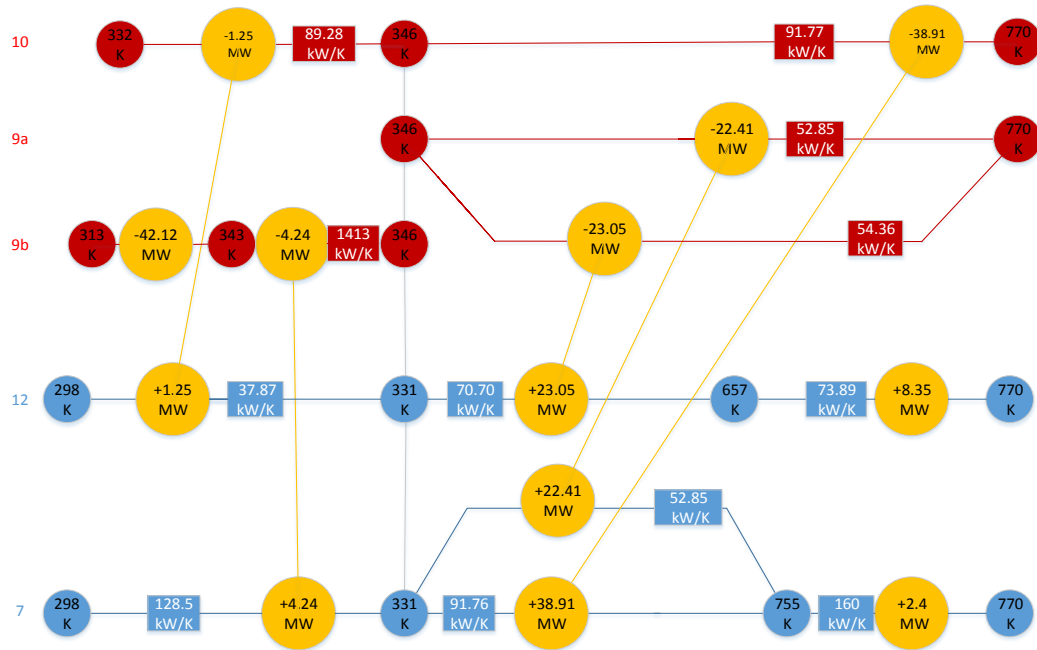


Figure 65: HEX network for dehydration step with three reactors.

From figure 65 and 63 we can see that the preheating of the cold stream is not completely fulfilled by the heat released by the hot streams and so the sun field has to provide about 10.75 MW to complete the preheating and so the total amount of power from the sun is 110.75 MW.

Then, considering the net heat that the hydration reactor can provide we found that after the pinch analysis the TES thermal efficiency is about 56.47 %. Table 32 shows a comparison of the system before and after the pinch analysis made with the same boundary conditions.

Parameter	Unit	Before	After
TES thermal efficiency	[%]	33.69	56.47
Power output	[MW]	101.23	62.54
Power input	[MW]	300.41	110.75

Table 32: before and after pinch analysis comparison.

The pinch analysis has brought to an increment of 22.77 percentage points in the TES efficiency with a reduction of the power requirement of 189.66 MW. The TES thermal efficiency after the pinch analysis is obtained as ratio of the reported values of power output and input as they represent respectively the available output of the hydration reactor and the sum of all the need heat of the system. The calculation is made using the power value instead of the energy values as the operational time of the charge and discharge are, as assumption, of the same length.

5.4. Hydration Pressure Modification

In this case the ambition is to work at higher pressure with only steam as the hydration reaction is well suited to this condition as high concentration of steam will mean a high rate of reaction. The goal could be having a higher temperature in the reactor in order to have a heat source of higher quality and so a higher maximum temperature in the power cycle to reach a higher efficiency. This can be achieved working at a higher partial pressure than the ambient one as for higher steam pressure also the temperature of reaction could be higher. The main positive results would be the release of heat at higher temperature and so a higher maximum temperature of the power cycle in order to reach a higher efficiency. An interesting work on this topic has been made by Schmidt et al [40] in a batch experimental reactor at three pressure levels of interest, 200, 270 and 470 kPa, at a reactor starting temperature of 500 °C. Figure 66 shows the main results of this experiment.

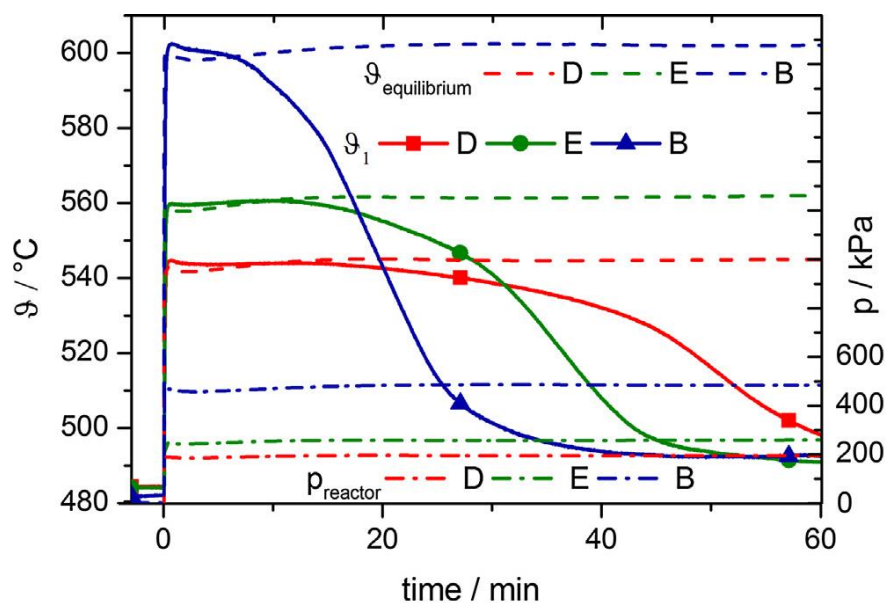


Figure 66: Hydration time behaviour at different temperatures and pressures during Schmidt's experiment [40].

The experimental reactor works with a fixed cooling load and the temperature in different part of the reactor are monitored. In figure 66 are shown the reactor temperature behaviour recorded by the first measurer for different reactor working pressure. As can be seen the temperature reached by the reactor when the reaction is running is the equilibrium one for the selected pressure.

The temperature remains at the equilibrium until the reaction in the neighbourhood of the measurer comes to the end. It is clear that for higher steam pressure the reaction goes faster and it can be also coupled with a higher working temperature. Another interesting result of this paper is that the length of the temperature plateau is dependent on the cooling load because they have seen that for higher cooling load the plateau is shorter.

Their conclusion is that at higher cooling loads the reaction seems to be faster and that at higher working pressure the hydration reaction could be very fast also at temperature very close to the equilibrium. The pressurization of the steam could be done at ambient temperature before the evaporation in order to exploit the fact that a pump specific energy requirement is really lower than the one needed by a compressor or a fan.

As reference, and to have a more conservative assumption, we can take a 50 K difference from the equilibrium temperature, as in the initial reference case, for any pressure tested in a range between 1 and 6 atmospheres.

Figure 67 shows the working conditions of the discharge step in the defined pressure range.

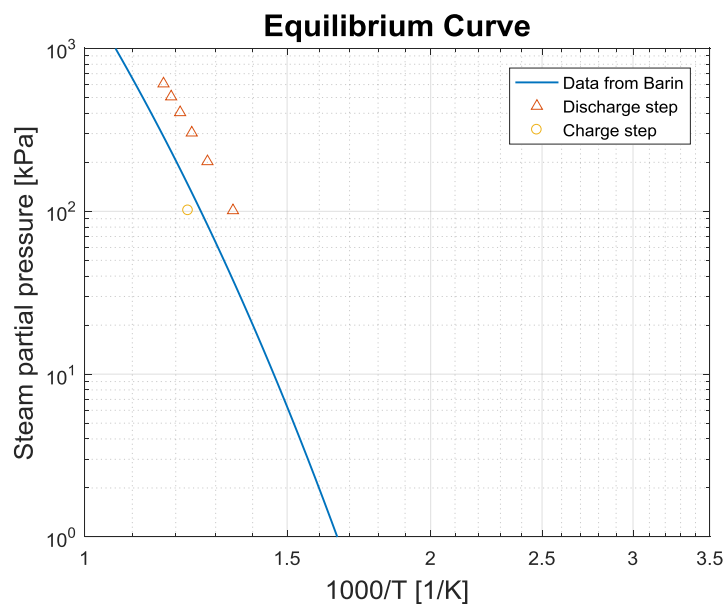


Figure 67: working point of the TES with different hydration pressures.

The reasonable range of temperatures at which heat can be provided by this chemical looping is comparable to the typical range of the common Rankine-Hirn steam cycle. Maximum temperature of a steam cycle is typically about 500-600 °C (773-873 K).

As can be seen these temperatures are higher or at least comparable to the one obtained from the initial discharge condition. With a high pressure and temperatures in the hydration reactor also the maximum temperature of the steam cycle could be higher and so the efficiency of the power block could be higher. Figure 68 shows the behaviour of the TES efficiency as function of the hydration pressure level.

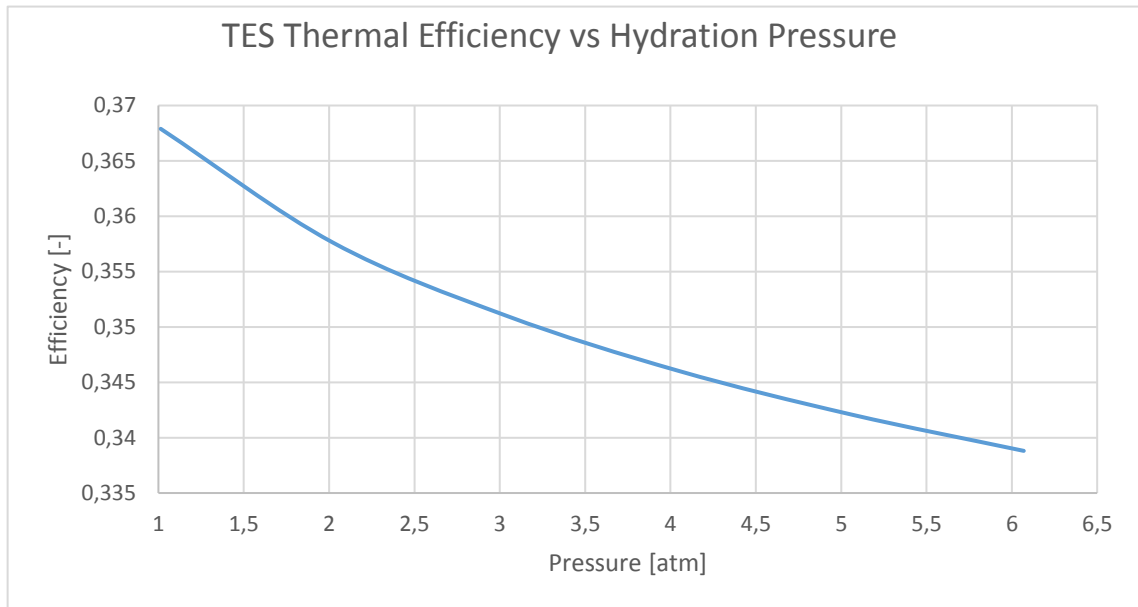


Figure 68: TES thermal efficiency for different hydration pressures.

As can be seen from figure 68, the pressurization and the increment of the hydration reactor temperature would mean a worst result in term of the efficiency of the TES system, as a higher temperature means also a higher heat requirement to preheat the inlet streams for the same power output. Moreover, a higher temperature of hydration means a lower specific heat of reaction and so the power output will be also lower.

The energy requirement for the pressurization is instead very low, as can be seen in table 29, and has not a noticeable influence on the TES performance. The increment of hydration pressure from 1 to 6 bars means a reduction of the TES efficiency of about 2.81 percentage points.

In table 29 are resumed the main results obtained for different hydration pressures.

Hydration Pressure [atm]	1,0	2,0	3,0	4,0	5,0	6,0
Hydration Temperature [K]	743	782	807	826	841	854
Hydration Reactor Duty [MW]	-101,72	-100,75	-100,07	-99,54	-99,10	-98,72
Dehydration Reactor Duty [MW]	100,00	100,00	100,00	100,00	100,00	100,00
HEX1 [MW]	40,97	44,71	47,12	48,96	50,42	51,64
HEX2 [MW]	59,91	61,39	62,34	63,06	63,64	64,11
HEX3 [MW]	-64,41	-70,59	-74,61	-77,71	-80,17	-82,20
HEX4 [MW]	75,62	75,62	75,62	75,62	75,62	75,62
HEX5 [MW]	-62,64	-62,64	-62,64	-62,64	-62,64	-62,64
HEX6 [MW]	-47,73	-47,73	-47,73	-47,73	-47,73	-47,73
PUMP [MW]	0,000	0,003	0,006	0,009	0,012	0,02
Mass Flow #7 [kg/s]	114,58	114,58	114,58	114,58	114,58	114,58
TES Thermal Efficiency [%]	36,79	35,76	35,10	34,60	34,21	33,88

Table 33: TES behaviour for different hydration pressures.

Figure 69 shows the system layouts for a 6 bars hydration pressure conditions.

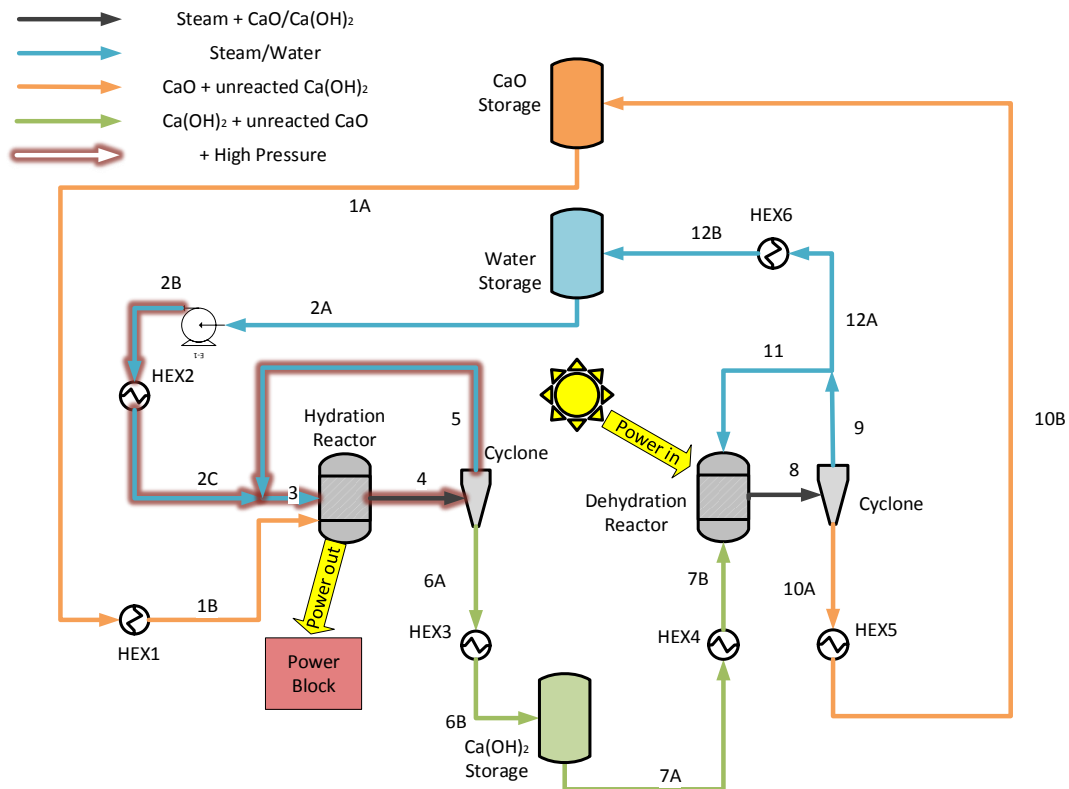


Figure 69: TES System layout with hydration high pressure.

Table 30 shows the equipment details of the layout shown in figure 69.

Equipment	Q or W	Pressure	Tin	Tout
Name	[MW]	[bar]	[K]	[K]
HEX1	51,64	1,01	298	854
HEX2	64,11	6,08	298	854
HEX3	-82,20	1,01	854	298
HEX4	75,62	1,01	298	813
HEX5	-62,64	1,01	813	298
HEX6	-47,73	1,01	813	298
Hydration reactor	-98,72	6,08	854	854
Dehydration reactor	100	1,01	813	813
Pump	0,02	6,08	298	298
CaO storage	0	1,01	298	298
Ca(OH)₂ storage	0	1,01	298	298
Water storage	0	1,01	298	298

Table 34: equipment of figure 69 main data.

Table 31 shows the data of the streams shown in figure 69.

Stream	Total Mass Flow	CaO	Water	Ca(OH)₂	Temperature	Pressure
Name	[kg/s]	[kg/s]	[kg/s]	[kg/s]	[K]	[bar]
1A	96,49	86,41	0,00	10,08	298,00	6,08
1B	96,49	86,41	0,00	10,08	854,00	6,08
2A	18,04	0,00	18,04	0,00	298,00	1,01
2B	18,04	0,00	18,04	0,00	298,07	6,08
2C	18,04	0,00	18,04	0,00	854,00	6,08
3	33,64	0,00	33,64	0,00	854,00	6,08
4	130,13	30,24	15,59	84,29	854,00	6,08
6A	114,53	30,24	0,00	84,29	854,00	6,08
6B	114,53	30,24	0,00	84,29	298,00	1,01
5	15,59	0,00	15,59	0,00	854,00	6,08
7A	114,58	30,24	0,00	84,33	298,00	1,01
7B	114,58	30,24	0,00	84,33	813,00	1,01
8	128,88	86,41	32,34	10,12	813,00	1,01

Stream	Total Mass Flow	CaO	Water	Ca(OH)₂	Temperature	Pressure
Name	[kg/s]	[kg/s]	[kg/s]	[kg/s]	[K]	[bar]
9	32,34	0,00	32,34	0,00	813,00	1,01
10A	96,53	86,41	0,00	10,12	813,00	1,01
10B	96,53	86,41	0,00	10,12	298,00	1,01
11	14,30	0,00	14,30	0,00	813,43	1,01
12A	18,05	0,00	18,05	0,00	813,43	1,01
12B	18,05	0,00	18,05	0,00	298,00	1,01

Table 35: main data of the streams in figure 69.

5.4.1. Pinch analysis

As for the previous cases the analysis is carried out with some fixed boundary conditions; among them there are: the conversion value settled at 0.65 for hydration and 0.88 for dehydration, the dehydration temperature fixed at 813 K, the power input of 100 MW to the dehydration reactor. In this case the analysis is made for a hydration pressure of 6 atmospheres and a hydration temperature of 854 K.

In table 30 are summarized all the streams and heat source or sink main information.

Stream / Source	Mass flow	T_{in}	T_{out}	C_p	C	Q	Cold / Hot
[#]	[Kg/s]	[K]	[K]	[kJ/kgK]	[kW/K]	[MW]	[-]
6	114,50	854	313	1,30	148,60	-80,39	hot
Hydration	-	854	854	-	-	-98,71	hot
1	96,50	298	854	0,93	89,59	51,69	cold
2a	18	298	432,5	4,22	76,13	10,24	cold
2b	18	432,5	432,5	-	-	37,6	cold
2c	18	432,5	854	2,14	38,64	16,29	cold
10	98,50	813	313	0,94	92,82	-46,41	hot
12a	18,00	813	373	2,05	36,95	-16,26	hot
12b	18,00	373	373	-	-	-40,70	hot
12c	18,00	373	313	42,97	773,50	-46,41	hot
7	114,50	298	813	1,28	146,83	75,62	cold
Dehydration	-	813	813	-	-	100,00	cold

Table 36: available heat sources and sinks of the system

In this case the dehydration step is similar to the one present in the base case as the pressure change only affect the hydration step. In tables 31 and 32 are respectively summarized the hot and the cold streams available during the dehydration step.

Hot side						
Stream/ Source	Mass flow	T _{in}	T _{out}	C _p	C	Q
[#]	[Kg/s]	[K]	[K]	[kJ/kgK]	[kW/K]	[MW]
12a	18	813	373	2,05303	36,95455	-16,26
12b	18	373	373	-	-	-40,7
12c	18	373	313	42,97222	773,5	-46,41
10	98,5	813	313	0,942335	92,82	-46,41

Table 37: hot streams and sources available during the charging step.

Cold side						
Stream/ Source	Mass flow	T _{in}	T _{out}	C _p	C	Q
[#]	[Kg/s]	[K]	[K]	[kJ/kgK]	[kW/K]	[MW]
7	114,5	298	813	1,281282	146,835	75,62
Dehydration	-	813	813	-	-	100

Table 38: cold streams and sources available during the charging step.

Figure 70 shows the hot and cold side heat cumulative of the charging step.

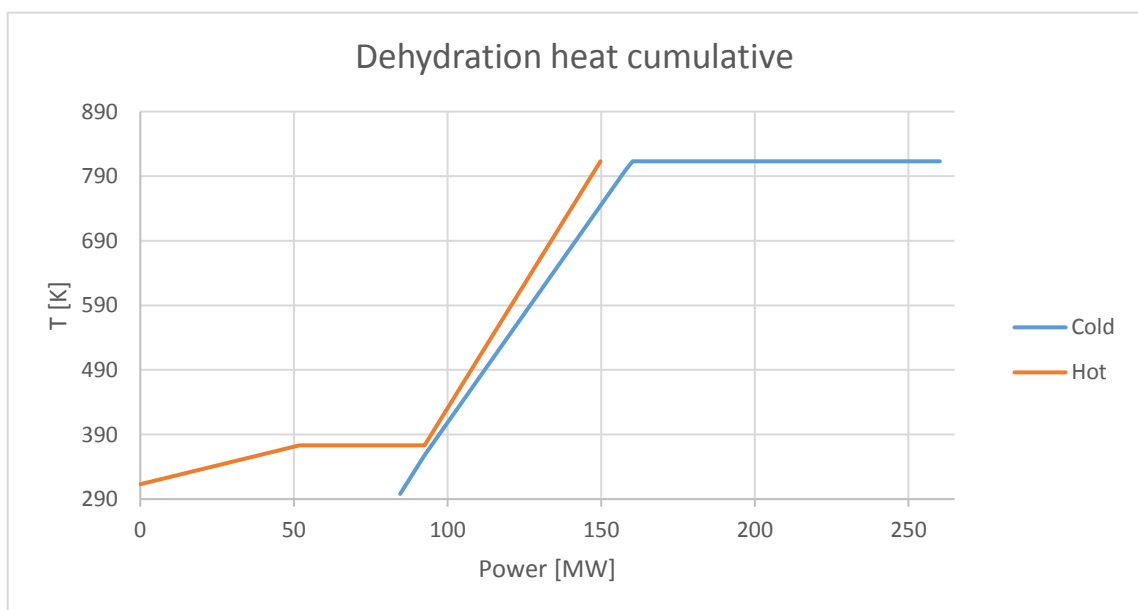


Figure 70: heat cumulatives of the charging step.

Cold side						
Stream/ Source	Mass flow	T _{in}	T _{out}	C _p	C	Q
[#]	[Kg/s]	[K]	[K]	[kJ/kgK]	[kW/K]	[MW]
1	96,50	298	854	0,93	89,59	51,69
2a	18	298	432,5	4,22	76,13	10,24
2b	18	432,5	432,5	-	-	37,6
2c	18	432,5	854	2,14	38,64	16,29

Table 40: cold streams and sources available during the discharge step.

Figure 72 shows the heat cumulative for the discharge step.

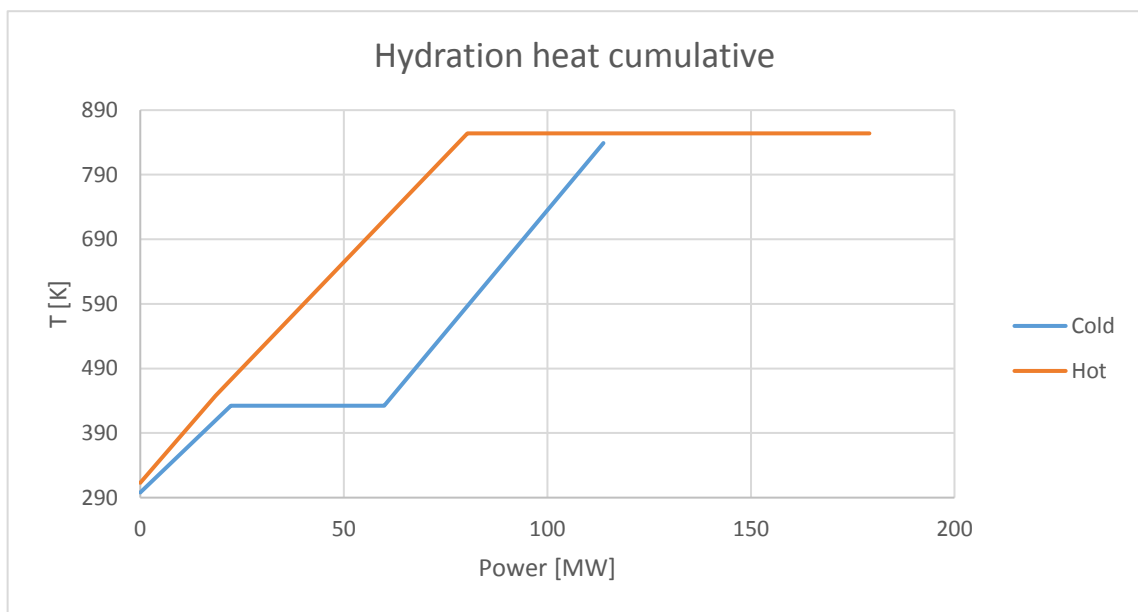


Figure 72: hot and cold heat cumulative of the discharge step.

The main change that can be seen in respect to the other cases in figure 72 is that the temperature of water evaporation is not anymore at 373 K but in this case is at 432.5 K. As the pinch point is always at 298 K for the cold side and at 313 K for the hot side the difference in respect to the previous case are not so much.

Figure 73 shows the HEX network for the discharge step at high pressure.

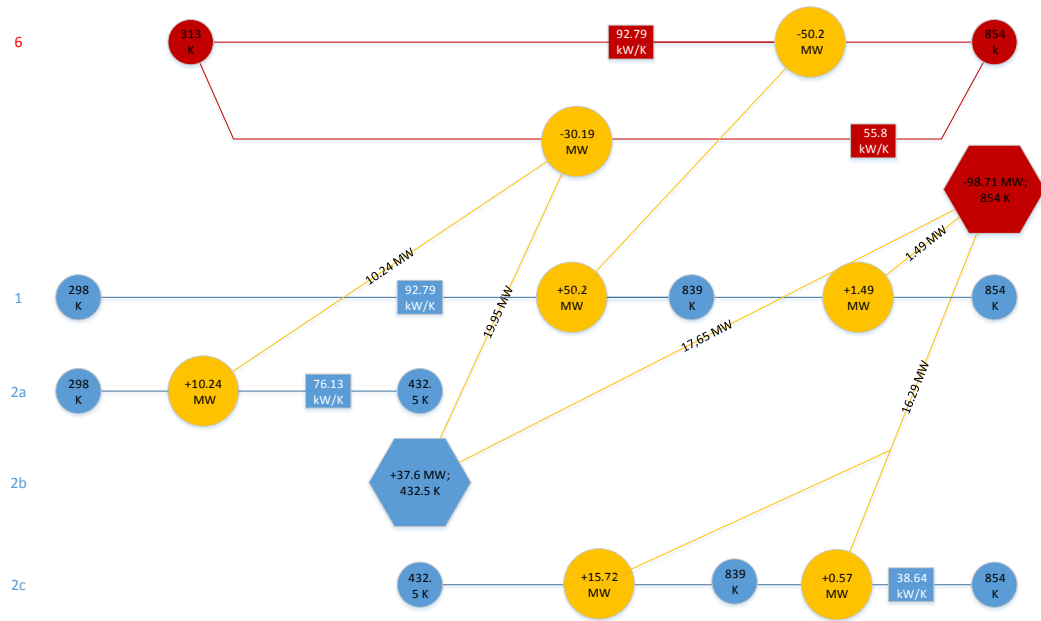


Figure 73: HEX network of the discharge step.

From figures 72 and 73 we can see that the hydration reactor has to provide 35.43 MW in order to cover the preheating of the cold streams during the discharge step, so the amount of power that can be employed in other applications is about 63.28 MW. Considering the total amount of heat needed to run the charging step, that is about 110.43 MW, and the power available from the hydration reactor, the TES thermal efficiency reached with the pinch analysis is about 57.30%.

Table 41 shows a comparison of the system before and after the pinch analysis taking into account the same boundary conditions.

Parameter	Unit	Before	After
TES thermal efficiency	[%]	33.87	57.30
Power output	[MW]	98.71	63.28
Power input	[MW]	291.44	110.43

Table 41: comparison before and after pinch analysis.

Table 41 shows that the pinch analysis has increased the TES efficiency of about 23,43 percentage points and has reduced the needed power input of about 181 MW. The efficiency is obtained as ratio of the power output and input as, for assumption, the time of charge and discharge are of the same length.

6. Power Block Integration

The following chapter is focused on the study of the possible way of power production using the heat released by the TES discharge step. The following list summarize the alternatives taken into account by the present work:

- Rankine-Hirn steam cycle, section 6.1, page 107. This section is about the study of the performance of a steam Rankine-Hirn power cycle with two pressure levels and a reheater to find the best coupling with the TES system. The coupling is done with: TES base case, TES with N₂ as dehydration fluidizing gas, TES with 3 dehydration reactors in series.
- Higher TES heat output temperature level by higher hydration pressure, section 6.2, page 118. This section studies the coupling of the Rankine-Hirn power cycle with two pressure levels and the reheater with a TES system where the hydration is run at higher pressure and temperature than the base case.
- Direct steam turbine integration, section 6.3, page 123. In this section has been analysed the direct integration of a steam turbine downstream of the hydration reactors worked at higher than atmospheric pressures.
- Organic Rankine cycle, section 6.4, page 137. In this section has been taken into account the coupling of an ORC power block with the base case TES layout worked at low hydration temperature using two different working fluids: toluene and cyclopentane.

6.1. Rankine-Hirn Steam Cycle

Taking into account the range of temperatures involved in the process the most compatible power cycle is the Rankine-Hirn with superheated steam cycle. As a starting point we can consider a situation in which the thermal coupling between the power cycle and the TES system is made considering only the heat provided by the hydration reactor to feed the boilers of the steam cycle. One of the most interesting things is that the power output from the hydration reactor is decoupled from the charging step and can work providing the required nominal power for all the time of operation. The only limitation is linked to the amount of stored energy.

With a hydration temperature of 470 °C (743 K) and, considering a direct integration with a minimum temperature approach of 15 K, the maximum temperature that the steam in the power cycle can reach is 455 °C (728 K). If we consider a mean ambient temperature of 25 °C (298 K) the condensation temperature should be higher than that to have a good heat exchanger configuration. Considering always a minimum temperature approach of 15 K the steam condensation has to be made at a temperature higher than 40 °C (313 K).

In figure 74 is shown the temperature and pressure conditions at which steam condensate in the range of 300 to 320 K with underlined the chosen condition for the steam condenser of the power block.

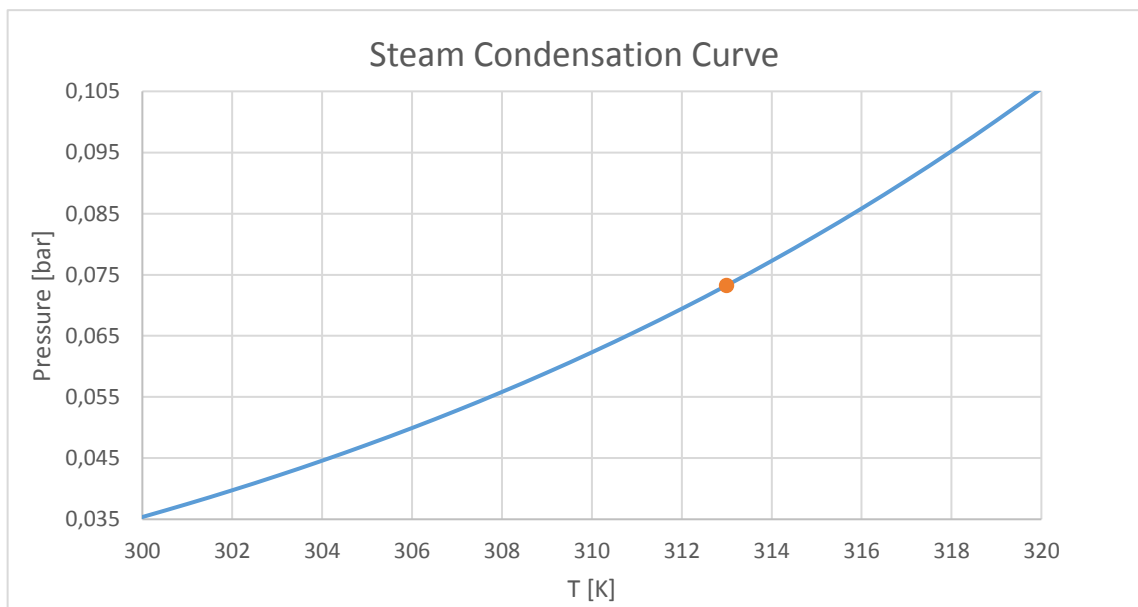


Figure 74: power block steam condenser temperature and pressure.

With the condensation temperature underlined in figure 74 the discharge pressure of the turbine has to be higher than the 0.074 bar or the condensation won't be at this temperature. In order to have a conservative and safe system the steam condensation has to be done with a grade of subcooling: in this way the pump cannot be reached by any amount of steam. We can consider a 2 K degree of subcooling and with this assumption the turbine outlet pressure cannot go under a pressure of about 0.08 bar.

It is recommendable that the turbine works in order to ensure a vapour fraction higher than 0.88 at the outlet as for lower value the turbine blade would suffer too much cavitation issues and so there will be the need to change them too often. As reference we can take a steam cycle with a double pressure level and a reheating system in order to have an already good performance. The reheating is done splitting the heat provided by the hydration reactor in order to reach the same temperature, 728 K, before the inlet of the turbines. This is managed changing the steam mass flow in the cycle.

Has already said the pressure of superheated steam for this kind of cycle is between 100 to 160 bar. In figure 75 is shown the result of a parametric analysis done varying both the high and the low-pressure levels in order to evaluate the efficiency behaviour of the steam cycle. The analysis is done varying the high-pressure level between 100 to 160 bar and the low-pressure level between 10 to 50 bar. The analysis shown in figure 75 is referred only to the power block without considering the TES performances but only the temperature level at which the heat is available and the amount of it that could be released by the TES.

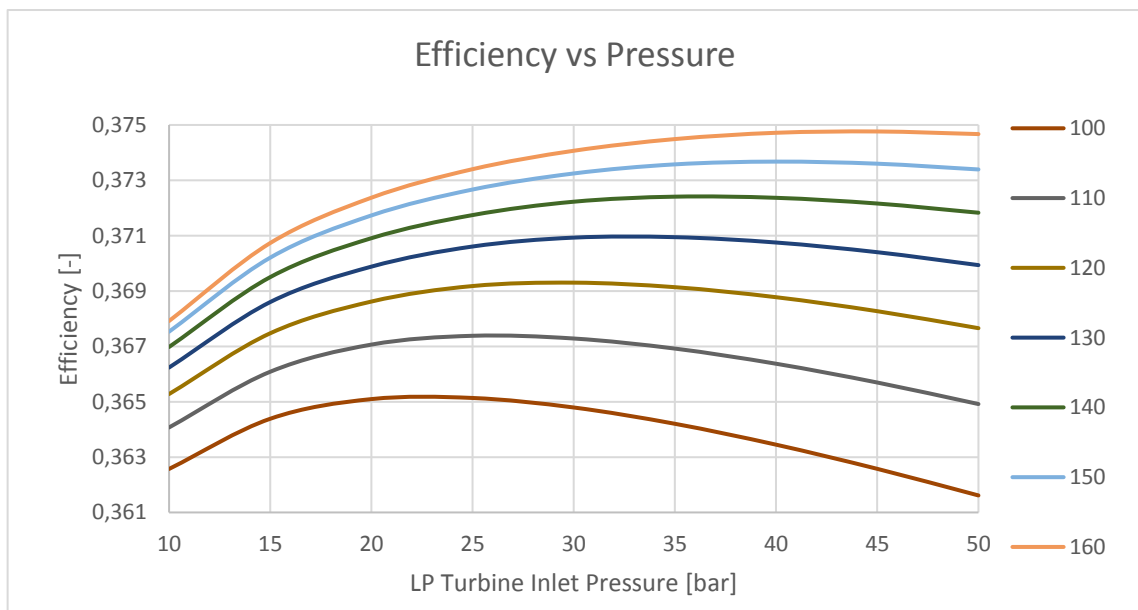


Figure 75: power block efficiency vs LP pressure.

The legend of figure 75 is referred to the inlet pressure level of the high-pressure turbine. The best efficiency results if the HP turbine inlet pressure is higher are obtained also for higher LP turbine inlet pressure levels. For a HP level of 100 bars the maximum efficiency is obtained for LP level around 22 bars. Instead for HP level of 160 bars the maximum is for LP around 45 bars. The power block thermal efficiency evaluated in figure 75 is obtained using equation number 19.

Equation 19

$$\eta_{PB} = \frac{abs(W_{turbineHP} + W_{turbineLP} - W_{pumps}) * t_{hyd,op}}{(Q_{Econ} + Q_{Boiler} + Q_{Sh} + Q_{Reheat}) * t_{hyd,op}}$$

Figure 77 shows the power block layout.

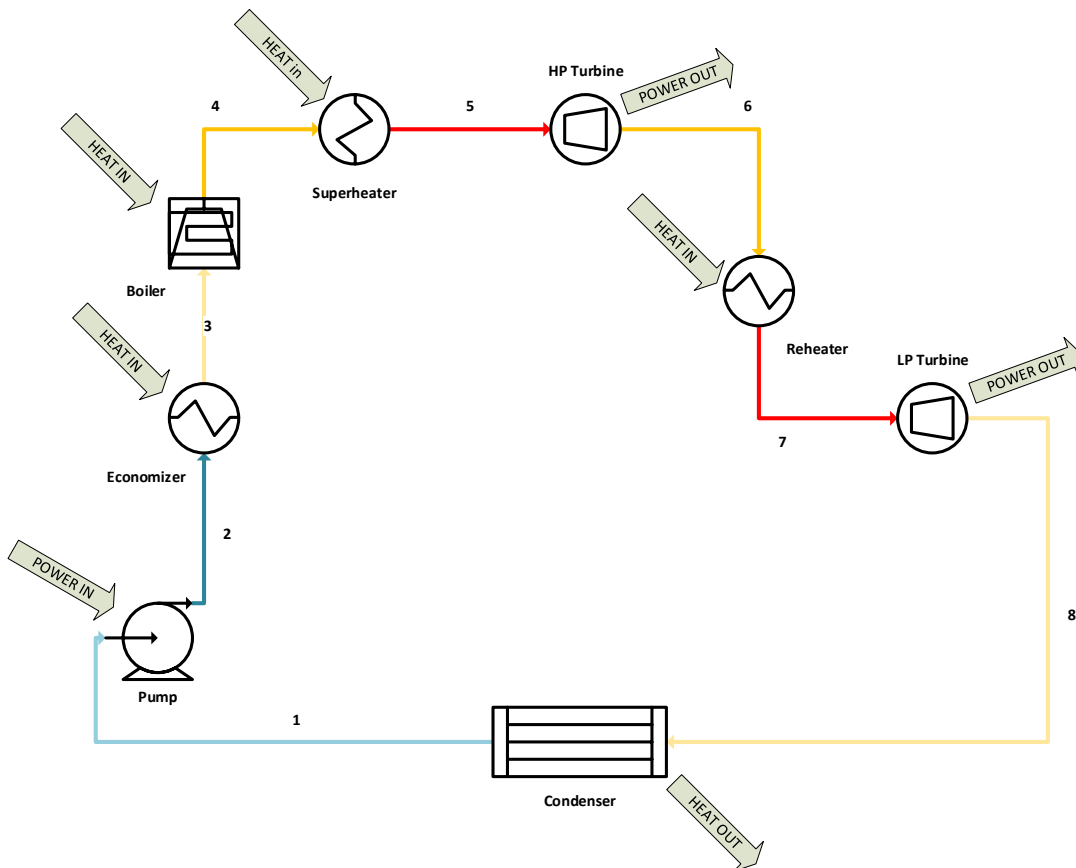


Figure 76: Steam power block layout.

The two working conditions show an efficiency gap of 1 percentage point. From the graph it can be seen that the efficiency gap between HP levels at the maximum efficiency point becomes

lower as the HP level increase. The parametric analysis is done considering the system adiabatic and any pressure loss equal to zero. The following efficiency parameters kept constant during the simulation:

HP Turbine	Isentropic Efficiency	[-]	0,88
LP Turbine	Isentropic Efficiency	[-]	0,88
Pump	Isentropic Efficiency	[-]	0,6

Table 42: isentropic efficiency of the power block's equipment.

In order to have the highest efficiency of the power block the chosen parameters are 160 bars for the HP level and 44 bars for the LP level. The LP turbine inlet pressure, that is also the pressure at which the steam is reheated, has to be chosen in order to have a steam fraction at the turbine outlet not lower than 0.88.

Figure 77 shows the steam fraction behaviour as function of the LP turbine inlet pressure with underlined the steam fraction obtained with the chosen inlet pressure and the limit of 0.88 as reference.

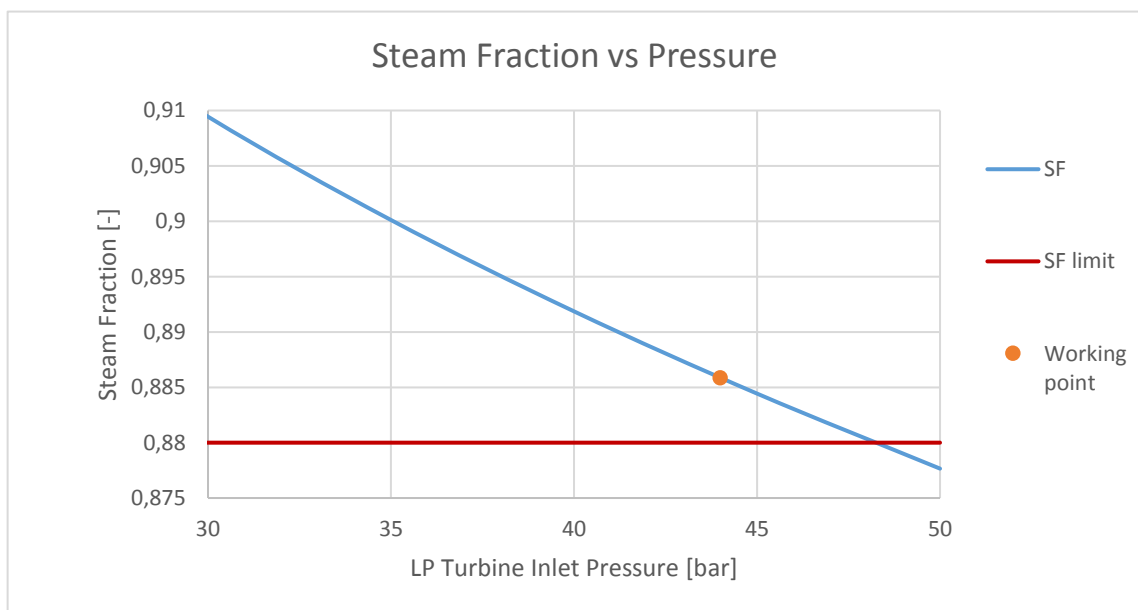


Figure 77: steam fraction at the outlet of the LP turbine as function of the LP inlet pressure.

The chosen working point permits to have a steam fraction at the LP turbine outlet of about 0.885 and so higher than the limit related to the cavitation problem. At the outlet of the HP turbine the limit is respected as the steam fraction is 1.

All the power block data referred to the chosen working point are reported in tables 43 and 44.

- Thermodynamic strongholds data:

#	T [K]	T [C]	P [bar]	s [kJ/kgK]	H [kJ/kg]
1	313	39,85	0,08	0,57	166,91
2	316	42,85	160	0,6037	193,46
3	620,5	347,35	160	3,745	1649,67
4	620,5	347,35	160	5,246	2580,8
5	728	454,85	160	6,116	3155,93
6	552	278,85	44	6,183	2881,95
7	728	454,85	44	6,904	3336,75
8	315	41,85	0,08	7,352	2302,37

Table 43: power block thermodynamic strongholds results.

- Component specifications:

HP Turbine	Power Output	[MW]	-8,15
LP Turbine	Power Output	[MW]	-30,79
Pump	Power Requirement	[MW]	0,82
Boiler-Economizer	Duty	[MW]	43,69
Boiler-Evaporator	Duty	[MW]	27,02
Boiler-Superheater	Duty	[MW]	17,48
Reheater	Duty	[MW]	13,53

Table 44: power block components results.

The data about the power input to the power block are the one that could be obtained coupling the power block with the TES of the base case layout of figure 20 with a power input to the dehydration reactor of 100 MW as described in the ‘plant configuration chapter’. With the previous data the net produced power by the steam cycle considering the heat input provided by the hydration reactor of the TES and the needed pump power provided by the turbines output, is about 38.12 MW. The hypothesis is to have the power block directly connected to the hydration reactor of the TES.

The power block with the previous data works with a steam mass flow of about 29.77 kg/s; The heat from the TES system is divided between the boiler and the reheater in order to reach in any configuration the same temperature at the inlet of the turbines.

Figure 78 show how the heat exchange between the TES system and the power block is made; as previously mentioned the described situation plans to use only the heat provided by the hydration reactor to provide the needed heat to the power block.

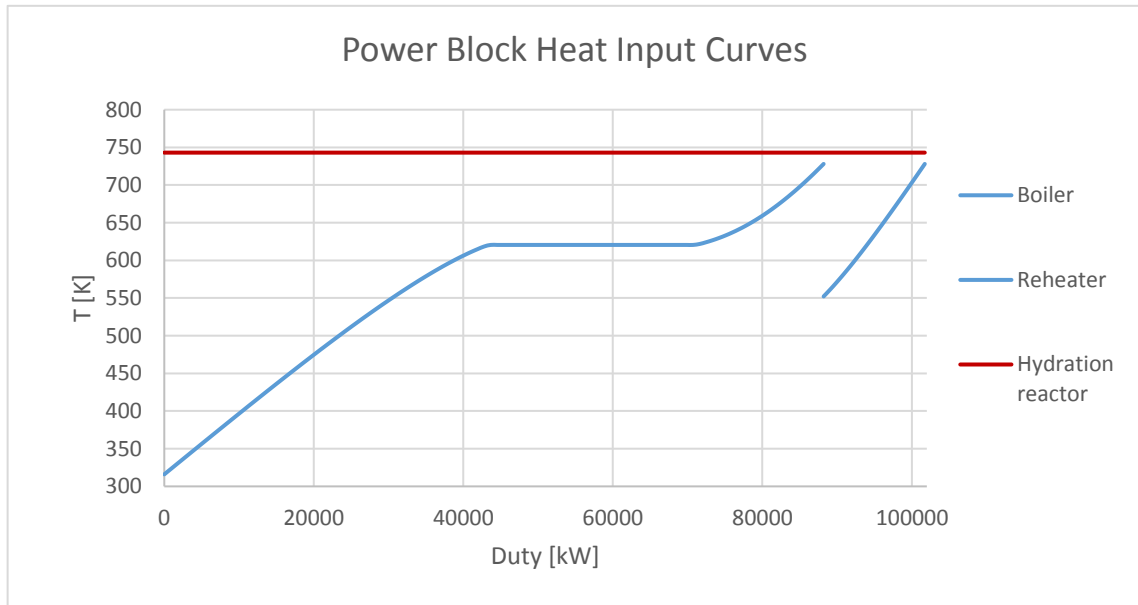


Figure 78: Heat coupling between hydration reactor and power block.

Figure 78 is related to a direct integration between the hydration reactor and both the boiler and the reheater and so there is not the need of an HTF.

In the case of an indirect integration with the exploitation of an HTF first the maximum temperature that the steam in the power block can reach would be a bit lower as also for the HTF a minimum temperature approach needs to be considered. If we consider always a minimum temperature approach of 15 K the maximum temperature that the steam can reach is then 713 K (440 °C).

In any case the direct integration of these components is for sure the best choice from a thermal point of view as the introduction of an HTF, as well as having to lower the steam maximum temperature, will also means the introduction of another HEX that means more losses and probably also a higher cost. Against could be technically more complex to have a direct integration instead of using an HTF.

If we want to evaluate the thermal efficiency of the TES system integrated with the power block referring to the previous configuration we can use the following formula:

Equation 20

$$\eta_{Overall} = \frac{abs(W_{turbineHP} + W_{turbineLP} - W_{pumps}) * t_{hyd,op}}{Q_{Dehy} * t_{dehy,op} + \sum(Q_{Hex,i} * t_{op,i})}$$

Where $Q_{Hex,i} * t_{op,i}$ represents all the energy transferred by the heaters needed to heat up the cold streams of the TES both in the hydration and the dehydration steps. The source of the heat needed by the HEXs to heat up the cold streams is not defined as this analysis is made to have an idea of the heat demand of the system for a given value of stored energy. The power block is assumed to work the same time of the hydration reactor as this is the heat source of the power block. On the base of the assumption that the times of charge and discharge of the TES are of the same length we can neglect the time factor and use equation 20 to evaluate the overall efficiency of both the TES and the power block coupled with a direct integration of the hydration reactor and the HEX of the power block.

For simplicity we can study the behaviour of both TES and power block system efficiency considering the TES without any streams thermal integration to have a thermal recovery. With the data and temperature and pressure of the TES of the base case we have that the system can reach an overall efficiency of 13.786 %. This efficiency is evaluated not considering the losses that affect the solar plant and is only referred to the TES and the power block.

6.1.1. Rankine-Hirne PB integration with base case TES layout after pinch analysis

The previous analysis is made without the HEX network obtained from the pinch analysis made in chapter 4.3. As reference we can take into account the system layout and results obtained with the pinch analysis made in chapter 4.3 and couple to it the steam Rankine-Hirn power block studied in this chapter with the best configuration obtained. Table 45 shows the main results of the system.

Equipment	Data	Value	Unit
Boiler	Duty	54,89	MW
	Output temperature	728	K
HP Turbine	Power output	-5,07	MW
	Pressure inlet	160	bar
Reheater	Duty	8,42	MW
	Output temperature	728	K
LP Turbine	Power output	-19,17	MW
	Pressure inlet	44	bar
Condenser	Duty	-39,58	MW
	Pressure	0,08	bar
	Temperature	313	K
Pump	Power inlet	0,51	MW
	Pressure outlet	160	bar
Hydration reactor	Duty	-63,32	MW
	Temperature	743	K
	Pressure	1	bar
TES Power input	Duty	110,43	MW

Table 45: TES and Power block data after integration.

The power block thermal efficiency is equal to 37.48 % and the steam mass flow is about 18.5 kg/s. As the TES base case layout, after the pinch analysis, has a power input of 110.43 MW, that has to be covered completely by the solar plant, and so with the data of table 45 we can evaluate the overall efficiency using equation 21.

Equation 21

$$\eta_{Overall} = \frac{abs(W_{turbineHP} + W_{turbineLP} - W_{pump,PB}) * t_{hyd,op}}{Q_{TES,input} * t_{dehy,op}}$$

The resulting value of the system overall efficiency is about 21.48 %. Equation 21 is used considering equal operation time for charge and discharge steps and so $t_{dehy,op} = t_{hyd,op}$.

The same thing can be made considering the layouts obtained from the pinch analysis made in chapters 5.2 and 5.3. The first one is referred to the TES with the nitrogen as fluidizing agent in the dehydration reactor and the second to the TES layout with more dehydration reactors putted in series.

6.1.2. Rankine-Hirne PB integration with N₂ modified TES layout after pinch analysis

The TES layout referred to the case with nitrogen as dehydration fluidizing agent is shown in chapter 5.2 and so the related pinch analysis. Table 46 shows the main results of the system after the integration.

Equipment	Data	Value	Unit
Boiler	Duty	54,69	MW
	Output temperature	728	K
HP Turbine	Power output	-5,05	MW
	Pressure inlet	160	bar
Reheater	Duty	8,39	MW
	Output temperature	728	K
LP Turbine	Power output	-19,1	MW
	Pressure inlet	44	bar
Condenser	Duty	-39,43	MW
	Pressure	0,08	bar
	Temperature	313	K
Pump	Power inlet	0,51	MW
	Pressure outlet	160	bar
Hydration reactor	Duty	-63,08	MW
	Temperature	743	K
	Pressure	1	bar
TES power input	Duty	110,25	MW

Table 46: TES and PB data after integration.

The power block thermal efficiency is equal to 37.47 % and the steam mass flow is about 18.5 kg/s. The modified TES system with nitrogen as fluidizing agent has a power input of 110.25 MW and so, using equation 21, the overall thermal efficiency of the system is about 21.44 %. As said before the charge and discharge operation time are considered equal and the power input to the TES system is all covered by the CSP plant.

6.1.3. Rankine-Hirn PB integration with modified 3 dehydration reactor TES after pinch analysis

In this case the modified TES system is the one with three dehydration reactors in series shown and analysed in chapter 5.3. Table 47 shows the main results of the system after the integration.

Equipment	Data	Value	Unit
Boiler	Duty	54,34	MW
	Output temperature	728	K
HP Turbine	Power output	-5,02	MW
	Pressure inlet	160	bar
Reheater	Duty	8,34	MW
	Output temperature	728	K
LP Turbine	Power output	-18,97	MW
	Pressure inlet	44	bar
Condenser	Duty	-39,18	MW
	Pressure	0,08	bar
	Temperature	313	K
Pump	Power inlet	0,5	MW
	Pressure outlet	160	bar
Hydration reactor	Duty	-62,68	MW
	Temperature	743	K
	Pressure	1	bar
TES power input	Duty	110,75	MW

Table 47: TES and PB data after integration.

In this case the PB thermal efficiency is about 37.47% with a steam mass flow of 18.3 kg/s. With the data of table 47 and equation 21 we can evaluate the system overall efficiency that is

equal to 21.21 %. Also in this case the charge and discharge times are equal and the power input to the TES system is covered entirely by the CPS plant.

6.2. Higher TES heat output temperature level by higher hydration temperature

As previously said the hydration reactor could be made working at higher than atmospheric pressure to ensure a higher hydration reaction temperature.

Figure 79 shows the behaviour of the TES and the Power Block efficiency for different pressures levels of the hydration reactor. The high and low pressures levels of the power block are the same founded as the best for the power block efficiency after the previous parametric analysis. Instead the maximum temperature reached by the steam in the boiler and in the reheater is changed in order to follow the temperature variation of the hydration reactor. The difference between the steam and the hydration temperature is fixed with a minimum temperature approach of 15 K.

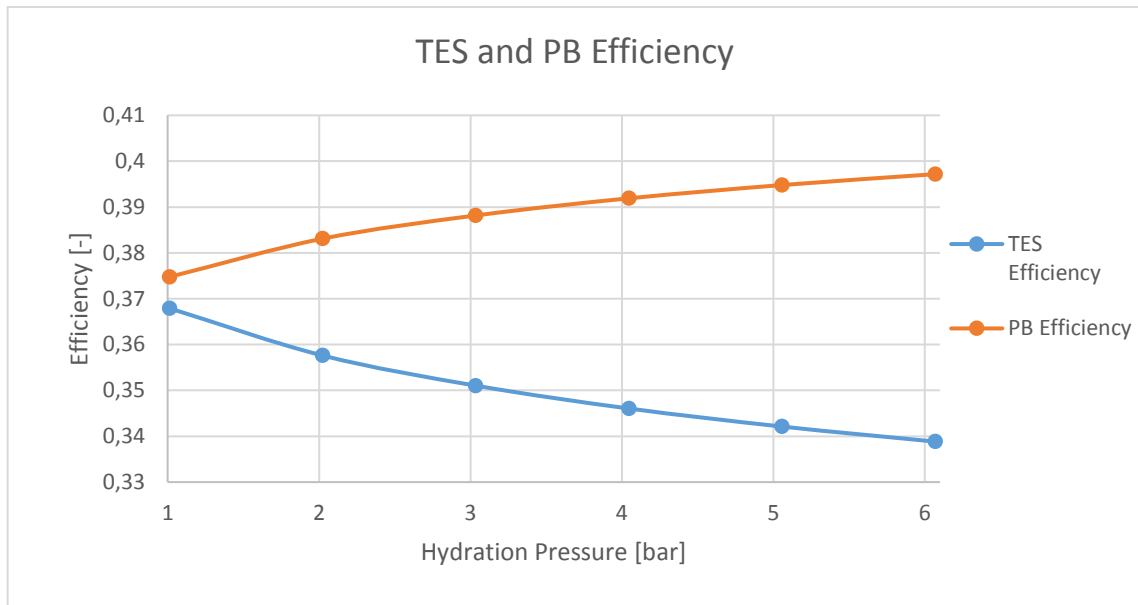


Figure 79: PB and TES efficiency vs hydration pressure.

The studied hydration pressure levels are the same reported in the analysis made in chapter 5.3 but is also considered an additional pressure level of 6 atmosphere that is necessary to reach the typical steam power cycle maximum temperature of 560 °C (833 K). The TES efficiency is the same obtained in this case while the power block efficiency is the result obtained from the integration of the two systems with the already explained boundary conditions.

As can be seen in figure 79 the power block efficiency has a positive trend with the increment of the hydration pressure level as this means also an increment of the hydration temperature and so the steam can be heated up to higher temperatures increasing the power block efficiency. It has to be clarified that in the power block efficiency evaluation is also counted the power needed to pressurize the water in the TES system.

The trend shown by the two curves is the same but with opposite sign; this behaviour is also related to the choice of having a constant relation between the pressure and temperature variations in the hydration reactor. The power block efficiency shows a lower increment with increasing hydration pressure in respect to the decrement of the TES efficiency and so the resulting overall efficiency is expected to be lower for higher hydration pressure.

Figure 80 shows the overall efficiency obtained with equation 19 for the same condition defined before.

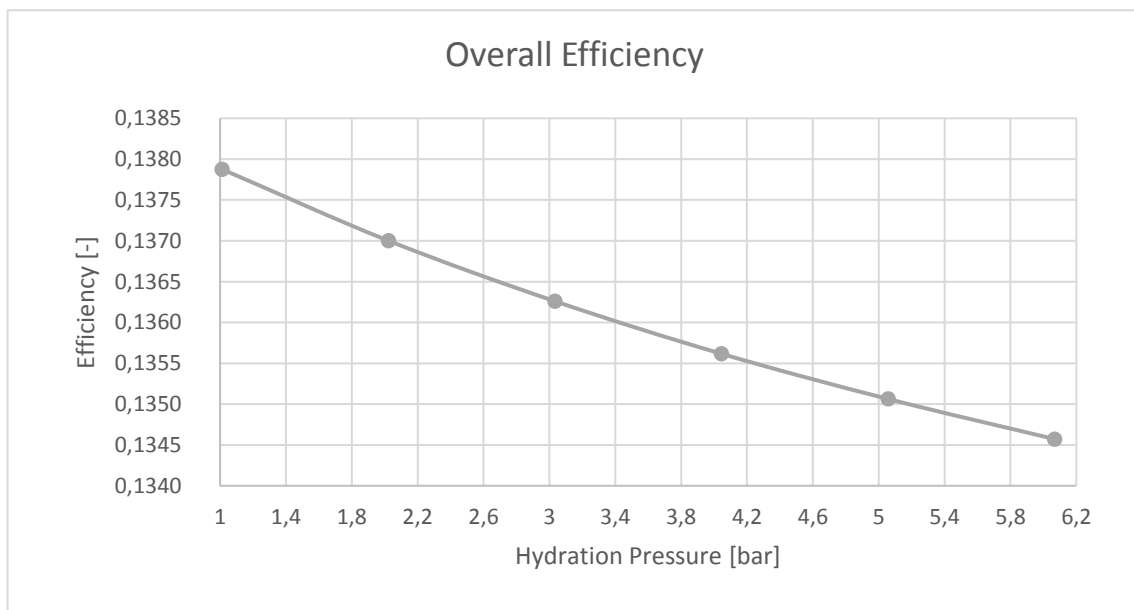


Figure 80: TES + power block overall efficiency vs hydration pressure.

As can be seen in figure 80 the overall efficiency, as expected, has a negative trend for increasing hydration pressures. The difference between the case with atmospheric pressure or 5 bars in the hydration reactors is not so high as the efficiency is affected less than 0.3%. But considering that this is the overall efficiency of both TES and power block system in nominal condition a little decrement in the efficiency could be not negligible.

The parametric analysis done before is made changing the hydration pressure to see the power block and the overall efficiency is made considering constant pressure condition at the inlet of

the turbines. In this configuration an increment of the steam temperature already means an increment of the power block efficiency. A change in the steam temperature after the boiler and the reheater means that the power cycle could have a better performance for different pressure level at the inlet of the turbines.

In figure 81 are shown the power block efficiency curves versus the LP level for different steam maximum temperature and for the same HP level, 160 bars.

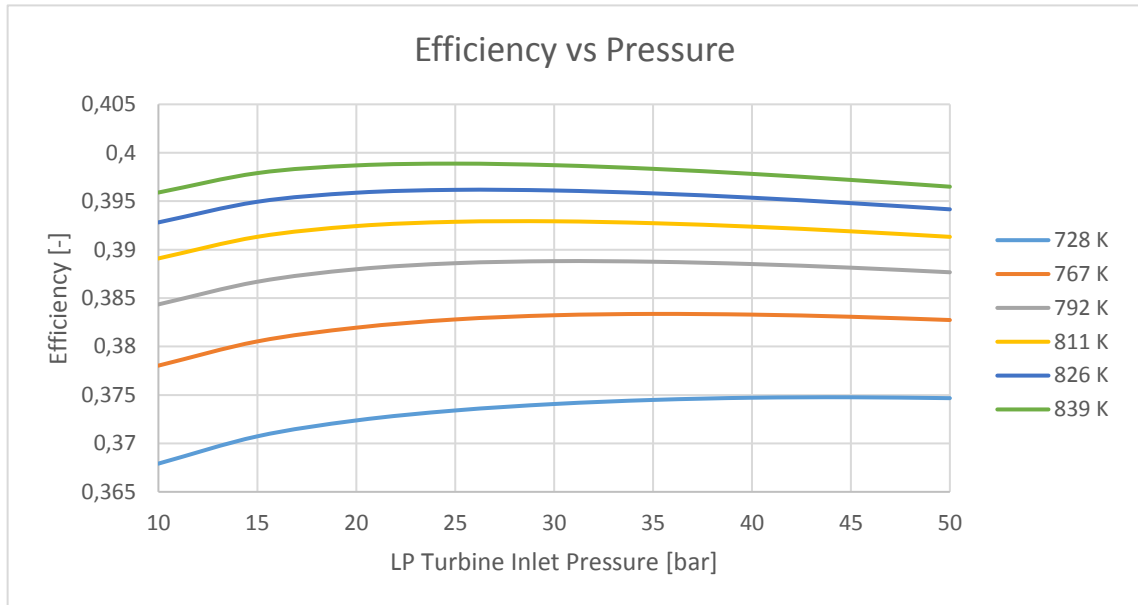


Figure 81: Power block efficiency vs LP turbine inlet pressure for different max steam temperatures.

As can be seen in figure 81, while the power block efficiency behaviour in respect to the HP level is more or less the same and for higher HP level the efficiency is higher also for increasing steam maximum temperature, the relationship between the efficiency and the LP level when the maximum steam temperature is changed is different. We can see that for higher temperature at the same HP level the highest efficiency is obtained for decreasing LP level. As already said if the hydration temperature is at 743 K (470 °C), and so the steam can reach a maximum temperature of 728 K (455 °C), the higher efficiency with a HP level of 160 bar is at a LP level of 44 bars. Instead if the hydration temperature is at 854 K (581 °C), and so the steam can reach a maximum temperature of 839 K (566 °C), the higher efficiency with a HP level of 160 bar is at a LP level of 25 bar.

For steam maximum temperature shifting from 728 K to 839 K the highest efficiency at constant HP level is obtained for decreasing LP level. The best performance obtained by the power block

is then about 39.88 %. The progressive approach of the efficiency curves for increasing temperature is mainly related to the fact that the shown temperature levels are also progressively approaching themselves as the increment of pressure in the hydration reactor does not lead to a linear temperature increment.

Table 48 shows the highest performance in respect to the maximum steam temperature and the correlated LP level:

Steam T [K]	LP Level [bar]	PB Efficiency [-]
839	24	39,89
826	26	39,61
811	29	39,29
792	32	38,89
767	36	38,34
728	44	37,48

Table 48: correlation between steam temperature, LP pressure and PB efficiency

Then we can evaluate again the, already defined by equation 20, overall efficiency of the TES plus the power block; the results are shown in figure 82.

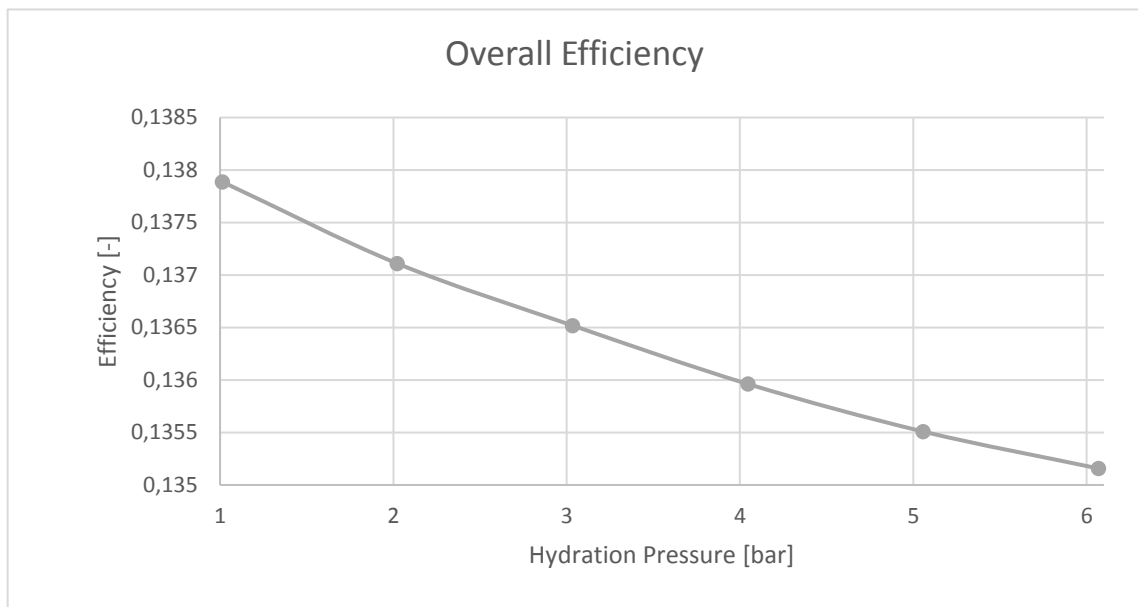


Figure 82: Overall efficiency vs hydration pressure.

The overall efficiency behaviour in figure 82 is the same as shown in figure 80, but the values are higher for the same hydration pressure level. The relative variation is very little; for

atmospheric pressure there is no variation in the efficiency while for increasing pressure the difference has an increment but at the end at 6 atmospheres the improvement in the overall efficiency is only of +0.05%.

To see the overall efficiency when the TES system is optimized by the pinch analysis we can take as reference, for the TES system the layout and the data obtained from the pinch analysis of chapter 5.4.1 on the TES with a hydration reactor pressure of 6 bars that means a hydration temperature of 854 K. In the present chapter we have seen that the steam Rankine-Hirn power block, if matched with a heat source at this temperature, has the best efficiency working at a LP pressure of 24 bars as reported in table 48.

Table 49 shows the main data referred to the system equipment with a focus on the power block with the modified power input.

Equipment	Data	Value	Unit
Boiler	Duty	55,16	MW
	Output temperature	839	K
HP Turbine	Power output	-6,21	MW
	Pressure inlet	160	bar
Reheater	Duty	8,11	MW
	Output temperature	839	K
LP Turbine	Power output	-19,43	MW
	Pressure inlet	39,89	bar
Condenser	Duty	-38,09	MW
	Pressure	0,08	bar
	Temperature	313	K
Pump	Power inlet	0,46	MW
	Pressure outlet	160	bar
Hydration reactor	Duty	63,27	MW
	Temperature	854	K
	Pressure	6	bar
TES Power input	Duty	110,43	MW

Table 49: TES and PB data after pinch analysis.

As can be seen from table 49 the power block has an input of 63.27 MW from the TES system, and the resulting overall efficiency is about 22.80%. The system overall efficiency is obtained using equation 22.

Equation 22

$$\eta_{Overall} = \frac{abs(W_{turbineHP} + W_{turbineLP} - W_{pump,PB} - W_{pump,TES}) * t_{hyd,op}}{Q_{TES,input} * t_{dehy,op}}$$

Also in this case the operational time of the discharge and the charge step are considered equal and so the operational times are equal. Furthermore, the PB is matched to the TES directly without the exploitation of an HTF between the hydration reactor and the HEXs of the PB. The heat input to the TES, after the pinch analysis, is all taken from the solar plant. The steam mass flow of the PB is in this case of 16.8 kg/s and its own thermal efficiency is about 39.79 %.

6.3. Direct Steam Turbine integration

The hydration reaction can be done in any case using steam also as fluidizing agent; this means that there is an excess of steam at high temperature that is recirculated in the reactor without any interaction other purpose. As seen before the hydration reaction could be reasonably done at higher than atmospheric pressure and so there is the potential to exploit the resulting pressurized steam in a steam turbine.

The exploitation of the hot pressurized steam that is recirculated in the hydration reactor in a steam turbine means that will be necessary to restore the temperature and the pressure before the recirculation. After the turbine the steam has to be pressurized again to reach the pressure level of the reactor, in order to spend the minimum amount of energy in this process the steam can be condensed and then pressurized with a pump.

The plant design already has a pump to pressurize the stoichiometric amount of water that is introduced in the reactor and so the pressurization of the water recirculation can be made using a single but bigger pump. In this way the two water streams are mixed and then pressurized with the pump. To have the same pressure level for the two water stream the pressure at the outlet of the turbine is fixed at ambient pressure.

With this choice the steam at the outlet of the turbine is at high temperature and has to be cooled down to be condensed. The steam can be also not condensed completely as part of the heat can be used to heat up the other water stream during the mixing. Is important that after the mixing the resulting stream has to be only of water as it will be then introduced into a pump.

For simplicity the steam cooling is brought to the complete condensation and then the two water streams at different temperature are mixed. As the steam employed in the hydration reactor comes into contact with solid particles the separation unit has to be truly performing in order to avoid the entry of the solid particles in the steam turbine.

Figure 83 shows the efficiency of the TES and of the power block with the introduction of the integrated TES steam turbine.

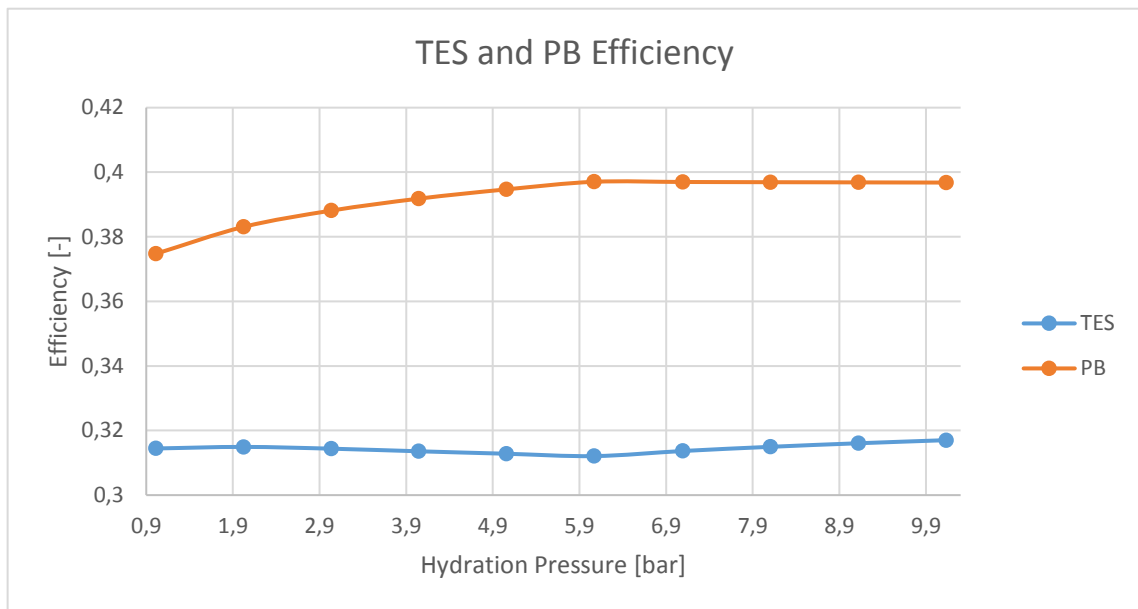


Figure 83: TES with integrated turbine and PB efficiency vs hydration pressure.

The efficiencies in figure 83 are obtained using equation 23 for the TES efficiency and equation 24 for the PB efficiency. Where equation 23 is defined as:

Equation 23

$$\eta_{TES} = \frac{abs(W_{turb\ int} - W_{pump} + Q_{hyd}) * t_{hyd,op}}{Q_{dehy} * t_{dehy,op} + \sum(Q_{Hex,i} * t_{op,hex,i})}$$

And equation 24:

Equation 24

$$\eta_{PB} = \frac{abs(W_{turbHP} + W_{turbLP} - W_{pump}) * t_{hyd,op}}{abs(Q_{hyd} * t_{hyd,op})}$$

In both the equations the terms related to the time can be simplified as all equal. The sum of the terms $Q_{Hex,i} * t_{op,hex,i}$ is referred to the heat needed by the TES system to preheat the cold streams. For this analysis the pressure in the discharge side of the TES system has varied between 1 to 10 atmospheres with steps of 1 atmosphere.

For pressure higher than 6 atmospheres the temperature of the hydration reaction is kept constant as it is comparable with the maximum temperature usually considered for steam turbine. Instead for pressure lower and equal to 6 atmospheres the temperature is changed as in the previous analysis. The turbine isentropic efficiency is kept constant at a value of 88% also in this case.

As can be seen from figure 80 the TES efficiency, that take account for the power produced by the integrated steam turbine, has a decreasing trend for pressure lower than 6 atmospheres while for higher pressure the trend is increasing. This behaviour is related to the already mentioned choice to work at fixed temperature for pressure higher than 6 atmospheres as this pressure should be enough to allow a high enough temperature for the steam turbine of the power block.

If we compare the TES efficiency of this case with the ones obtained without integrated turbine we can see that last ones are lower as there is the necessity to heat up more water, about the double, with practically the same specific energy requirement.

From 9 atmospheres the TES efficiency overcome the performance obtained for lower pressures. The power block efficiency curve is the same as the previous case for pressure lower than 6 atmospheres and then shows a constant behaviour as the maximum steam temperature is kept fixed.

Figure 84 shows a comparison of the overall efficiency vs the hydration pressure between with and without integrated steam turbine that are respectively defined in figure 86 and 20 of chapter 3.3.

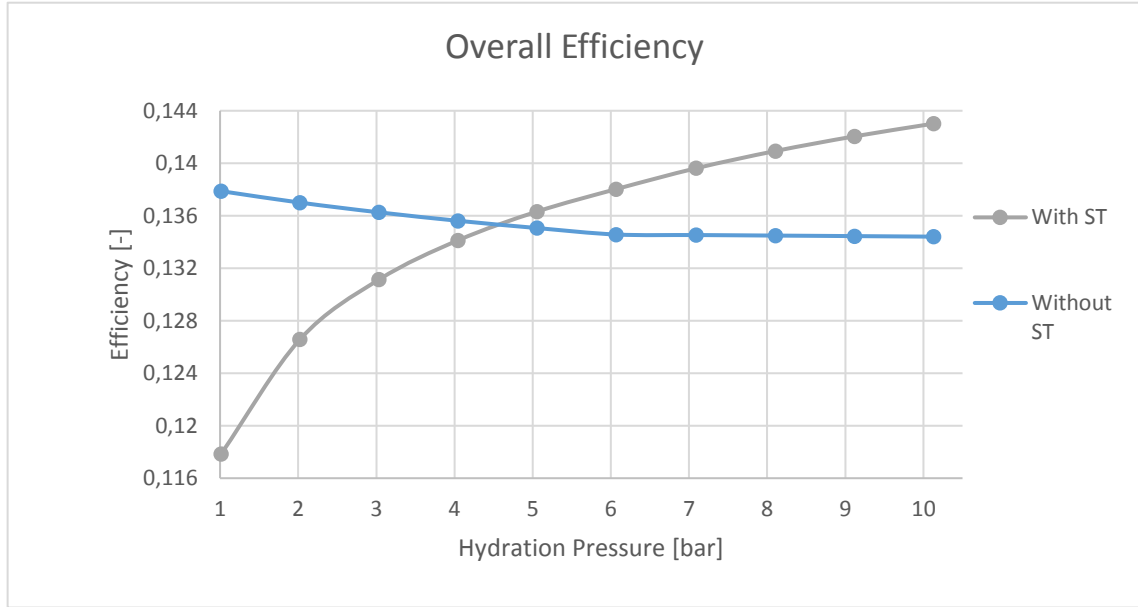


Figure 84: with and without integrated TES turbine overall efficiency comparison.

The efficiency of the curve in figure 84 related to the system without integrated turbine is referred to the base case TES system with a dehydration heat input of 100MW and coupled to the power block defined in chapter 6.1. This efficiency is obtained using equation 20; the efficiency of the system with the integrated turbine is obtained using equation 25.

Equation 25

$$\eta_{overall,ST} = \frac{abs(W_{turb,int} - W_{pump,PB} + Q_{hyd} + W_{turbHP} + W_{turbLP} - W_{pump,int}) * t_{hyd,op}}{Q_{dehy} * t_{dehy,op} + \sum(Q_{Hex,i} * t_{op,hex,i})}$$

As can be seen in figure 84, in the case of the integrated turbine the overall efficiency trend is positive and overcome the overall efficiency obtained by the system without the steam turbine integration for pressure higher than 4.5 atmospheres. At pressure higher than 6 atmosphere the overall efficiency of the system with the integrated steam turbine overcome also the best performance obtained without integrated steam turbine. The quasi constant trend of the overall efficiency in the case without the integrated steam turbine is due to the fixation of the hydration

temperature; in reality is slightly decreasing due to the higher requirement of the water pump in the TES hydration side. The choice to fix the outlet pressure of the integrated steam turbine to atmospheric condition is a limitation on its efficiency as it enable the exploitation of a non-negligible enthalpy jump. If the outlet pressure of the steam turbine is lower than the atmospheric ones there is the need to introduce another pump to cover the pressure gap between the water recirculation outlet stream from the turbine and the stoichiometric reaction water inlet stream. As the pressurization of the recirculation stream happens in liquid phase the energy requirement is not high.

Figure 85 shows the overall efficiency of the system with different integrated steam turbine discharge pressures compared with the overall efficiency obtained without the integrated steam turbine.

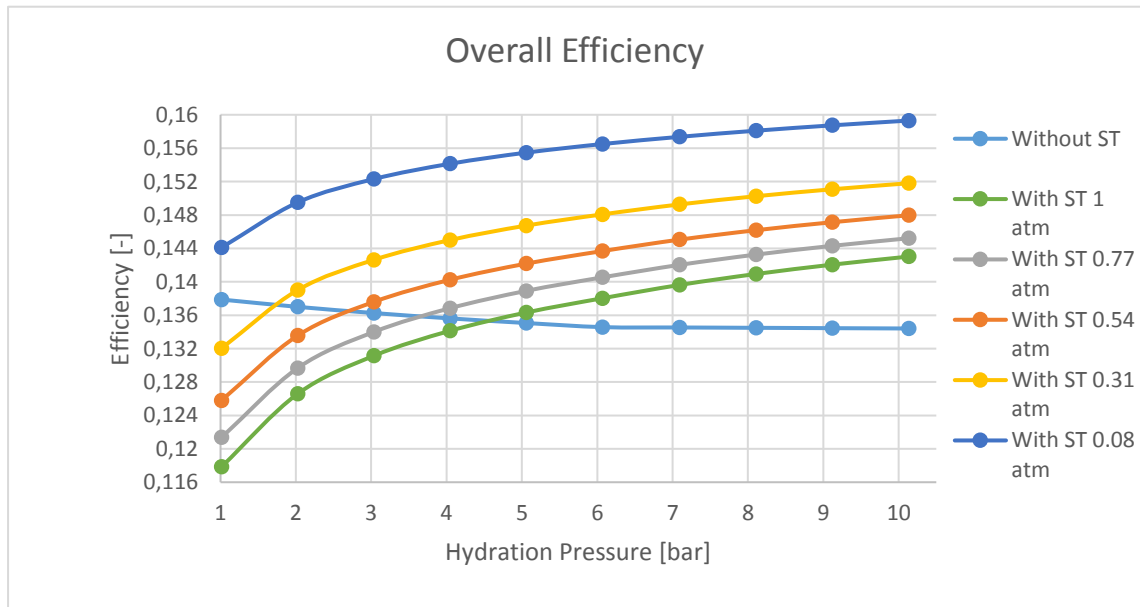


Figure 85: Comparison between overall efficiency obtained with and without integrated turbines for different hydration pressures and LP turbine discharge pressures

As can be seen from figure 85 the reduction of the outlet pressure of the integrated steam turbine has an interesting effect on the overall efficiency. The legend reports the discharge pressure of the integrated steam turbine. The positive effect increment becomes higher as the outlet pressure becomes lower. Is interesting to see that also with an atmospheric hydration pressure the overall efficiency grows of some percentages in respect to the case with atmospheric discharge pressure if the integrated steam turbine outlet pressure is decreased. For a fixed value of integrated steam turbine outlet pressure the increment of the hydration pressure brings a higher benefit in the

range between 1 to 6 atmospheres while after that value the overall efficiency grows slower. Due to the low pressure reached by the steam and the high temperatures the expansion in the turbine doesn't lead to the appearance of a liquid phase in the turbine. In respect to the case without the integrated steam turbine the overall efficiency obtained with low integrated steam turbine discharge pressure are higher and show that the exploitation of this steam stream in the power production is important to have a better performance of the system. The exploitation of this steam stream can be also done by a direct integration in the power block system in the LP turbine. In that case the condition at the inlet of the LP turbine has to be the same as the steam from the hydration reactor and after the condensation the steam recirculation to the hydration reactor as to be pressurized with its own pump. The gain is the use of a single LP turbine instead of two. Figure 86 shows the layout the system described before for a hydration pressure of 5 bars without considering the external power block.

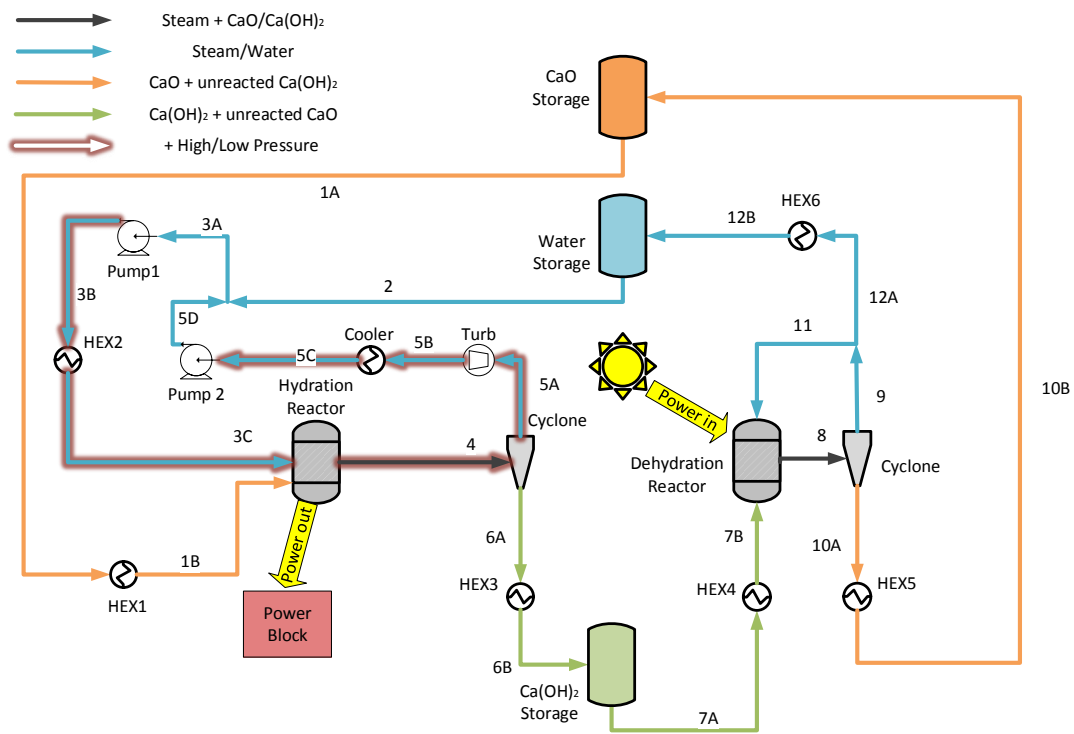


Figure 86: System layout with turbine direct integration.

Table 50 shows the main data about the equipment of figure 86.

Equipment	Q or W	Pressure	Tin	Tout
Name	[MW]	[bar]	[K]	[K]
HEX1	51,1	1,01	298	841
HEX2	115,8	5,07	318	841
HEX3	-80,17	1,01	841	298
HEX4	75,62	1,01	298	813
HEX5	-62,63	1,01	813	298
HEX6	-47,73	1,01	813	298
Cooler	-41,19	0,31	498	341
Hydration	-99,1	5,07	841	841
Dehydration	100	1,01	813	813
Pump	0,02	5,07	318	318
PumpINT	0	1,01	341	341
TurbineINT	-11,05	5,07	841	498
Water storage	0	1,01	298	298
CaO	0	1,01	298	298
CaOH	0	1,01	298	298

Table 50: main data of the equipment in figure 86.

Table 51 shows the main data about the streams in figure 85.

Stream	Total mass flow	CaO	Water	Ca(OH)₂	Temperature	Pressure
Name	[kg/s]	[kg/s]	[kg/s]	[kg/s]	[K]	[bar]
1A	96,49	86,41	0,00	10,08	298,00	6,08
1B	96,49	86,41	0,00	10,08	848,00	6,08
2	18,04	0,00	18,04	0,00	298,00	1,01
3A	33,64	0,00	33,64	0,00	318,09	1,01
3B	33,64	0,00	33,64	0,00	318,19	6,08
3C	33,64	0,00	33,64	0,00	848,00	6,08
4	130,13	30,24	15,59	84,29	848,00	6,08
5A	15,59	0,00	15,59	0,00	848,00	6,08
5B	15,59	0,00	15,59	0,00	485,87	0,31
5C	15,59	0,00	15,59	0,00	341,31	0,31

Stream	Total mass flow	CaO	Water	Ca(OH)₂	Temperature	Pressure
Name	[kg/s]	[kg/s]	[kg/s]	[kg/s]	[K]	[bar]
5D	15,59	0,00	15,59	0,00	341,32	1,01
6A	114,53	30,24	0,00	84,29	848,00	6,08
6B	114,53	30,24	0,00	84,29	298,00	1,01
7A	114,58	30,24	0,00	84,33	298,00	1,01
7B	114,58	30,24	0,00	84,33	813,00	1,01
8	128,88	86,41	32,34	10,12	813,00	1,01
9	32,34	0,00	32,34	0,00	813,00	1,01
10A	96,53	86,41	0,00	10,12	813,00	1,01
10B	96,53	86,41	0,00	10,12	298,00	1,01
11	14,30	0,00	14,30	0,00	813,43	1,01
12A	18,04	0,00	18,04	0,00	813,43	1,01
12B	18,04	0,00	18,04	0,00	298,00	1,01

Table 51: main data of the streams in figure 86.

6.3.1. Pinch analysis

The introduction of the steam turbine directly in the TES system means that another water stream has to be heated up during the TES functioning. To carry out the pinch analysis of this system has been chosen the case with a hydration pressure of 5 bars because, as is shown in figure 81, the overall efficiency of the system with the integrated turbine working at 5 bars is already higher than the efficiency obtained without the integrated turbine by the same system in the same conditions. Table 52 shows the hot and cold streams of the system under analysis.

Stream/ Source	Mass flow	T_{in}	T_{out}	C_p	C	Q	Cold/ Hot
 [#]	 [Kg/s]	 [K]	 [K]	 [kJ/kgK]	 [kW/K]	 [MW]	 [-]
5	15,60	498	341,3	26,95	420,42	-65,88	hot
Hydration	-	841	841	-	-	-99,10	hot
1	96,50	298	841	0,96	92,85	50,42	cold
3a	33,60	298	425,5	16,49	554,18	15,24	cold
3b	3,60	425,5	425,5	-	-	70,84	cold
3c	33,60	425,5	841	1,71	57,59	29,69	cold
10	98,50	813	313	0,94	92,82	-46,41	hot
13a	18,00	813	373	2,05	36,95	-16,26	hot
13b	18,00	373	373	-	-	-40,70	hot
13c	18,00	373	313	37,69	678,33	-40,70	hot
7	114,60	298	813	1,28	146,83	75,62	cold
Dehydration	-	813	813	-	-	100,00	cold
6	114,50	841	313	1,33	151,83	-80,17	hot

Table 52: hot and cold streams and sources available in the system.

In this case the dehydration step is similar to the one present in the base case as the pressure change and the introduction of the integrated turbine only affects the hydration step. In the hydration step there is also the introduction of another hot sources, the stream number 5.

In tables 53 and 54 are respectively summarized the hot and the cold streams available during the hydration step.

Hot side						
Stream/ Source	Mass flow	T _{in}	T _{out}	C _p	C	Q
[#]	[Kg/s]	[K]	[K]	[kJ/kgK]	[kW/K]	[MW]
Hydration	-	841	841	-	-	-99,1
5	15,6	498	341,3	26,95	420,42	-65,88
6	114,50	841	313	1,33	151,83	-80,17

Table 53: hydration step available hot and cold streams and sources

Cold side						
Stream/ Source	Mass flow	T _{in}	T _{out}	C _p	C	Q
[#]	[Kg/s]	[K]	[K]	[kJ/kgK]	[kW/K]	[MW]
1	96,5	298	826	0,962223	92,85	48,95
3a	33,6	298	425,5	16,49351	554,1818	15,24
3b	3,6	425,5	425,5	-	-	70,84
3c	33,6	425,5	826	1,714124	57,59457	28,63

Table 54: hydration step available cold streams and sources.

With the data contained in tables 53 and 54 we can build the heat cumulative of the hydration step.

Figure 87 shows the heat cumulative of the hydration step.

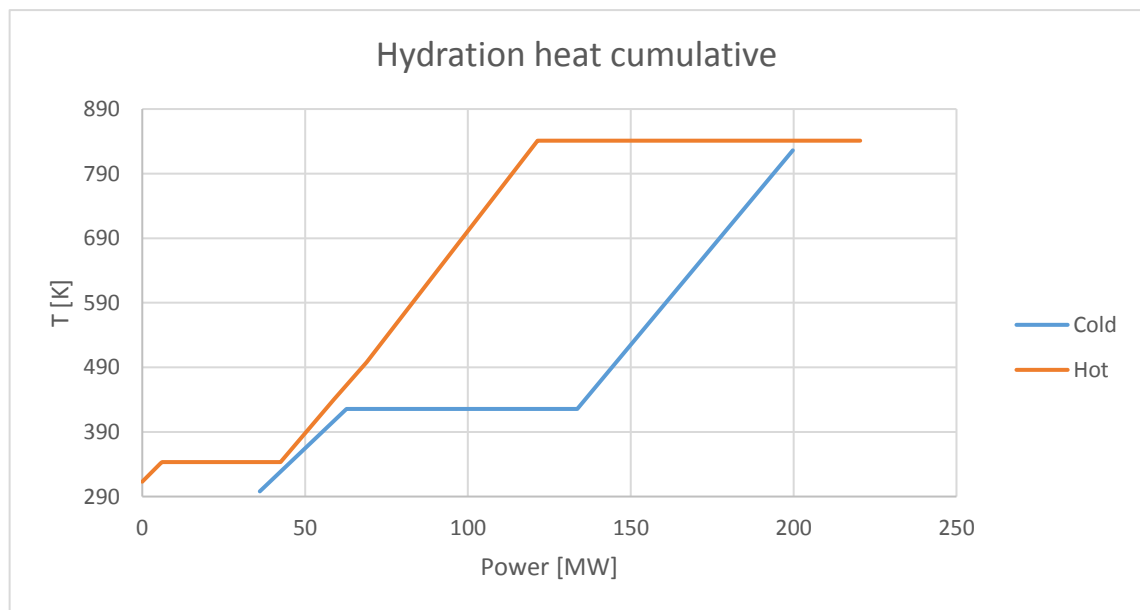


Figure 87: hot and cold heat cumulative of the hydration step.

From figure 87 we can already see that the introduction of the internal turbine affects strongly the quantity of heat that the hydration reactor can provide for other purposes despite the self-sustainment of the discharge step. In this case the pinch point is located at 343.3 K for the hot side and at 328.3 K for the cold side. We can also see that there is a certain quantity of heat available under the pinch point that is not useful for the preheating of the cold streams.

Figure 88 shows the HEX network of the hydration step.

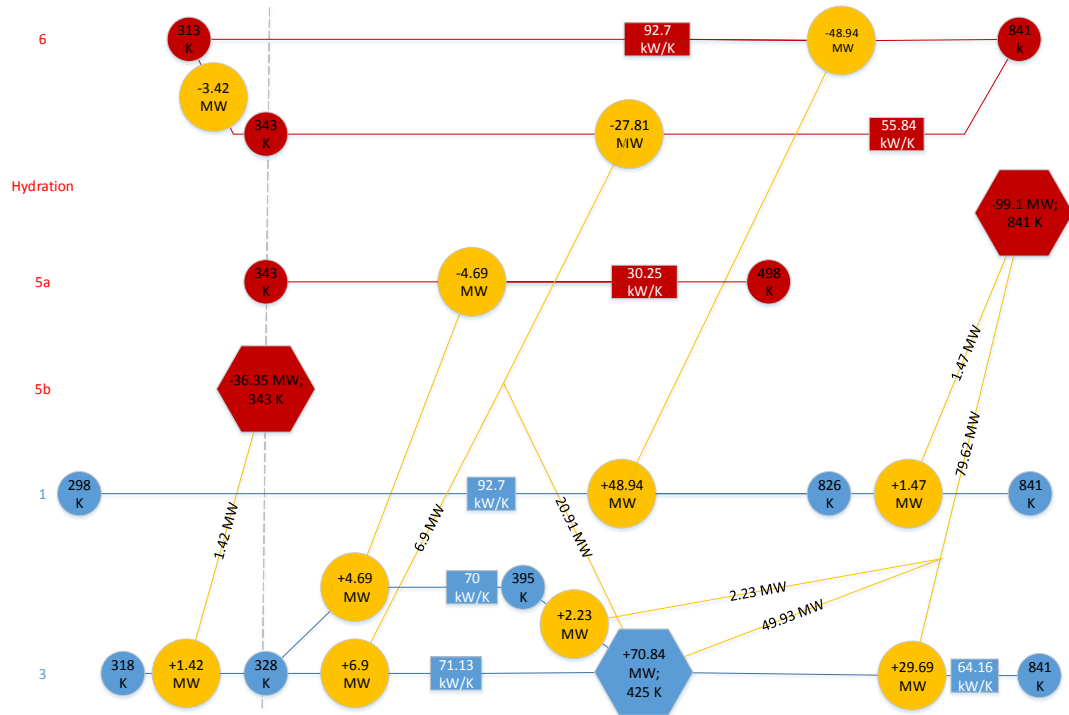


Figure 88: HEX network of the hydration step.

As already said the dehydration step is not changed unless for some secondary aspect as some little variation on the mass flows and then on the heat exchanged. Tables 55 and 56 show the respectively the hot and the cold streams and sources available during the dehydration step.

Hot side						
Stream/ Source	Mass flow	Tin	Tout	Cp	C	Q
[#]	[Kg/s]	[K]	[K]	[kJ/kgK]	[kW/K]	[MW]
13a	18	813	373	2,05303	36,95455	-16,26
13b	18	373	373	-	-	-40,7
13c	18	373	313	37,68519	678,3333	-40,7
10	98,5	813	313	0,942335	92,82	-46,41

Table 55: hot streams and sources available in the charging step.

Cold side						
Stream/ Source	Mass flow	T _{in}	T _{out}	C _p	C	Q
[#]	[Kg/s]	[K]	[K]	[kJ/kgK]	[kW/K]	[MW]
7	114,6	298	798	1,281282	146,835	73,19
Dehydration	-	813	813	-	-	100

Table 56: cold streams and sources available in the charging step.

Figure 89 shows the heat cumulative of the dehydration.

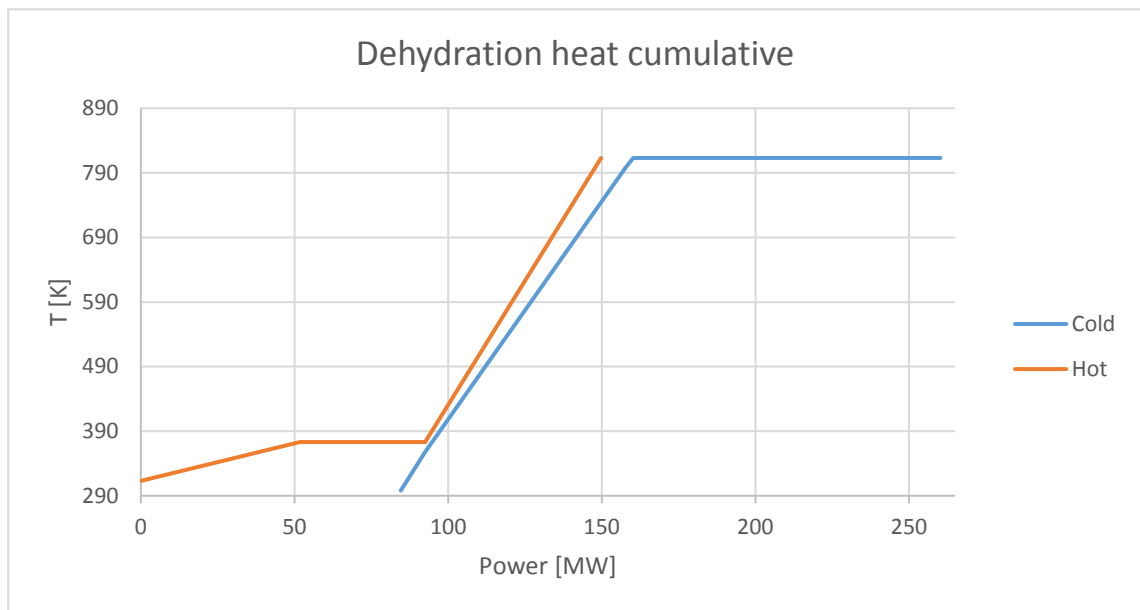


Figure 89: hot and cold heat cumulative of the charging step.

In figure 89 we can see that the hot streams can only provide a part of the heat needed to preheat the cold streams and that a certain amount of heat under the pinch point from the hot streams is in excess and can't be used in the system. As can be seen from figure 85 and 86 the pinch point for the hot side is at 373 K while for the cold side is at 358 K

Figure 90 shows the HEX network of the dehydration step.

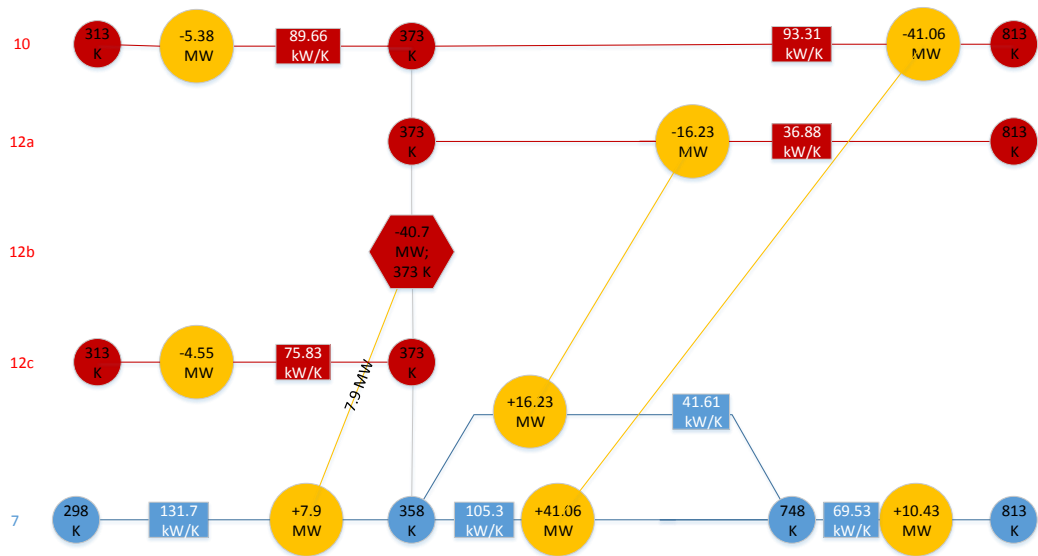


Figure 90: HEX network of the dehydration step.

From figure 90 we can see that the amount of heat from the hot side that is lost is about 42.73 MW. Instead the amount of heat needed to complete the preheating of the cold streams is about 10.43 MW. The total amount of heat to run the dehydration step needed from the sun is then about 110.43 MW.

Table 57 shows a comparison of the system before and after the pinch analysis taking into account the same boundary conditions.

Parameter	Unit	Before	After
TES mechanical efficiency	[%]	3.22	9.98
TES Thermal efficiency	[%]	29.20	16.3
TES overall efficiency	[%]	32.42	26.30
Thermal power output	[MW]	99.81	18.01
Net mechanical power output	[MW]	11.03	11.03
Power input	[MW]	341.81	110.43

Table 57: before and after pinch analysis comparison.

In table 57 the evaluated efficiencies are referred to the TES system without the external power block. In this case the only way to cover the heat needs for the preheating of the streams during the hydration step is to use a large amount of the heat released by the hydration reactor leading to a condition in which the remaining heat for other applications is very low.

The only case in which the pinch analysis has a positive result is if we only take into account the mechanical power produced by the integrated turbine as the output of the system. After the

pinch analysis the available heat is only 18 MW and is not anymore enough to fuel a large-scale power block.

The problem related to the introduction of the integrated turbine is the fact that also the recirculation water has to be reheated before entering the hydration reactor. As the heating of the water is made after the pressurization of the stream the phase change happens at 425.5 K and the only way to cover the heat demands is to use the hydration thermal output. The introduction of the integrated turbine seems to be applicable only if the heat needed to cover the water stream evaporation could be taken from other sources.

6.4. Organic Rankine Cycle

We have seen that the chosen chemical couple, calcium hydroxide and calcium oxide, involved in the TES chemical loop has shown that at ambient pressure the temperature level at which the heat can be released during the discharge step is around 740 K (467 °C). In any case the discharge temperature can't be higher than 792 K (519 °C) without increasing the hydration pressure. As already said and studied this range of temperature can be coupled with a steam Rankine-Hirn power cycle in order to produce mechanical energy and then electricity.

From the point of view of the TES the reduction of the hydration reaction temperature means a benefit in the TES efficiency. This is due to mainly two facts: for lower reaction temperatures the heat of reaction increases and the energy for the preheating of the streams that are introduced in the reactor is reduced. While for the dehydration process if the reaction temperature is increased the role of the streams preheating is stronger than the reduction of the heat of reaction in this case both the variations are advantageous and so there is a final benefit.

In figure 91 is shown the TES efficiency trend for hydration temperatures between 230 and 380 °C.

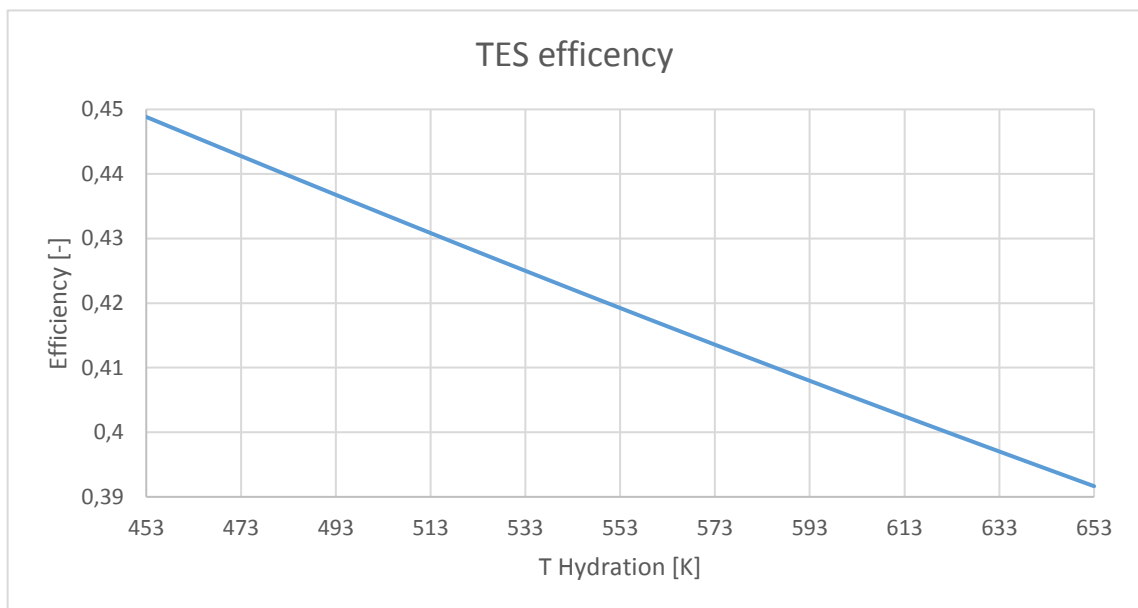


Figure 91: TES efficiency vs low hydration temperature

As can be seen in figure 91 the TES efficiency is linearly dependant from the hydration temperature and in a range of 150 k it shows a change of about 6 percentage points. Figure 91 is made using equation 16.

The reduction of the hydration reaction temperature means also that the reaction conditions are farther from the equilibrium condition and so this means that the kinetics of the reaction is enhanced.

As already known the efficiency of the steam Rankine cycle gets lower and lower as the maximum temperature is reduced. Instead, thanks to the thermodynamic properties of the involved working fluids, the organic Rankine cycles can be adapted to work with good efficiency with temperature that are not useful for a steam Rankine cycle. For maximum working temperatures lower than 574 K (300 °C) the ORC are well imposed as the best choice for medium and small scale applications [41],[42].

For higher temperatures, until 773 K (500 °C), that from the ORC point of view can be defined as high or very high working temperatures, the thermal efficiency competition between ORC and SRC is open and the result is in many case correlated to the choice made for the working fluid of the ORC [41].

6.4.1. Toluene

Between the fluids that can be used in a ORC at high and very high temperatures [41],[43] I have chosen to select the toluene. The choice of the toluene as the working fluid of the ORC is made as in literature is reported that it can be used for high and very high working temperatures and because in another study [44] is underlined as a working fluid which allows very high thermal performances compared to the other studied fluids.

Toluene is reported to has been studied up to a temperature of 400 °C (673 K). In the same study of Nishith et al [44] is also reported that the exploitation of toluene is not very cheap in comparison with the other studied fluids and that its impact on the environment is quite low.

Toluene is an aromatic hydrocarbon with C_7H_8 as chemical formula. Toluene is a flammable compound usually used, in many applications, as substitute of benzene. Toluene is a very toxic substance but is widely used in the industry and is also present in some products.

Due to its toxicity there are many issues about is storage and its handling. This fluid has already been used as fluid for ORC in some studies and applications; from a thermodynamic point of view can be classified as a dry fluid as can be seen in the following T-s graph comparison with other ORC working fluids of figure 92.

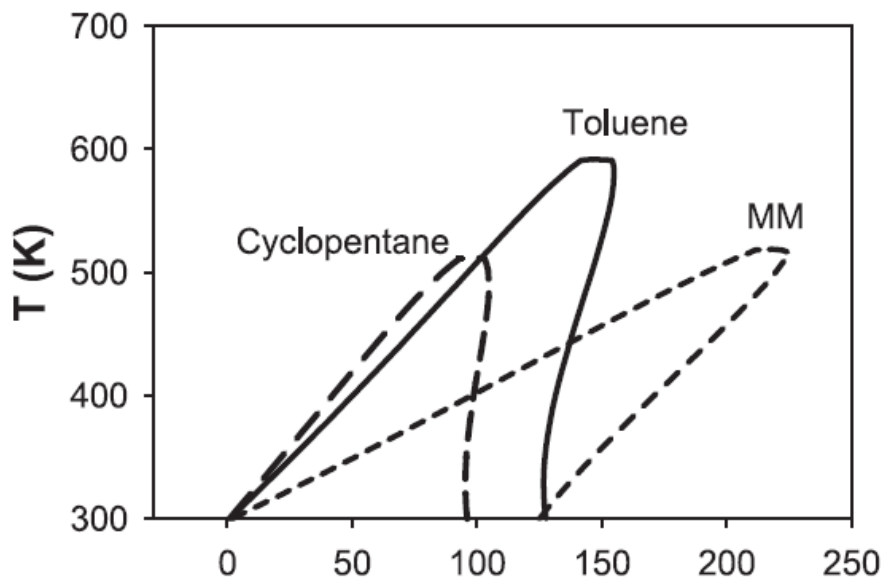


Figure 92: T-s comparison of three different ORC fluids [43].

As can be seen from figure 92 toluene has a critical temperature near to 600 K, exactly 591.6 K (318.6 °C). The toluene critical pressure is instead 42.12 bars. The layout of the ORC used

with toluene, as comparison with the steam Rankine cycle, is a simple one that have only a turbine. This kind ORC layout is quite similar to a simple SRC but, for the peculiar thermodynamic working conditions and behaviour of this kind of fluids, there is the need of having an internal heat exchanger in order to reuse the amount of heat at useful temperature still brought by the fluids at the outlet of the turbine. If the internal heat exchanger is not included the amount of wasted heat would be very high and the efficiency of the power block couldn't be competitive.

Figure 93 shows the power block layout of the ORC with the internal heat exchanger.

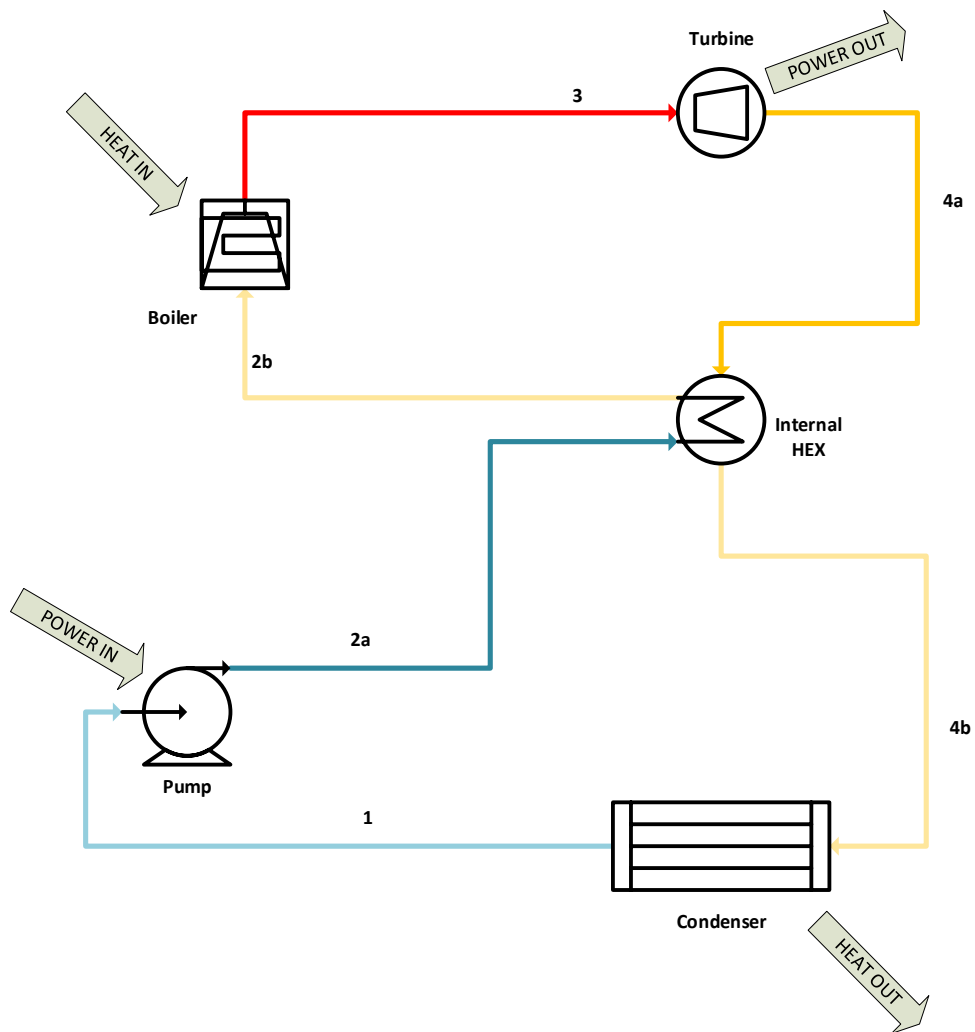


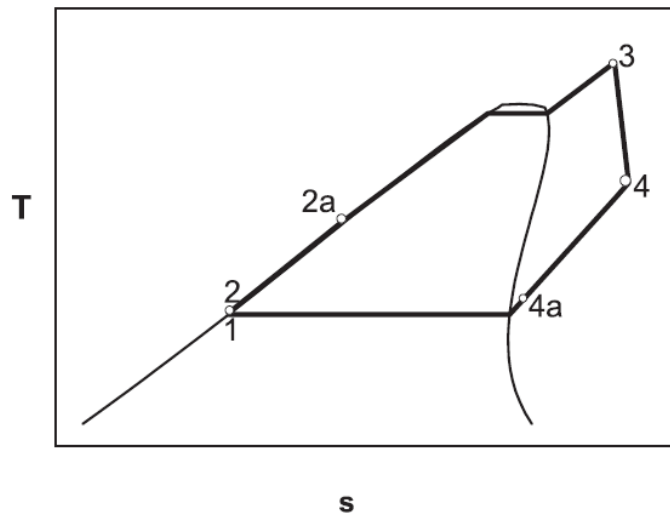
Figure 93: schematic representation of the ORC power block layout[43][43][43][43].

Figure 93 shows the configuration of the main components needed by the ORC power cycle taken as reference. We can see two heat exchangers put in series, the first one after the turbine is the internal heat exchanger used to recover the heat at the outlet of the turbine while the second is the one uses for the fluid condensation.

This ORC needs only one pump that is placed after the condensation HEX and before the cold side of the internal HEX. After the internal HEX cold side is placed the heat exchanger with the external heat source that has to bring the working fluid to the required condition at the inlet of the turbine.

As reported by Ngoc et al. [43] the ORC can work in different configurations:

1. Subcritical maximum pressure and superheated vapours at the inlet of the turbine, figure

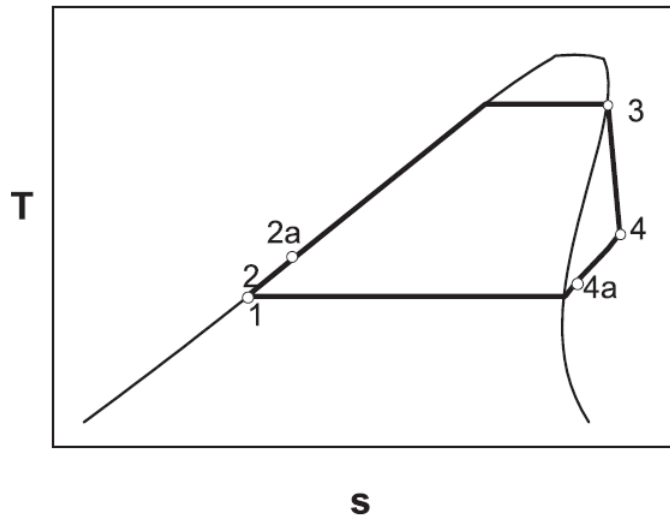


94;

Figure 94: T-s representation of the subcritical with superheated vapour configuration [43].

Figure 94 and 95 are referred to the configuration used in the analysis; the third scheme is not taken into account because the thermal integration with the TES source would be less convenient.

2. Subcritical maximum pressure and saturated vapours at the inlet of the turbine, figure



95;

Figure 95: T-s representation of the subcritical with saturated vapour configuration [43].

3. Supercritical maximum pressure and superheated vapours at the inlet of the turbine, figure 96.

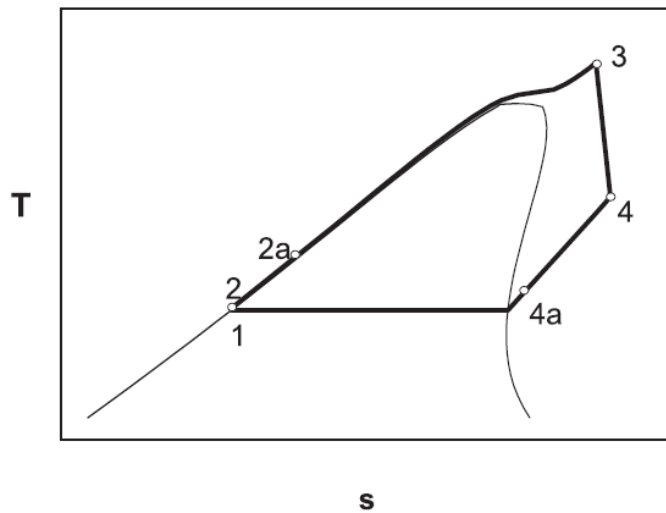


Figure 96: T-s representation of the supercritical vapour configuration [43].

In figures 93 to 96 it can be seen the internal heat exchanger connection: from point 4 to point 4a the hot fluid at low pressure that is coming out from the turbine is cooled down without reaching the saturated steam curve, the extracted heat is then provided to the cold fluid to cover the enthalpy gap between point 2 and 2a.

This heat exchanger couple thermally the fluid at the turbine outlet with the fluid after the pump. In the following analysis the amount of heat exchanged in this HEX is dependent on the temperature difference between the hot outlet stream and the cold inlet stream temperatures that is fixed equal to 15 K.

The heat exchanger is needed as the relatively low maximum pressure of the system coupled with relatively high maximum temperatures brings to a turbine outlet streams at low pressure but still at high temperature.

Could be also very interesting to use a configuration based on case 1 as the TES heat source provides heat at a constant temperature and so the coupling would be easier and more convenient.

Figure 97 shows the power block efficiency obtained with the toluene ORC on a temperature range between 553 K (250 °C) and 653 K (350 °C). The pressure range covered is between 20 to 40 bars.

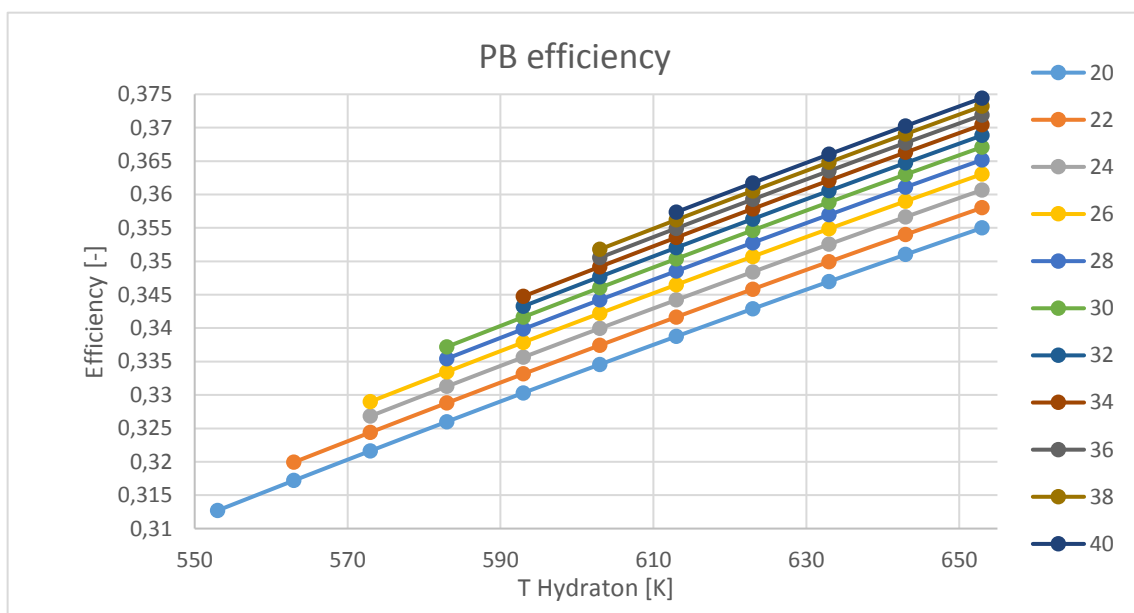


Figure 97: toluene ORC power block efficiency vs pressure and temperature.

The toluene ORC thermal efficiency shown in figure 97 has a linear trend for increasing maximum temperature. The increment of the maximum cycle pressure is also a way to increase the thermal efficiency but, the gain obtained at constant maximum temperature, is not linear and it decrease with the increase of the pressure. The power block efficiency in figure 97 is obtained using equation 26.

Equation 26

$$\eta_{PB} = \frac{abs(W_{turb} - W_{pump}) * t_{hyd,op}}{abs(Q_{hyd} * t_{hyd,op})}$$

In equations 26 the terms related to the time are equal and can be simplified.

Figure 97, for each pressure, shows data only for temperatures higher than a certain limit as, for lower temperature, at a given pressure, the fluid is not fully evaporated at the inlet of the turbine and so the system can't work properly. Of consequence the points reported at the lowest temperature for a certain pressure are basically cases in which the fluid at the inlet of the turbine has a low or any degree of superheating

Figures 97 and 98 about the power block and the overall efficiency are obtained using power blocks components efficiencies and working condition shown in table 58.

Item	Specification	Value	unit
Pump	Isentropic efficiency	0.6	[-]
Turbine	Isentropic efficiency	0.85	[-]
	Discharge pressure	0.086	[bar]
Condenser	Subcooling degree	2	[K]

Table 58: efficiency and working conditions of the power block equipment.

The choice of the turbine discharge pressure is done in order to have a condensation temperature of the ORC fluid that allows to use the external environment as heat sink. With a discharge pressure of 0.1 bar the condensation temperature is at 318 K and so there is a temperature difference with the environment temperature that is 15, the minimum temperature approach used until now in the heat exchangers, plus 2 k of subcooling degree.

Figure 98 shows the overall thermal efficiency obtained with the union of the TES system and the toluene ORC power block.

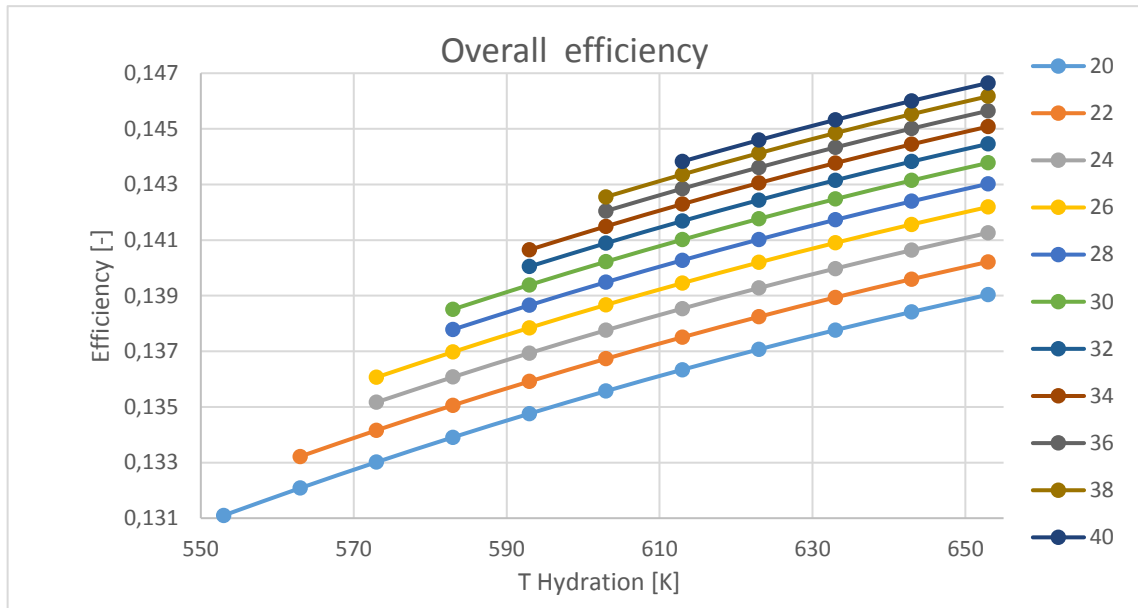


Figure 98: overall efficiency vs power block pressure and hydration temperature.

The efficiency in figure 98 is obtained using equation 27 where the terms related to the time are all equal and can be simplified. Furthermore, the terms of the summation are referred to the heat needed by the HEXs in the TES to preheat the cold streams.

Equation 27

$$\eta_{overall} = \frac{abs(W_{turb} - W_{pump}) * t_{hyd,op}}{Q_{dehyd} * t_{dehyd,op} + \sum(Q_{Hex,i} * t_{op,hex,i})}$$

The obtained overall efficiency behaviour shown in figure 98 is similar to the one for the ORC power block only but we can see a slight deviation from the linear path with the temperature increment. This is clearly related to the behaviour of the TES system for increasing hydration reaction temperature as shown before. From the results is clear that in this range of temperatures also with the ORC would be better to reach the highest possible temperature in order to have the highest overall efficiency. At the end the temperature related enhancement of the TES efficiency is not affecting the overall efficiency behaviour but the combination of the choice of having an ORC power block and a lower hydration temperature is able to permit overall efficiency that are comparable with the ones obtained with the steam Rankine cycle and in some cases also better.

6.4.2. Toluene ORC PB integration with low hydration temperature TES

In this case the TES layout taken as reference is the base case of chapter 4. The Difference is that the hydration temperature is lower as the ORC needs a lower heat source temperature. The coupling is made considering an ORC power block that works with a maximum pressure of 40 bars and a maximum temperature of 638 K in order to have the highest possible efficiency of the PB and, on the basis of figure 98, also of the complete system. The reduction of the hydration temperature doesn't affect the pinch analysis result as the temperature variation means only that all the temperature of the streams during the hydration step are lowered of the same amount without touching the pinch point. Table 59 shows the main data of the system.

Equipment	Data	Value	Unit
Boiler	Duty	63,31	MW
	Output temperature	638	K
Turbine	Power output	-24,44	MW
	Pressure inlet	40	bar
Condenser	Duty	-39,59	MW
	Pressure	0,085	bar
	Temperature output	313	K
Pump	Power inlet	0,74	MW
	Pressure outlet	40	bar
Hydration reactor	Duty	-63,31	MW
	Temperature	653	K
	Pressure	1	bar
TES power input	Duty	110,43	MW

Table 59: TES and PB data after pinch analysis and integration

In this case the toluene mass flow is about 92.6 kg/s and the PB efficiency is 37.43%. With the data in table 59 and equation 28 the overall efficiency of the system is about 21.46 %.

Equation 28

$$\eta_{overall} = \frac{abs(W_{turb} - W_{pump}) * t_{hyd,op}}{Q_{TES,input} * t_{dehyd,op}}$$

6.4.3. Cyclopentane

In order to have a further reduction on of the hydration reaction we can try to integrate an ORC with another working fluid. The choice can be made considering that the power block would work under the critical pressure of the fluid in order to have the phase change at a fixed temperature. Between the fluids listed in literature cyclopentane has recorded very good performances and, as displayed in figure 92, compared to toluene has a lower critical temperature and a slightly higher critical pressure. Exactly these values are: 511.7 K and 45.1 bar. The auto ignition temperature is 634.15 K.

Cyclopentane is also a dry fluid and the internal heat exchanger is quite important to get high thermal efficiency and so the power block layout is the same as in the case of toluene. The chemical formula of cyclopentane is C_5H_{10} and is another hydrocarbon used in many industrial applications and also as a substitute of the more environmentally harmful working fluids of domestic fridge and freezers.

The power block layout is the same used for the Toluene and described in figure 93. In this case the pressure range used for the parametric analysis is the same as before, from 20 to 40 bars, while the hydration reaction temperature range is between 493 to 593 K. The minimum temperature approach in the HEX between hydration reactor and the cyclopentane is 15 K as before; the other power block specifications are resumed in table 60.

Item	Specification	Value	unit
Pump	Isentropic efficiency	0.6	[-]
Turbine	Isentropic efficiency	0.88	[-]
	Discharge pressure	0.8	[bar]
Condenser	Subcooling degree	2	[K]

Table 60: efficiency and specifications of the power block equipment.

As reported in table 60, the turbine discharge pressure has been chosen, also in this case, in order to have a condensation temperature of 315 k and so, with a subcooling degree of 2 k, a power block minimum temperature 15 k higher than the environment.

Figure 99 shows the power block efficiency obtained with the parametric analysis with the already defined boundary conditions. The graph is made using equation 26 as in the case of toluene.

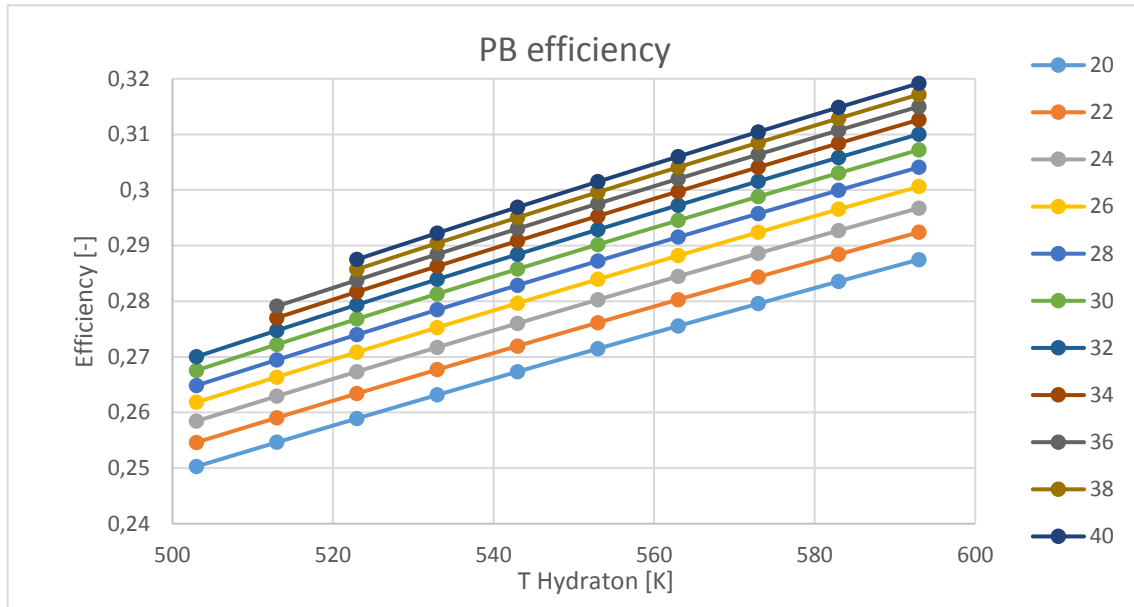


Figure 99: Cyclopentane ORC power block vs temperature and pression.

Figure 99 shows that also in this case the power block thermal efficiency shows a linear trend in respect to the temperature increment of the hydration reaction, and so in respect to the maximum temperature of the cycle itself.

The increment of the maximum power cycle pressure shows also, as consequence, a higher thermal efficiency and as in the previous case this increment becomes slower as the pressure becomes higher. Also in the case, for high pressure and low temperature, the working fluid at the inlet of the turbine is not completely evaporated so the graph show only the points for whom the turbine can work properly

If compared to the results obtained for the toluene we can see that in the range of temperature and pressure that is in common the cyclopentane shows lower performances of about 4- 5 percentage points. The power block efficiency is really affected by the discharge pressure of the turbines that in the case of cyclopentane is of 0.8 bars while the toluene can reach, with the previously mentioned boundary conditions, a discharge pressure of 0.086 bars.

Figure 100 shows the overall efficiency obtained with the TES hydration reaction temperature reaction and the cyclopentane ORC. The graph is made using equation 27 as in the case of toluene.

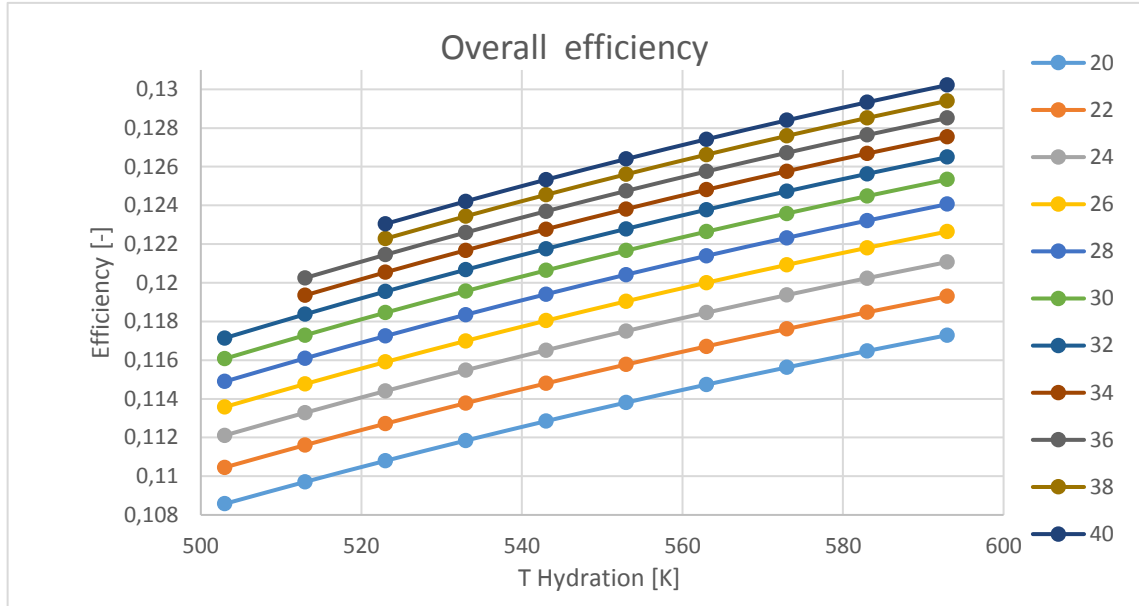


Figure 100: overall efficiency of TES + cyclopentane PB vs hydration temperature and ORC max pressure

As can be seen from figure 100 the cyclopentane ORC overall efficiency has the same trend shown by the toluene ORC. In this case the reduction of the hydration temperature and the increment of the TES thermal efficiency seems to be not enough to overcome the power block efficiency reduction. In this case, as already said, the role of the discharge pressure has an important role in having a not so-high power block efficiency.

6.4.4. Cyclopentane ORC PB integration with low hydration temperature TES

Cyclopentane ORC power block has been studied in a range of lower temperature than toluene but also in this case the reduction of the hydration reaction temperature in the TES system doesn't affect the pinch analysis resultant layout and the integration of the PB can be done with the TES layout obtained at the end of the pinch analysis of chapter 4.

The PB chosen working point is with a maximum pressure of 40 bars and a maximum temperature of 578 K. Also in this case all the temperature in the discharge step are lowered of the same amount of hydration temperature without touching the pinch point and so the HEX network is not changed. In table 61 are shown the data related to the integration.

Equipment	Data	Value	Unit
Boiler	Duty	63,52	MW
	Output temperature	578	K
Turbine	Power output	-21,22	MW
	Pressure inlet	40	bar
Condenser	Duty	-39,58	MW
	Pressure	0,08	bar
	Temperature outlet	313	K
Pump	Power inlet	0,51	MW
	Pressure outlet	160	bar
Hydration reactor	Duty	-63,52	MW
	Temperature	593	K
	Pressure	1	bar
TES power input	Duty	110,43	MW

Table 61: TES and PB data after pinch analysis and integration.

The power block efficiency is 32.60 % with a cyclopentane mass flow of 102.9 kg/s. Using equation 28 and the data of table 61 we can obtain the overall efficiency that is equal to 18.75 %.

7. Conclusions

The present thesis is focused on the study of thermal energy storage via the exploitation of a chemical looping that is a new and innovative way of approaching this kind of applications. This thermal energy storage concept has its own functioning linked to the chemical species that are involved in the process as different species would bring to very different needs, solutions and results in relation to the intended working conditions. This kind of technology has already been studied in the past for many kinds of applications, as mentioned before, and only recently it has been taken into account for applications like thermochemical energy storage power production plant. The interest for this kind of process in the present work is related to the possibilities to use it as thermal storage in relation to CSP power plants.

This technology could be of interest for many other applications but, each analysed case would probably bring to a different final choice on the involved chemicals in order to have the best match with the process needs. In the field of CSP thermal storage application, where the purpose is to collect thermal energy at medium high temperature and to store it for variable time length in order to ensure the highest possible power production availability during the year, in the last years have been studied different chemical loops [45], [46], as solutions in respect to the common thermal storage technology that is represented by sensible, or more recently, latent heat storage.

As reported in the first part of this work the thermochemical energy storage shows a very interesting alternative to classical heat storage method due to its intrinsic characteristics that, overall, brings to the possibilities to store thermal energy for long time periods without needs of thermal barriers and without losses as the storage method is not related to the temperature level of the storage medium during the storage period and so thermal losses are not present. Sensible and latent thermal storage as storage time increases are more and more affected by thermal losses; very high temperature difference with the external environment would also bring to high losses or high costs to prevent them.

Another limitation of sensible and latent heat storage is that the discharge temperature cant' be higher than the one during the charging procedure instead the thermochemical heat storage via chemical loop, as it has the charging and discharging reaction can be run separately, could be used to release energy at higher temperature than the one of the used sources as a chemical heat pump and in facts there are many studies about this topic [16]. As can be seen from literature thermochemical heat storage in many of its variants is in fact only at an experimental or

conceptual stage with many open questions on the best way to technically build the system and make it works.

The present work, as it is related to CSP thermal storage, is focused on a specific chemical looping that can be matched with the typical conditions and needs of this kind of plants. Between the chemicals that are listed in literature this work is focused on the chemical loop based on the use of the hydration of calcium oxide as discharge reaction and the dehydration of calcium hydroxide as charge reaction. The behaviour of the reactions and the characteristics of the involved chemical species have been studied in respect to the main variables, temperature and pressure, and presented in chapter 2 to have a better comprehension of the TES medium.

The raw materials involved in the process, as reported before, are cheap and widely used in many industrial applications, and so, in respect to the cost related to common sensible heat storage this means an advantage. From figure 4 we can see that Hitec and solar salt have a cost respectively of about 10.4 and 5.9 US dollar per kWh stored with an exploitable temperature difference of 200 K. If instead we consider that the energy mass density of a mixture made of calcium hydroxide by 90 % in mass, and for the rest made of calcium oxide, we have a mass energy density value of about 242 kWh/kg and that a mean cos for each kilogram of calcium hydroxide is about 0.15 US dollar [47] we have that the solid mixture has a price, per each kWh of stored energy, of 0.00062 US dollar, that is really lower compared to common HTF costs.

From another point of view the use of HTF and in general of fluids to store energy means the employment of pumps that, usually are not very expensive in term of energy and so are good solutions. The reactions on which the chemical loop of the calcium hydroxide dehydration/hydration is based are solid-gas reaction and so there is the needs both of compatible reactors and of a proper way to move the solid streams in the system. For the solid medium transportation are already available and widely used many solutions like tape and screw conveyors or also pneumatic transportation [48] that can be also used at pressure higher than atmospheric.

For the reactor choice the best solution founded from literature for large scale systems and that gives a good velocity of functioning is represented by the fluidized bed reactor. This kind of reactor, as already said, is quite complicated but it represents one of the most common solutions for gas solid reactions where mass and thermal distributions are crucial.

The coupling between the charging step reaction and the solar plant is then taken into account and the solutions that can be potentially used are represented by direct and indirect integration.

First solution means the employment of an HTF with, as seen in chapter 4, limitations on the maximum temperature that can be reached by the system during the dehydration reaction linked to the maximum working temperature that the common HTF can reach. The other solution is technically more complex, but it doesn't put limitation on the maximum temperature. The direct integration means that the fluid bed reactor where the dehydration reaction takes place has to be directly irradiated by the concentrated solar irradiation. This kind of technology is not very common and, as told before, is still under development and brings with it more complexity and uncertainties.

An aspect that has not been deeply analysed in the present work, and so has to be further investigated, is the problem related to the solid powder fluidization as the involved solids are classified as C type on Geldart's scale and so the fluidization of them would need the introduction of some expedients among the ones listed in chapter 3. In the case of the introduction of an inert in the flows it would mean a drastic reduction of the system thermal efficiency, as reported in the cited works, and the needs of a bigger size of the equipment in order to have the same size power. The other solutions instead would mean a lower efficiency as it would be necessary to give energy to the equipment introduced like agitators. Moreover, has not been taken into account the energy needed by the fans and the pumps needed to the gaseous and liquid flows.

Also the heat exchangers that have to work with solid-solid or solid-gas add some complexity to the system but, as already said in paragraph 3, and discussed by [24], the HEX can be of fluidized bed type (FBHEX) when there are solid streams involved. The solid-gas separation units are instead based on quite common commercial solutions.

After the choice of the main technical direction that has to be followed in order to build up the system, following the conceptual design proposed by [24], a first layout has been created. The boundary conditions of the proposed layout are, in some cases, different from the ones proposed in the reference paper; the most important difference is related to the choice of having the storage at ambient temperature and so only chemical storage. From the comparison with the results obtained in the reference papers, but also from the analysis shown in figure 34, the contribution of the storage temperature to the efficiency of the TES system is in any case very important and has not to be forgotten as an increment of the solid storage temperature of 100 K means a mean thermal efficiency increment of about 5.25 percentage points.

The proposed layout has been tested by two parametric analysis. First parametric analysis is made showing thermal efficiency and power output and input as function of temperature and

reaction conversions alternatively of both the reactors in a range of values that are near to the starting point data. This analysis shown that the relations between these variables in the system are mostly linear and, in some cases, there are no influence. A higher conversion in any case means a higher efficiency while a higher temperature in each of the reactors means a lower efficiency. Already from this point is clear that to have a higher temperature of discharge is more expensive in term of energy and also the energy output from the reaction is lower, while a lower temperature in the charging step means a higher energy needs to reach the reaction temperature but a lower expenditure to run the reaction and break the chemical bounds of the calcium hydroxide.

Then a second parametric analysis has been made for constant temperatures in the reactors varying the conversion in both the reactors between 0.1 to 1. The chosen temperature are the ones provided by the conceptual design paper [24]. The output variables are the efficiency and the power output and input to and from the TES system during a complete cycle of charge and discharge.

In this case the system response shows how should be important to reach at least a conversion for both the reactions that should be higher than 0.4 in order to have already a good level of thermal efficiency. Moreover, to have a low conversion of only one of the reactions means in any case an increment of the solid mass flow needed to chemically absorb or release the same amount of energy as can be seen in figure 101 where the legend is referred to the dehydration conversion.

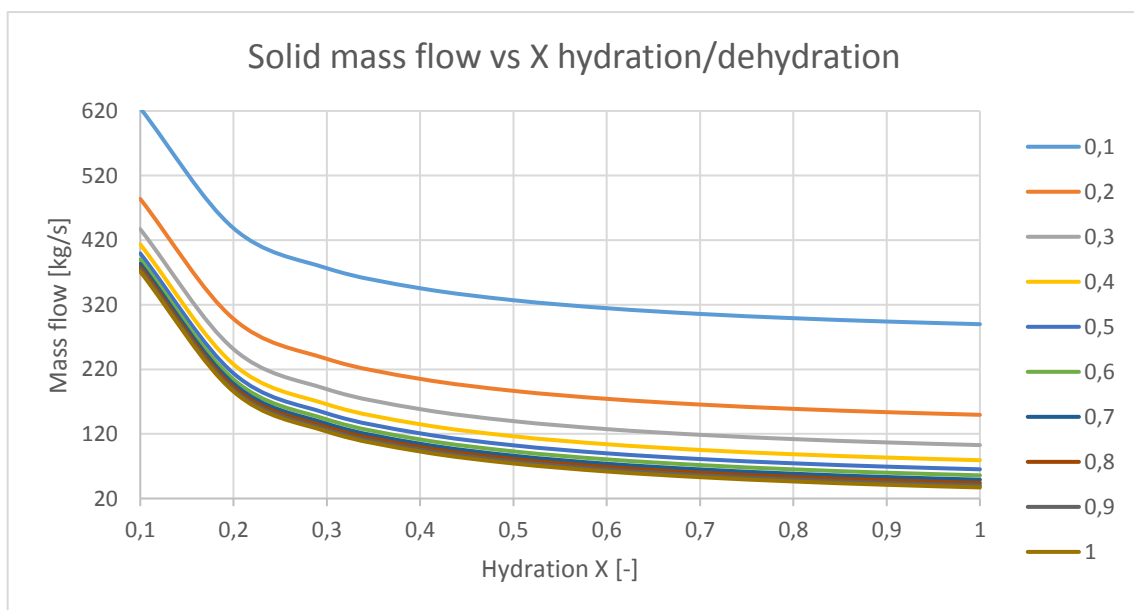


Figure 101: hydraion/dehydration conversion influence on the dehydration solid mass flow.

Figure 101 is obtained fixing the power input to the dehydration reactor at 50 MW and show us that when with only one of the reaction conversions over 0.4 the mass flow needed by the system has been heavily reduced but, in relative terms, also when both the conversions are over 0.6 the mass flow reduction can be very important for increasing conversion values. A lower solid mass flow for the same power input or output means also a lower needed energy to preheat those streams and so a higher thermal efficiency.

It has to be taken into account that the amount of water needed for the hydration reaction is linked directly to the amount of calcium oxide that react and that the specific energy needed to preheat this stream is higher than the one needed for the solid streams, ratio of about 6 to 1, but the needed energy is lower as the mass flow of the inlet water stream is lower and so only if the hydration and the dehydration conversions becomes very high the preheating needed energy are comparable.

Figure 102 shows a comparison between the power needed to preheat the solid mass flow inlet to the hydration reactor and the water mass flow inlet as function of the conversions of both the reactors.

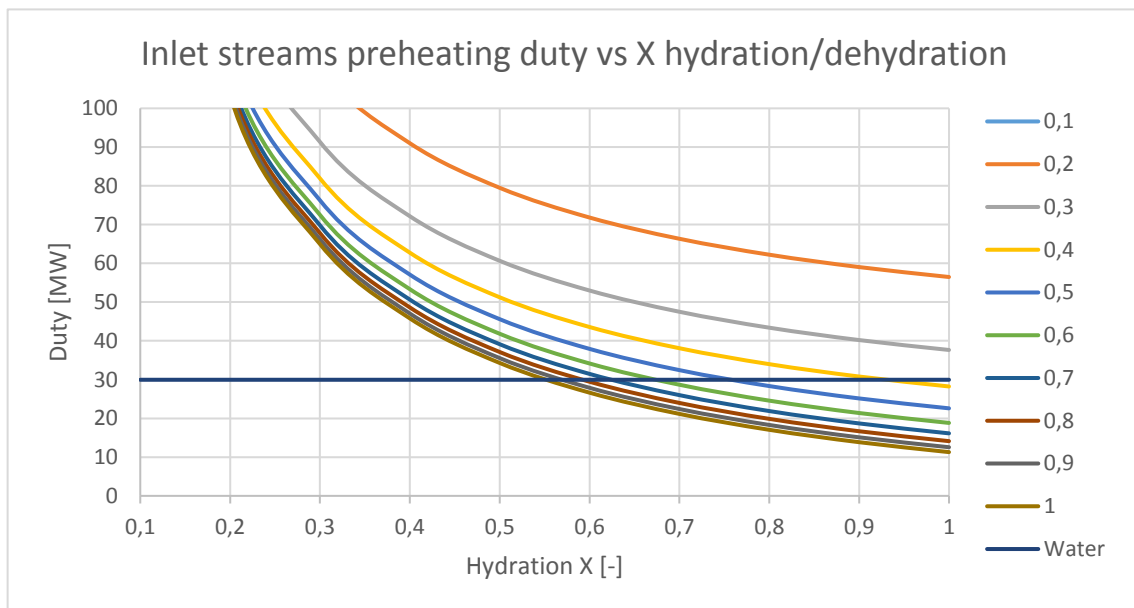


Figure 102: Inlet streams preheating duty vs X hydration/dehydration.

As can be seen from figure 102 the preheating duty needed for the solid stream is higher of the one needed to preheat the water stream unless the reaction conversions are high enough. The water stream preheating duty is constant as the calculation is made for a constant level of power

input to the dehydration reaction and so also the output is always the same and so the needed stoichiometric amount of water as the two step works for the same amount of time.

After the parametric analysis has been made a first pinch analysis to see how the system thermal efficiency can be improved in order to make a comparison with the system thermal efficiency obtained in the reference paper.

Then the work has been developed in order to have base layout with some fixed condition that can be used as point of comparison with modified versions of the system base layout. The main fixed conditions are: the power input to the dehydration reactor, for which has been chosen a value of 100 MW, the dehydration and the hydration conversion values that are fixed respectively to 0.88 and 0.6. On this layout has been also made a pinch analysis always for further comparison. The power input level has been chosen referring to the typical values founded in literature for the solar towers CSP plant types.

7.1. TES system modification results and analysis

The present work has taken into account several possible changes of the TES system in order to find way to enhance the thermal efficiency of the system. The reactions involved in the chemical loop are relatively simple as they involve at most two reactants or two products and from the physical point of views the only parameters that can be changed in order to have a different system behaviour are temperature and pressure.

The first modification taken into account has been the reduction of the dehydration temperature in order to reduce the energy needed to the preheating of the inlet stream of the charging step to see if the efficiency could be enhanced. As the reaction temperature is directly linked to the steam partial pressure and the reduction of the reaction temperature is possible only if also the pressure is lowered the only way to reduce the temperature is working on the dehydration steam partial pressure. As reference we can remind that at ambient pressure the dehydration process happens at temperature higher than 792 K.

The method used to reduce the dehydration steam partial pressure has been discussed in chapter 5.2 and involves the introduction of a neutral gas, instead of steam, as fluidizing agent in order to dilute the steam and so have a reduction of its partial pressure. The chosen neutral gas is the nitrogen as in literature are present some works where this element is used in some experiment on the same topic without any change in the reaction behaviour. Moreover, nitrogen is also a

commonly used substance. The introduction of the nitrogen rises the needs of the separation between it and the steam generated in the reaction. The proposed solution is the condensation of the steam, process that is not anymore at constant temperature due to the mixture of gaseous species.

The results of this first test is that the dehydration temperature can be reasonably lowered only of some tens of degrees. Moreover, the efficiency of the system is not improved as the lower heat needs for the preheating of the streams is lower than the increment of heat needed to run the dehydration reaction due to the reduction of temperature.

The second try is to introduce a series of dehydration reactors in order to be able to have always the same final dehydration conversion but with lower steam production in each reactor and so a lower steam partial pressure that can be exploited to reduce more the temperature. This study has been made using a number of reactors between 2 and 5. The result is that the temperature reduction is also in this case not so high and in any case the thermal efficiency shows a further reduction.

The present work has taken into account only physical expedients in order to reduce the dehydration temperature but, it could be interesting, to make some studies about the possibilities of employ catalysts in the dehydration process to reach lower temperatures.

Also the hydration reaction conditions have been modified but in order to increase the temperature at which the TES can release the stored heat. The physical way to do that is the increment of the hydration pressure. The study on the hydration pressure increment ranges between 1 to atmospheres and in conjunction with the temperature increment it brings also a thermal efficiency decrement due to the higher stream preheating needs.

After all the system modifications have been also made a pinch analysis for a specific case in order to have a more real idea of the potential thermal efficiency of the TES.

Figure 103 shows a comparison between the efficiency obtained before and after the pinch analysis for all the for all the TES modification cases for which have been made the pinch analysis.

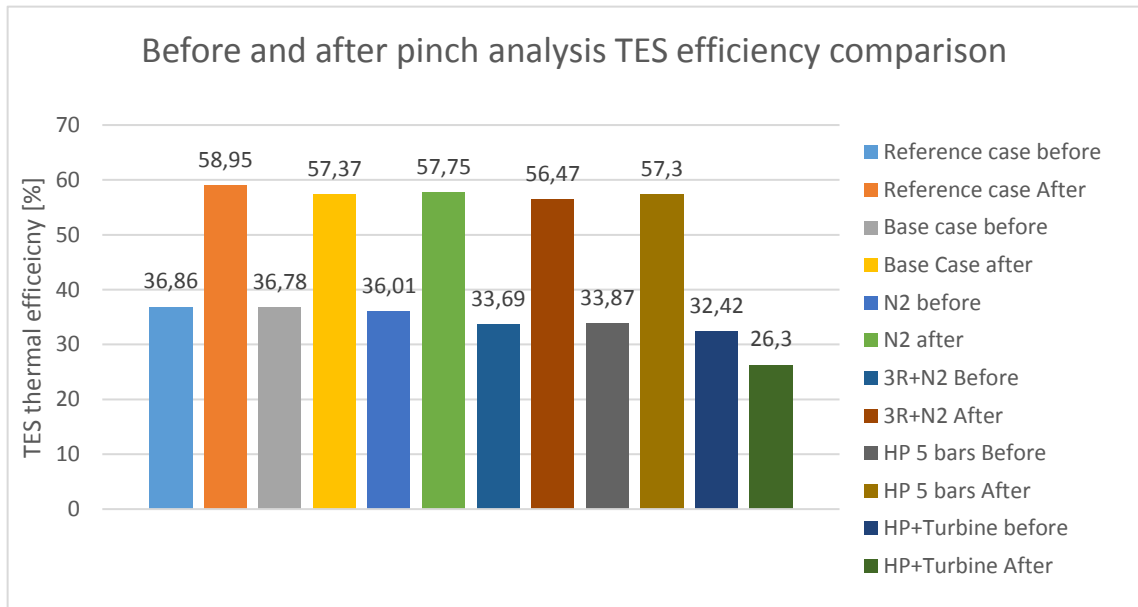


Figure 10325: TES thermal efficeicny comparison before and after pinch analysis.

As can be seen from figure 103 the efficiency for the TES systems before the pinch analysis show lower and mainly very similar values. Between the base case and the case with the addition of the nitrogen the difference before the pinch analysis are very low.

The efficiency of the cases with three reactors in series and the one with higher hydration pressure before the pinch analysis have similar efficiencies that show both a percentage gap of about 2 or 3 points in relation to the base case and the case with the addition of nitrogen.

After the pinch analysis the thermal efficiency of all the cases are very similar and are between 56.5 to 59 %; the only case in which the efficiency is remarkably lower is related to the turbine direct integration. It can be seen that from the TES thermal efficiency point of view any kind of physical modifications made to have some kind of improvements brings to a lower thermal efficiency but, in most of the cases, a well made network of HEX is able to reduce these differences.

The pinch analysis seems to have a higher influence in the TES layouts with higher hydration pressure and the one with three dehydration reactors in series as they have a lower initial thermal efficiency and after the pinch analysis they reach an efficiency more similar to the one of the other cases that have as starting point already a higher efficiency.

7.2. Power block integration results and analysis

The last part of the present work is focused on the integration of the system that is in charge for the production of the mechanical power that can be then transformed into electricity. The power block is supposed to work only when the hydration process is on duty.

As reported the discharge step needs to employ also an amount of the heat release by the hydration reactor in order to preheat the reactant needed by the process and so best integration with the power block is to use the remaining amount of energy released by the reactor to heat up the working fluid of the power block as all the other heat sources available in the TES system during the discharge step are used to cover the preheating needs of the TES system itself.

As previously discussed the temperature level at which the heat is available from the hydration reactor is high enough to fuel a Rankine-Hirn steam power cycle. Starting from the available conditions at which the heat is released by the base case TES system a steam Rankine-Hirn cycle with two level of pressure has been studied in order to find the working point with the best efficiency working both on the maximum temperature and pressure of the system and also the low-pressure level.

As the steam cycle performance shows that a higher maximum pressure and temperature links to better efficiency the conclusion is that this kind of coupling could be improved modifying the temperature at which the TES release the power. As we have already seen the increment of the TES discharge temperature can be made increasing the pressure at which the hydration reaction works but this brings to a reduction of the TES efficiency and so it as to be investigated if this modification makes sense or not.

Moreover, we have seen that the TES system has a better performance if the hydration temperature is decreased but if it is too low is not convenient anymore to use a steam Rankine-Hirn cycle as power block as lowering the temperature at which the energy is available links to an efficiency reduction.

In parallel a higher pressure condition in the hydration reactor has been taken into account to study the introduction of an integrated steam turbine linked to the discharge step of the TES. This solution, after the pinch analysis, brings to a very low thermal output that can be used for other applications making not applicable the coupling with an external large-scale power block. The integrated turbine can be maybe interesting for low scale TES where in any case also the power block would have a low power output.

Instead, with a lower temperature available heat source the power block choice could be direct towards the use of an organic Rankine power cycle. This alternative has been studied taking into account two different working fluids, toluene and cyclopentane, that are commonly used in the industry and are feasible to work in a temperature range between 250 and 380 °C.

The power block layout used for both the ORC is with a single pressure level and an internal heat exchanger to get better efficiency. The TES starting point layout is represented by the base case layout in which the hydration reaction temperature has been reduced in order to have higher TES efficiency and matching the ORC working temperature level.

Figure 104 shows a comparison between the overall efficiency obtained in the cited cases.

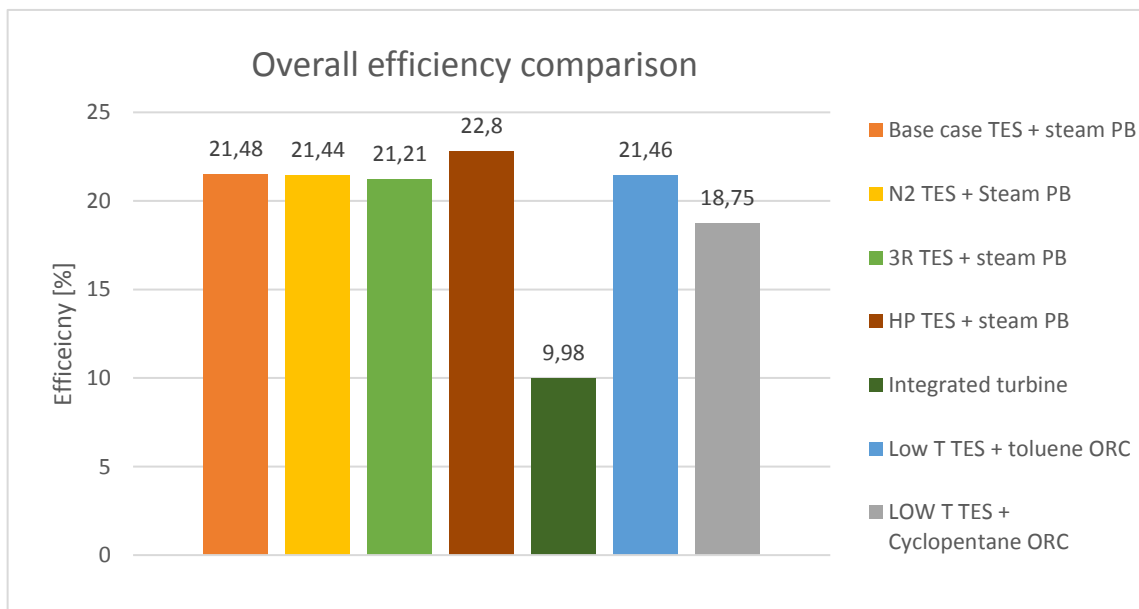


Figure 104: Overall efficiency comparison.

Figure 104 is a comparison of the overall efficiency obtained combining the studied power block with the TES systems cases for which it have been made a pinch analysis. The one referred to the integrated steam turbine takes into account as usefull output only the net mechanical energy provided by the turbien itself without considering the low amount of heat that the hydration reactor can still provide. The such system at the end has the lowest overall efficiency. The best performance is obatine dcombining the steam power block with the hydration reactor at a pressure of 6 bars in order to have the released heat at higher temperature.

The combination of the steam PB with the TES systems that use nitrogen in the dehydration step as fluidizing agent brings to overall efficeincies comparable to the one obtained with the

combination of the steam PB and the TES base case. Also the toluene ORC power block combined with the low hydration temperature TES shows a overall efficiency that is comparable to the ones obtained with the TES base case and the steam power cycle.

The combination of the cyclopentane ORC power block with the low hydration temperature TES instead brings to the second worst overall efficiency also if the related hydration temperature is lower than the one of the case with the toluene ORC PB and so the TES thermal efficiency should be higher.

With the studied TES and power block there are other combinations that can be done like both hydration high pressure and dehydration with nitrogen and steam cycle based power block or ORC based power block combined with low temperature hydration reactor and dehydration with nitrogen as fluidizing agent TES and many more. The analysis made on the TES system takes into account several system modifications but one by one and only on one of the TES steps. In this way it can be seen the system response to the single modifications.

As the two steps of the TES are not completely coupled the modification on one of the steps has a low influence on the behaviour of the other side. Due to the way the system has been built the modifications on the dehydration side of the TES affect more all the system while the modifications on the discharge side are less influential. This is due to the fact that the mass flows of all the system are defined by the power input to the dehydration reactor.

The resulting overall efficiency are not so high if compared to the one of actual CSP plants like the ones shown in figure, but it has to be reminded that the efficiency obtained are only referred to the mechanical power that can be provided with the heat provided by the TES and so is not taking into account the power that can be produced directly when the sun is available. Furthermore, in the analysis done in this work is not considered the efficiency of the solar plant and also the conversion efficiency from mechanical power to electricity.

The next step should be a deeper analysis of this kind of system during a typical day other than the study of the process in terms of real experimentation both at lab and at application scales.

8. Bibliography

- [1] M. Aneke and M. Wang, 'Energy storage technologies and real life applications – A state of the art review', *Appl. Energy*, vol. 179, pp. 350–377, 2016.
- [2] K. C. Divya and J. Østergaard, 'Battery energy storage technology for power systems- An overview', *Electr. Power Syst. Res.*, vol. 79, no. 4, pp. 511–520, 2009.
- [3] M. Liu *et al.*, 'Review on concentrating solar power plants and new developments in high temperature thermal energy storage technologies', *Renew. Sustain. Energy Rev.*, vol. 53, pp. 1411–1432, 2016.
- [4] P. Pardo, A. Deydier, Z. Anxionnaz-Minvielle, S. Rougé, M. Cabassud, and P. Cognet, 'A review on high temperature thermochemical heat energy storage', *Renew. Sustain. Energy Rev.*, vol. 32, pp. 591–610, 2014.
- [5] A. G. Fernández, S. Ushak, H. Galleguillos, and F. J. Pérez, 'Development of new molten salts with LiNO₃ and Ca(NO₃)₂ for energy storage in CSP plants', *Appl. Energy*, vol. 119, no. 3, pp. 131–140, 2014.
- [6] E. B. Fox, T. C. Paul, N. J. Bridges, J. A. Khan, A. K. M. M. Morshed, and A. E. Visser, 'Thermal performance of ionic liquids for solar thermal applications', *Exp. Therm. Fluid Sci.*, vol. 59, pp. 88–95, 2014.
- [7] C. Xu, X. Li, Z. Wang, Y. He, and F. Bai, 'Effects of solid particle properties on the thermal performance of a packed-bed molten-salt thermochemical thermal storage system', *Appl. Therm. Eng.*, vol. 57, no. 1–2, pp. 69–80, 2013.
- [8] J. C. Kurnia, A. P. Sasmito, S. V. Jangam, and A. S. Mujumdar, 'Improved design for heat transfer performance of a novel phase change material (PCM) thermal energy storage (TES)', *Appl. Therm. Eng.*, vol. 50, no. 1, pp. 896–907, 2013.
- [9] A. F. Elmozughi, L. Solomon, A. Oztekin, and S. Neti, 'Encapsulated phase change material for high temperature thermal energy storage - Heat transfer analysis', *Int. J. Heat Mass Transf.*, vol. 78, pp. 1135–1144, 2014.
- [10] C. W. Robak, T. L. Bergman, and A. Faghri, 'Enhancement of latent heat energy storage using embedded heat pipes', *Int. J. Heat Mass Transf.*, vol. 54, no. 15–16, pp. 3476–3484, 2011.

- [11] N. Gokon, D. Nakano, S. Inuta, and T. Kodama, 'High-temperature carbonate/MgO composite materials as thermal storage media for double-walled solar reformer tubes', *Sol. Energy*, vol. 82, no. 12, pp. 1145–1153, 2008.
- [12] W. E. Wentworth and E. Chen, 'Simple thermal decomposition reactions for storage of solar thermal energy', *Sol. Energy*, vol. 18, no. 3, pp. 205–214, 1976.
- [13] A. Farhad and Z. Mohammadi Esfahan, 'Calcium hydroxide: a review Chemical characteristics of calcium hydroxide', *Int. Dent. J.*, vol. 55, pp. 293–301, 2005.
- [14] F. Schaube, L. Koch, A. Wörner, and H. Müller-Steinhagen, 'A thermodynamic and kinetic study of the de- and rehydration of Ca(OH)₂ at high H₂O partial pressures for thermo-chemical heat storage', *Thermochim. Acta*, vol. 538, pp. 9–20, 2012.
- [15] L. André, S. Abanades, and G. Flamant, 'Screening of thermochemical systems based on solid-gas reversible reactions for high temperature solar thermal energy storage', *Renew. Sustain. Energy Rev.*, vol. 64, pp. 703–715, 2016.
- [16] H. Ogura, S. Abliz, and H. Kage, 'Studies on applicability of scallop material to calcium oxide/calcium hydroxide chemical heat pump', *Fuel Process. Technol.*, vol. 85, no. 8–10, pp. 1259–1269, 2004.
- [17] J. Montagu, M. Configurations, B. Deflection, and S. Technologies, 'United States Patent (19)', no. 19, 1993.
- [18] P. E. L. Green, 'U . S . Patent Apr . 25 , 1989', no. 19, 1989.
- [19] M. E. Perez-davis, B. I. McKissock, and F. DiFilippo, 'Thermochemical Energy Storage for a Lunar Base', *Int. Sol. energy Conf.*, p. 8, 1992.
- [20] Y. A. Criado, M. Alonso, and J. C. Abanades, 'Kinetics of the CaO/Ca(OH)₂ hydration/dehydration reaction for thermochemical energy storage applications', *Ind. Eng. Chem. Res.*, vol. 53, no. 32, pp. 12594–12601, 2014.
- [21] Y. Wang, S. Lin, and Y. Suzuki, 'Effect of CaO content on hydration rates of Ca-based sorbents at high temperature', vol. 9, pp. 2–8, 2007.
- [22] S. Lin, Y. Wang, and Y. Suzuki, 'High-Temperature CaO Hydration/Ca(OH)₂ Decomposition over a Multitude of Cycles', vol. 23, no. June, 2009.
- [23] P. Pardo, Z. Anxionnaz-Minvielle, S. Rougé, P. Cognet, and M. Cabassud,

- ‘Ca(OH)₂/CaO reversible reaction in a fluidized bed reactor for thermochemical heat storage’, *Sol. Energy*, vol. 107, pp. 605–616, 2014.
- [24] Y. A. Criado, M. Alonso, J. C. Abanades, and Z. Anxionnaz-Minvielle, ‘Conceptual process design of a CaO/Ca(OH)₂ thermochemical energy storage system using fluidized bed reactors’, *Appl. Therm. Eng.*, vol. 73, no. 1, pp. 1085–1092, 2014.
- [25] M. Angerer *et al.*, ‘Design of a MW-scale thermo-chemical energy storage reactor’, *Energy Reports*, vol. 4, pp. 507–519, 2018.
- [26] D. Geldart, ‘Types of gas fluidization’, *Powder Technol.*, vol. 7, no. 5, pp. 285–292, May 1973.
- [27] C. Roßkopf, M. Haas, A. Faik, M. Linder, and A. Wörner, ‘Improving powder bed properties for thermochemical storage by adding nanoparticles’, vol. 86, pp. 93–98, 2014.
- [28] I. Barin and F. Sauert, *Thermochemical Data of Pure Substances*, no. parte 1. VCH, 1993.
- [29] E. Agrawal and P. Jha, ‘Chemical reaction engineering’, vol. 2, pp. 20–23, 2017.
- [30] A. Johansson, F. Johnsson, B. Leckner, and F. Scalo, ‘Solids back-mixing in CFB boilers’, *Chem. Eng. Sci.*, vol. 62, no. 1–2, pp. 561–573, 2007.
- [31] F. Scalo, ‘Fluidized Bed Technologies for Near-Zero Emission Combustion and Gasification’, *Fluidized Bed Technologies for Near-Zero Emission Combustion and Gasification*. 2013.
- [32] ‘Perry’s chemical engineers’ handbook’, *Choice Reviews Online*, vol. 35, no. 06. pp. 35-3079-35–3079, 2013.
- [33] R. I. Olivares, ‘The thermal stability of molten nitrite / nitrates salt for solar thermal energy storage in different atmospheres The thermal stability of molten nitrite / nitrates salt for solar thermal energy storage in different atmospheres’, *Sol. Energy*, vol. 86, no. 9, pp. 2576–2583, 2017.
- [34] ‘Thermal performance of a 30 kW fluidized bed reactor for solar gasification A CFD DEM stud.pdf’ . .
- [35] ‘Heat transfer and particulate flow analysis of a 30 kW directly irradiated solar

fluidized bed reactor for thermochemical cycling.pdf' . .

- [36] C. Tregambi, R. Chirone, F. Montagnaro, P. Salatino, and R. Solimene, 'ScienceDirect Heat transfer in directly irradiated fluidized beds', *Sol. Energy*, vol. 129, pp. 85–100, 2016.
- [37] S. Bellan, N. Gokon, and K. Matsubara, 'ScienceDirect Numerical and experimental study on granular flow and heat transfer characteristics of directly-irradiated fluidized bed reactor for solar gasification', *Int. J. Hydrogen Energy*, vol. 43, no. 34, pp. 16443–16457, 2018.
- [38] C. Tregambi, P. Salatino, R. Solimene, and F. Montagnaro, 'An experimental characterization of Calcium Looping integrated with concentrated solar power', *Chem. Eng. J.*, vol. 331, no. August 2017, pp. 794–802, 2018.
- [39] M. Schmidt, A. Gutierrez, and M. Linder, 'Thermochemical energy storage with CaO/Ca(OH)₂– Experimental investigation of the thermal capability at low vapor pressures in a lab scale reactor', *Appl. Energy*, vol. 188, pp. 672–681, 2017.
- [40] M. Schmidt and M. Linder, 'Power generation based on the Ca(OH)₂/ CaO thermochemical storage system – Experimental investigation of discharge operation modes in lab scale and corresponding conceptual process design', *Appl. Energy*, vol. 203, pp. 594–607, 2017.
- [41] P. Systems *et al.*, 'ScienceDirect ScienceDirect ScienceDirect High Temperature Systems The 15th High Temperature ORC Temperature ORC Systems Assessing the feasibility of using the heat district heat demand forecast', *Energy Procedia*, vol. 129, pp. 82–89, 2017.
- [42] U. K. Deiters, A. Groniewsky, I. Lassu, and A. R. Imre, 'Novel classification of pure working fluids for Organic Rankine Cycle for Gy o', vol. 145, pp. 288–300, 2018.
- [43] N. A. Lai, M. Wendland, and J. Fischer, 'Working fluids for high-temperature organic Rankine cycles', *Energy*, vol. 36, no. 1, pp. 199–211, 2011.
- [44] N. B. Desai and S. Bandyopadhyay, 'Thermo-economic analysis and selection of working fluid for solar organic Rankine cycle', vol. 95, pp. 471–481, 2016.
- [45] R. Chacartegui, A. Alovio, C. Ortiz, J. M. Valverde, V. Verda, and J. A. Becerra, 'Thermochemical energy storage of concentrated solar power by integration of the

- calcium looping process and a CO₂power cycle’, *Appl. Energy*, vol. 173, pp. 589–605, 2016.
- [46] C. Chen, L. Zhao, and A. S. Lavine, ‘Feasibility of using ammonia-based thermochemical energy storage to produce high-temperature steam or sCO₂’, *Sol. Energy*, vol. 176, no. September 2017, pp. 638–647, 2018.
- [47] Intratec, ‘Hystorical calcium hydroxide price’ . .
- [48] G. E. Klinzing, ‘A review of pneumatic conveying status , advances and projections’, *Powder Technol.*, vol. 333, pp. 78–90, 2018.